# Southeastern Geology: Volume 31, No. 2 September 1990

Edited by: S. Duncan Heron, Jr.

**Abstract**

Academic journal published quarterly by the Department of Geology, Duke University.

# SOUTHEASTERN GEOLOGY

PUBLISHED AT DUKE UNIVERSITY DURHAM, NORTH CAROLINA

VOL. 31, NO. 2 SEPTEMBER 1990

# SOUTHEASTERN GEOLOGY

PUBLISHED

AT

DUKE UNIVERSITY



This journal publishes the results of original research on all phases of geology, geophysics and geochemistry as related to the Southeast. Send manuscripts to **S. DUNCAN HERON, JR., DUKE UNIVERSITY, DEPARTMENT OF GEOLOGY, OLD CHEMISTRY BUILDING, DURHAM, NORTH CAROLINA 27706**. Observe the following:

1) Type the manuscript with double space lines and submit in duplicate.
2) Cite references and prepare bibliographic lists in accordance with the method found within the pages of this journal.
3) Submit line drawings and complex tables reduced to final publication size (no bigger than 8 x 5 1/8 inches).
4) Make certain that all photographs are sharp, clear, and of good contrast.
5) Stratigraphic terminology should abide by the North American Stratigraphic Code (Am. Assoc. Petroleum Geologists Bulletin, v. 67, p. 841-875).

Subscriptions to *Southeastern Geology* are $12.00 per volume (US and Canada), $16.00 per volume (foreign). Inquires should be sent to: **SOUTHEASTERN GEOLOGY, DUKE UNIVERSITY, DEPARTMENT OF GEOLOGY, OLD CHEMISTRY BUILDING, DURHAM, NORTH CAROLINA 27706**. Make checks payable to: *Southeastern Geology*.

ISSN 0038-3678

# SOUTHEASTERN GEOLOGY

**Table of Contents**

Vol. 31, No. 2

September 1990

1. The Princess N. 6 Middle Pennsylvanian Volcanic Ash Fall (Tonstein), Kentucky and West Virginia, Central Appalachian Basin

William F. Outerbridge
Don M. Triplehorn
Paul C. Lyons
63

2. An Anomalous Mass-Flow Deposit in the Lee Formation (Pennsylvanian), Eastern Kentucky Coal Field

Stephen F. Greb
Donald B. Chesnut
Oscar B. Davidson
Rene Rodriguez 79

3. Deformation History of an Outcrop-Scale Fault System in the Central Appalachian

Philip B. Scott
William M. Dunne 93

4. Trace-Element Geochemistry and an Oceanic Origin for the Hammett Grove Meta-Igneous Suite, South Carolina

Steven K. Mittwede
W. E. Sharp 109

# THE PRINCESS NO. 6 MIDDLE PENNSYLVANIAN VOLCANIC ASH FALL (TONSTEIN), KENTUCKY AND WEST VIRGINIA, CENTRAL APPALACHIAN BASIN

WILLIAM F. OUTERBRIDGE[1]

DON M. TRIPLEHORN[1,2]

PAUL C. LYONS[1]

[1]*U.S. Geological Survey*
*MS 956 National Center*
*Reston, VA 22092*

[2]*University of Alaska,*
*Fairbanks, AK 99708*

## ABSTRACT

A thin claystone unit below the Princess No. 6 coal zone of northeastern Kentucky and adjacent parts of West Virginia contains euhedral β-quartz crystals (some with glass inclusions), euhedral zircon, and anatase(?). The limited suite of minerals, the bimodal size distribution, and the euhedral character of the β-quartz grains indicate that the claystone originated as a volcanic ash fall of acidic composition and is, therefore, a tonstein of volcanic origin.

## INTRODUCTION

It is well known that the Fire Clay or Hazard No. 4 coal bed (Middle Pennsylvanian) of Kentucky and the correlative Hernshaw coal bed of West Virginia of Westphalian B age (Englund and others, 1979) contain an altered volcanic ash deposit or tonstein (Seiders, 1965; Bohor and Triplehorn, 1981; Chesnut, 1985; Keiser and others, 1987, 1989; Belkin and Rice, 1989). Although the occurrence of other tonstein beds in the Pennsylvanian rocks of the Appalachian Basin has been suggested (Burger, 1985a; Burger and Damberger, 1985), none of these have been adequately described or positively identified mineralogically as being tonsteins. This paper presents evidence for another tonstein in the upper part of the Breathitt Formation and its lateral equivalent in West Virginia, the Charleston Sandstone. This tonstein occurs about 400 ft stratigraphically above the Fire Clay coal bed in northeastern Kentucky and adjacent West Virginia.

### Importance of the Tonstein

Volcanic ash beds in coal-bearing rocks have been used as marker beds in coal correlation (Rogers, 1914). Because a volcanic ash fall is geologically an instantaneous event and is, therefore, the same geologic age everywhere, it can be a critical marker bed for regional correlation. If volcanic ash beds contain isotopically datable minerals, such as sanidine (Lippolt and Hess, 1985) and zircon, then it may be possible to propose a geochronologic framework for part of the Pennsylvanian System of the Appalachian basin. Volcanic ash beds can provide data resolving spatial and temporal relations of individual coal beds and associated facies (e.g., Ryer and others, 1980).

## Definitions of Terms

Tonstein, which is German for claystone (Williamson, 1970), is applied in this paper to claystone derived from a volcanic ash fall. In general, there is no simple way to identify altered volcanic ash in the field. Any thin widespread unit may be a tonstein, but confirmation of a volcanic ash origin requires laboratory analysis of texture and mineralogy.

Flint clay is a field term for a claystone that breaks along a conchoidal or blocky fracture and does not soften in water. Some tonstein is also flint clay, but we use "flint clay" as a lithologic term without any genetic connotation. Our usage follows the definition of flint clay that is found in Howell (1960) and that was used by early workers in the central Appalachian basin who recognized thin widespread claystone units in several places in the Middle Pennsylvanian sequence. These units are notably more resistant than the enclosing mudrock.

β-quartz is the polymorph of quartz that exists between 573 and 870° C. It characteristically crystallizes as hexagonal bipyramids that do not change their shape on inversion to α-quartz at 573° C. Such forms are common in silicic volcanic ash and are an important criterion for the identification of altered volcanic ash layers (Triplehorn, 1976; Blatt and others, 1980; Bohor and Triplehorn, 1981). They range from perfect forms with sharp crystal faces and subspherical forms with vague crystal faces to completely rounded forms; the subspherical and rounded forms are presumably due to increasing degrees of resorption in the magma chamber.

## Previous Work

The flint clay (tonstein) that is associated with the Fire Clay coal bed and correlative coal beds was reported in Kentucky by McFarlan (1943), in Virginia by Giles (1934), and in West Virginia by Hennen and Teets (1919). This flint clay was described as a volcanic ash fall in the Pardee coal bed in Virginia by Nelson (1959), the Fire Clay coal bed in Kentucky by Seiders (1965) and Huddle and Englund (1966), and the Hernshaw coal bed in West Virginia by Keiser and others (1987). It has been reported to be about 311 Ma on the basis of $^{40}Ar/^{39}Ar$ dates on sanidine and plagioclase (Hess and others, 1988). Hoehne (1957) described flint clays from the Fire Clay, Windrock, Upper Hignite, Leatherwood, and Index Hill coal beds in the central Appalachian basin; in them he found quartz splinters and euhedral zircon, but did not conclude that they were of volcanic origin.

Thin claystone or flint clay associated with the Princess No. 6 coal zone has been used as a marker bed in northeastern Kentucky and adjacent areas of West Virginia (Sheppard and Ferm, 1962; Dobrovolny and others, 1963; Spencer, 1964; Carlson, 1965; Dobrovolny and others, 1966; Sharps, 1967; Carlson, 1971; Outerbridge, 1977; Connor and Flores, 1978; Outerbridge, 1978; Ward, 1978; and Pillmore and Connor, 1978). It was described as a distinctive black or dark-gray flint clay at or near the base of the Princess No. 6 coal zone or at the top of the underlying thick underclay known as the Hitchens clay in Kentucky, the Elk fire clay in West Virginia, and the Lawrence clay in Ohio (Stout and others, 1931; Outerbridge and others, 1988; Outerbridge, 1989). The flint clay marker bed occurs about 400 ft above the Fire Clay flint clay in the Louisa quadrangle of Kentucky and West Virginia (Connor and Flores, 1978) and the adjoining Webb quadrangle (Ward, 1978) in the general area of our investigation (Figure 1).

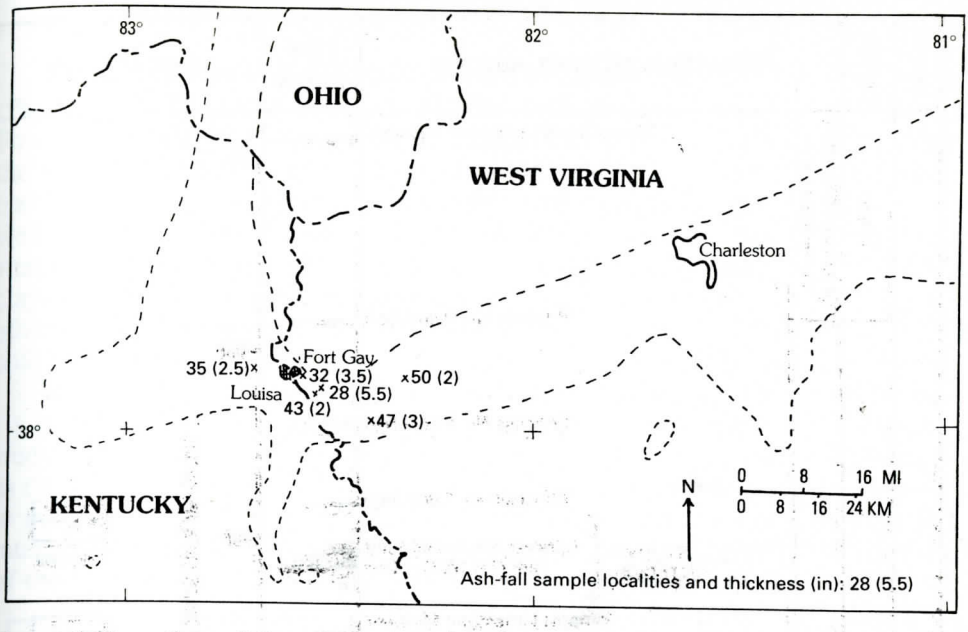


**Figure 1. Location of the study area showing sample localities and thicknesses of the flint clay marker bed just below the Princess No. 6 coal zone. Numbers 28, 32, 35, 43, 47, and 50 are LOT sample numbers. Dashed lines enclose outcrop area of upper part of Middle Pennsylvannian.**

## METHOD OF STUDY

A 5- to 10-gm sample from each of six localities (Figure 1) was ground to less than 200-mesh for X-ray diffraction analysis. Semiquantitative determinations of major minerals were made by using a computer program developed and described by Hosterman and Dulong (in press).

Coarse silt-sized grains and sand were concentrated by dispersing a second sample from each locality in water and decanting the clay and fine silt. Those samples that contained major amounts of illite broke down into mud spontaneously or with little agitation. Other samples required vigorous methods, such as mechanical crushing and ultrasonic vibration. Some samples proved resistant to breakdown by mechanical means and were partially digested in dilute HF, which preferentially dissolves the fine-grained groundmass. All the samples contained up to a few percent of fine sand- to silt-size grains.

Residues were dried and examined under a binocular microscope. Depending on the minerals present and their volume, the residues were sieved to various sizes (greater than 20, 20-60, 60-100, 100-140, 140-200, and less than 200 mesh), separated in bromoform by specific gravity [S.G. greater than quartz (2.65), S.G. ≈ quartz, S.G. ≈ K-feldspar (2.56), S.G. less than feldspar], or both. Some size fractions were panned under water in a petri dish to concentrate minerals by specific gravity. Individual mineral grains recovered in the concentrates were tentatively identified by their morphology and chemical composition as revealed by an SEM equipped with a KEVEX analyzer.

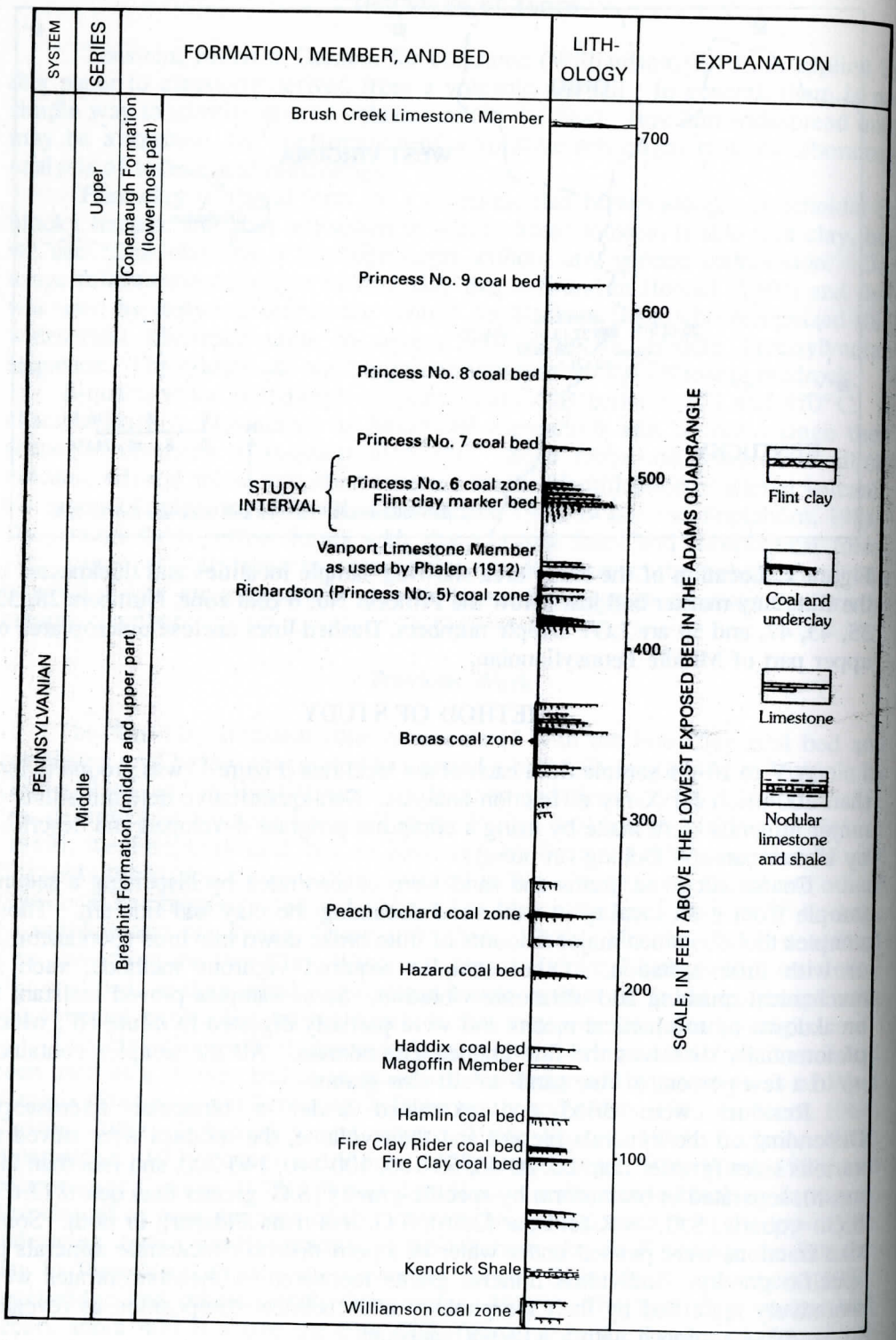


Figure 2. Key mapping units near Louisa, Ky. Modified from (Ward, 1978).

## GENERAL GEOLOGY AND SAMPLE LOCALITIES

The study area is located near Louisa, Kentucky and Fort Gay, West Virginia (Figure 1). This area contains Middle Pennsylvanian strata of the Breathitt Formation (upper part) or Charleston Sandstone and Upper Pennsylvanian strata of the Conemaugh Formation. The Middle Pennsylvanian strata, which consist of nonmarine sandstone, siltstone, shale, claystone, coal, underclay, and flint clay, as well as marine limestone and shale, are generally gray. The Upper Pennsylvanian strata are partly reddish brown to dusky red and generally contain more shale and claystone than the Middle Pennsylvanian strata. Middle Pennsylvanian coal and other key beds exposed in the Louisa-Fort Gay area are shown in Figure 2. The coal in this area is of high volatile B bituminous rank (Hayes and Connor, 1982).

We directed our initial effort to the vicinity of Louisa, Ky., where we measured six sections, (Figure 3) but recognized that this tonstein extends well beyond our study area (Figure 1). We have traced the tonstein bed from Yatesville Dam, Ky., as far east as Kiahsville, W. Va., which is a distance of about 20 mi. We have also in a recent study (Lyons and others, 1990) found more than one tonstein in the interval from the Vanport Limestone Member as used by Phalen (1912) to the top of the Princess No. 6 coal zone. We therefore consider correlations tentative.

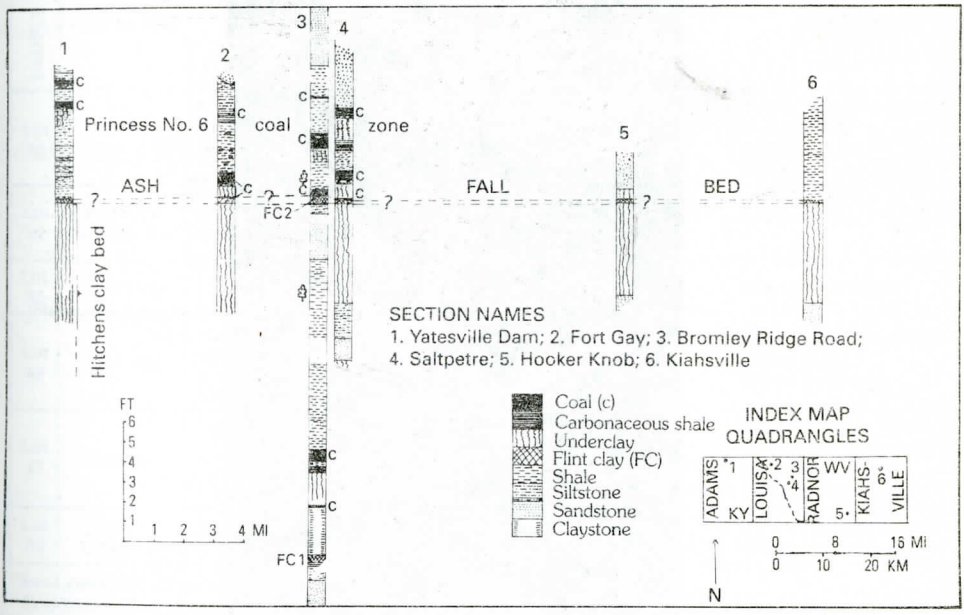


**Figure 3. Stratigraphic sections across the ash-fall bed just below the Princess No. 6 coal zone. Correlations between the Yatesville Dam section and the Fort Gay section and among the Saltpetre, Hookers Knob, and Kiahsville sections are tentative. Leaf symbol indicates abundant plant megafossils.**

### Measured Sections

The six sections including the tonstein bed of the Princess No. 6 coal zone were measured in the Adams, Ky., Louisa, Ky. and W. Va., Radnor, W. Va., and Kiahsville, W. Va. 7-1/2-minute quadrangles (Figure 3). Note that in five of the six sections, a tonstein bed is at or near the top of a thick, widely, but sporadically,

distributed underclay. The thick underclay is a general marker bed.

At each of the six localities, 1- to 2-lb channel samples of all the thin claystones, including underclay and shale beds, were taken. The claystones that proved to be tonsteins in these six sections vary from brownish gray to dark brownish gray (Table 1) and commonly have sharp contacts with the beds above and below (Figure 4). We also examined a claystone near the base of the Bromley Ridge Road section (FC1, Figure 3) and found no β-quartz pseudomorphs or other evidence of volcanic origin. At sections 4 and 5 (Figure 3), the tonstein occurs as nodules or discontinuous bands in the underclay. The thin claystone lies near the top of a thick underclay in five of the six sections, but in section 3 (Figure 3), it is between a coal bed and a carbonaceous shale bed (Figure 4), an indication of facies variation.

Lithologic differences between the tonstein beds and surrounding rocks are subtle in places, but the former generally has a distinctive appearance in the field. It is more resistant than the surrounding clay or claystone and weathers out as a


**Figure 4. Part of the section showing outcrop of the upper flint clay in the Bromley Ridge Road section (fig. 3, section 3).**

small ledge, has a blocky appearance, and commonly is a darker shade of gray than surrounding claystone, siltstone, or underclay. Where best developed, the tonstein is resistant to weathering and forms pebble- to cobble-sized angular fragments on the soil surface.

## LITHOLOGY AND MINERALOGY OF THE PRINCESS NO. 6 TONSTEIN BED

### Lithology

The gross physical appearance and properties of hand specimens of the six tonstein samples are shown in Table 1. Sample LOT-28 is from Bromley Ridge Road; LOT-32, from Fort Gay; LOT-35, from Yatesville Dam; LOT-43, from Saltpetre; LOT-47, from Hookers Knob; and LOT-50, from Kiahsville (Figure 3). Sample LOT-50 was taken at the approximate position of the other samples but the correlation of the tonstein bed at this location is uncertain (Figure 3).

**Table 1. Physical features of hand specimens of the six sampled claystones of volcanic origin (tonsteins) in this study.**

| SAMPLE NO. | LITHOLOGY | COLOR | FOSSILS | CHARACTERISTICS ON WETTING | REMARKS |
|---|---|---|---|---|---|
| Lot 28 | Semiflint clay | Brownish gray 5YR5/1[+] | Stigmarian rootlets medullosan seed fern rodlets* | Exfoliates easily | Blocky to subconchoidal fracture, siderite crystallites on fractures |
| Lot 32 | Semiflint clay | Dark brownish gray 5YR3/1 | Stigmarian rootlets, medullosan seed fern rodlets | Exfoliates rapidly, softens | Blocky fracture |
| Lot 35 | Flint clay | Dark brownish gray 5YR3/1 | Medullosan seed fern rodlets | Exfoliates | Slightly translucent |
| Lot 43 | Flint clay | Light gray N7 light to dark brownish gray 5YR7-3/1 | Stigmarian rootlets | Exfoliates | Mottled Mn + Fe oxides on fractures blocky fracture |
| Lot 47 | Flint clay | Light to medium brownish gray 5YR6-5/1 | Medullosan seed fern rodlets | Very slight exfoliation | Mn + Fe oxides on conchoidal fractures medium gray N7 lenticular inclusions |
| Lot 50 | Semiflint clay | Brownish gray 5YR4/1 | None | Exfoliates and softens | Brown ooids (siderite?) in dark gray matrix |

*See Lyons and others (1982).
[+]Goddard and others (1948).

### Mineralogy of the Claystones

Figure 5 shows X-ray diffraction patterns for the six samples, and the bulk mineralogy calculated from these is shown in Table 2. Sample LOT-47 is composed predominantly of well-crystallized kaolinite as indicated by the relatively strong prism reflections between 18-22 and 34-40 degrees 2θ. This sample breaks along a distinct conchoidal fracture (Table 1) and was the hardest and most resistant to dispersion in water. Samples LOT-28, LOT-32, and LOT-50 are composed of abundant quartz and significant amounts of illite (Table 2); in

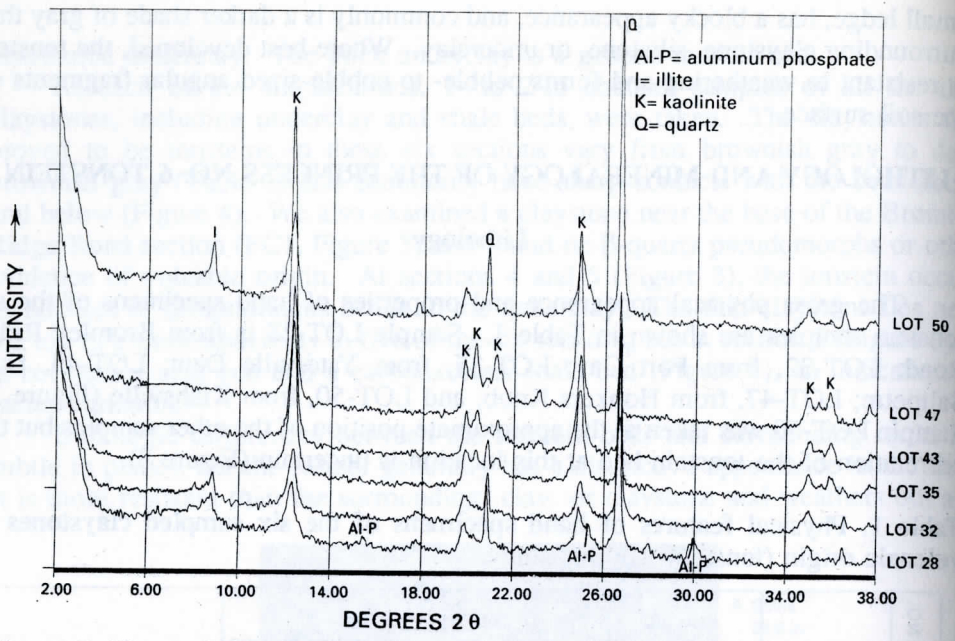


**Figure 5. X-ray diffraction patterns for six tonstein samples from just below the Princess No. 6 coal zone.**

**Table 2. Bulk mineralogy of the tonstein samples based on X-ray diffraction analysis [Numbers are weight percentages calculated from peak statistics according to a standardized program of the U.S. Geological Survey, Reston (Hosterman and Dulong, in press) Trace indicates <5 percent.**

| SAMPLE NO. | QUARTZ | KAOLINITE | ILLITE | FELDSPAR | PYRITE |
|---|---|---|---|---|---|
| Lot 28 | 50 | 35 | 15 | Trace | |
| Lot 32 | 40 | 40 | 20 | | Trace |
| Lot 35 | 25 | 75 | | | Trace |
| Lot 43 | 10 | 90 | | | Trace |
| Lot 47 | 10 | 90 | | | |
| Lot 50 | 50 | 40 | 10 | | |

sample LOT-50, these may be related, at least in part, to detrital influence. Sample LOT-28 shows definite peaks at about 15.7 and 30 degrees 2θ, as well as a shoulder on the high-angle side of the 25-degree 2θ kaolinite peak. These peaks suggest the presence of an alumino-phosphate mineral, probably crandallite or goyazite (see Triplehorn and Bohor, 1983). The marked differences in mineralogical composition of the six tonstein samples (Table 2) suggest two or more tonstein beds that are stratigraphically close together.

Nine samples of underclay or other claystone over and under the thin clay layer described above also were examined. All contained substantial amounts of illite and/or chlorite, as well as kaolinite. In these samples, sand-sized quartz grains lacked β-quartz forms and water-clear, sharply angular grains with flake and blade shapes. Quartz grains were present in a variety of shapes, but most were

equant and finer than the coarsest sizes present in the layer described above. Panning revealed a variety of heavy minerals (not identified), each present in only trace quantities. Zircon grains were subhedral to rounded and much less abundant than in the tonstein samples.

**Quartz:** Quartz is by far the most abundant primary mineral in the Princess No. 6 tonstein bed. It is clear and free from fractures and impurities except for uncommon glass and mineral inclusions (Figure 6). There is a variety of shapes, but almost all, including the euhedral forms, are very angular.

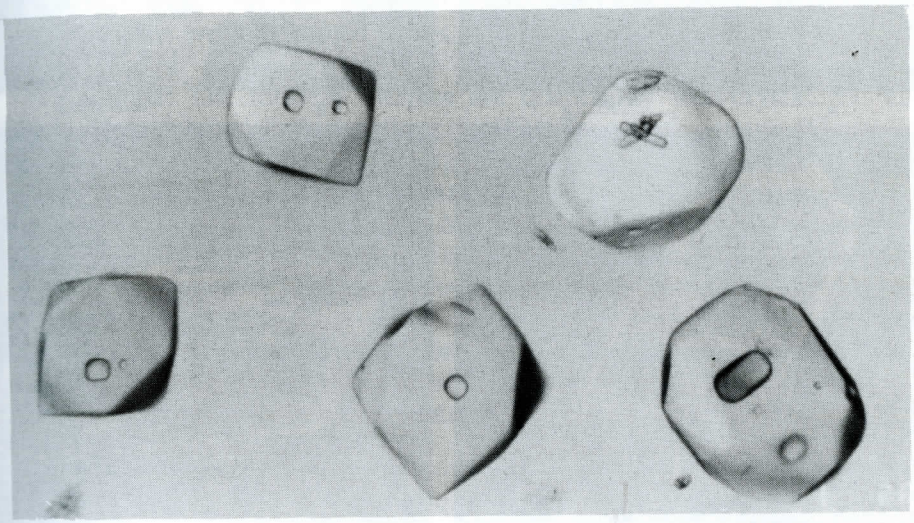

**Figure 6. α-Quartz pseudomorphic after β-quartz with glass (round) and crystal inclusions from sample LOT 47. Average grain size ≈ 190 μm, slightly oblique illumination, cross-polarized light rotated 45°. Note quartz with crystal inclusions has rounded corners, probably due to resorption.**

The sharp edges and well-developed conchoidal fracture of most of the clear broken quartz grains and the presence of dipyramid faces on some of them indicate that these are splinters or fragments from larger euhedral grains. HF treatment of claystone fragments revealed these splintery quartz shapes (Figure 7B) etched in positive relief in place, thus proving that they are original and not produced by grinding the samples in a mortar.

A small number of quartz grains display the bipyramidal crystal form of high-temperature β-quartz (Figure 7A). Some grains contain subspherical glass blebs and unidentified crystals (Figure 6). β-quartz forms are the best indicators of volcanic origin (Triplehorn, 1976; Blatt and others, 1980) in the Princess No. 6 flint clay. They are present in all six flint clay samples but are not present in nine other claystone samples taken above and below the Princess No. 6 marker bed.

The largest quartz grains in all six samples are between 150 and 250 μm. Most of the quartz fragments are less than 150 μm. Etching flint clay fragments by using HF brings the quartz into positive relief (Figure 7B) and illustrates the strongly bimodal grain size distribution (i.e., scattered sand-sized grains "floating" in clay). This is interpreted to be a result of alteration of volcanic ash, which

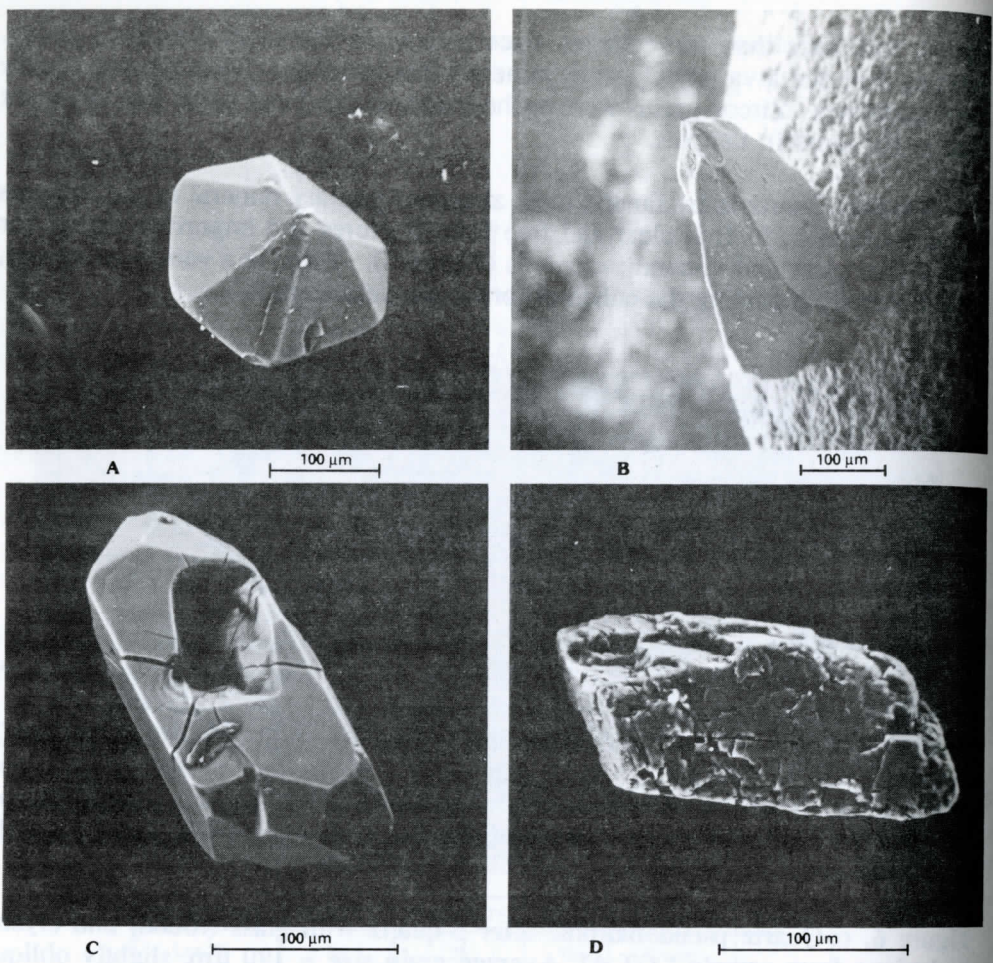


**Figure 7. Scanning Electron Microscope micrographs of selected minerals in the tonstein samples from just below the Princess No. 6 coal zone. A, Euhedral crystal of α-quartz pseudomorphic after β-quartz (high temperature polymorph of quartz). B, Shard-like quartz in groundmass of clay revealed by HF etching. C, Euhedral zircon with radial fractures around a crystal void, D, Single grain of K-feldspar. Scale A, B, C = 100 µm; D=10 µm.**

leaves resistant, broken microphenocrysts scattered in a clay matrix (formerly glass).

Authigenic (?) quartz is the second most abundant secondary mineral in the rock. It occurs as a microcrystalline phase intimately mixed with kaolinite, especially in specimens in which the kaolinite is poorly crystallized (Figure 5; Table 2).

**K-feldspar:** Figure 7C shows a HF-treated cleavage fragment grain with a Si-Al-K chemical signature, which is indicative of K-feldspar (Welton, 1984, p. 27) as determined with the SEM-KEVEX system.

**Zircon:** In all six tonstein samples, zircon occurs as pale-yellow to yellowish-brown, sharply euhedral crystals, most of which are about twice as long as they are

wide. Some grains contain mineral and silicate-melt inclusions. Figure 7C shows an unusual zircon crystal found in these samples. In sample LOT-50, very rare rounded zircons are found; these are probably due to resorption in the magma.

**Anatase(?):** Brownish, porous, Ti-rich grains occur in trace amounts in samples LOT-28, LOT-32, and LOT-47, and some display a hexagonal or pseudohexagonal platy shape. Similar grains are common in the Fire Clay volcanic ash parting and have been identified as anatase (Bohor and Triplehorn, 1981 or brookite (Lyons and others, in press) by X-ray diffraction techniques. Furthermore, Bohor and Triplehorn (1981) found that some grains in the Fire Clay include a black, metallic, weakly magnetic core of Fe and Ti composition which is probably ilmenite. Such hexagonal platy grains are common in volcanic ashes and tonsteins in the western United States.

**Kaolinite:** The tonstein samples are dominantly well-crystallized kaolinite (Figure 5), which is mainly in microcrystalline form in the matrix (Figure 7B). A minor amount occurs as relatively large single crystals, which occur as vermicules (elongate stacks of mica-like kaolinite platelets). In the disaggregated samples these vermicules are often broken. Most of the larger observed kaolinite grains are between 100 and 200 μm. The vermicules are obviously authigenic, and their fragile nature argues against any transport after their formation.

**Pyrite:** Framboidal pyrite is present in most samples. Pyrite occurs as framboids, layered forms, and octahedra intimately associated with coal fragments and clay matrix. It probably formed after deposition of the ash and before lithification.

## DISCUSSION

The presence of euhedral β-quartz forms, glass inclusions in quartz, euhedral zircons, bimodal grain size of the minerals, restricted suite of nonclay minerals, and the thin, widespread character of this Princess No.6 tonstein bed are consistent with an air-fall of rhyolitic to dacitic volcanic ash. A water-laid, detrital origin would have resulted in the presence of abundant abraded grains, the absence of euhedral β-quartz crystals, and the inclusion of a variety of additional minerals, such as tourmaline and garnet, which are generally present in the waterlaid beds of the Breathitt Formation (Huddle and Englund, 1966).

Most tonsteins are distal products of the more explosive types of volcanos that are characterized by a silica-rich magma of probable rhyolitic composition (see Belkin and Rice, 1989). The ash probably consisted mostly of glass and a small amount of microphenocrysts. This glass, along with biotite and amphibole, readily alters to produce a clay matrix (Severson and Shacklette, 1988). The microphenocrysts of quartz were probably shattered by explosive or thermal shock and fell as angular particles.

Before this study, only the Fire Clay flint-clay parting was proven to be volcanic in origin (Seiders, 1965) in Pennsylvanian rocks of the Appalachian basin. Its volcanic origin has been accepted only recently after some controversy (Tankard and Horne, 1979; Stevens, 1979; Bohor and Triplehorn, 1981; Chesnut, 1985; Eble, 1988).

In contrast, tonsteins (in the nongeneric sense of kaolinitic claystones) have

been known for a long time from coal-bearing strata of Carboniferous age in Europe. They are conspicuous and fairly common there; for example, Burger (1985b) listed 46 tonsteins in the Lower Rhine-Westphalia region of the Federal Republic of Germany. They have been used for coal-bed correlation for the better part of a century (Zaritsky, 1971; Burger, 1985c,d), even though general acceptance of their volcanic origin has come only in the last two decades (Spears and Duff, 1984).

Further work is necessary to determine the regional extent and the lateral changes in thickness and composition of the tonstein or tonsteins just below the Princess No. 6 coal zone. Studies of changes in thickness of the tonstein bed and in the grain size of the coarse fraction, and detailed mineralogical and geochemical analyses may permit interpretation of the direction of the source volcano.

## CONCLUSIONS

Volcanic ash of probable rhyolitic to dacitic composition fell just before the beginning of peat accumulation in the Princess No. 6 coal swamps (Middle Pennsylvanian) in the central Appalachian basin and subsequently altered to a tonstein. The volcanic origin of the tonsteins is established by the limited and distinctive mineralogy of the residue of the claystone after HF digestion. Other volcanic beds (tonsteins) are present in the Carboniferous of the central Appalachian basin (Lyons and others, in press), but they are outside of the scope of this paper.

## ACKNOWLEDGEMENTS

J.R. Evans (U.S. Geological Survey) took the SEM micrographs, and H.E. Belkin (U.S. Geological Survey) gave an interpretation of the probable origin of the inclusions in the quartz pseudomorphs. J.W. Hosterman (U.S. Geological Survey) supplied the X-ray diffraction data and provided critical comments on early drafts of this paper. C.W. Connor (U.S. Geological Survey) supplied samples and preliminary sections from localities in the Louisa quadrangle. W.J. Betterton (U.S. Geological Survey) took the photograph shown in Figure 6. We are grateful for their help and that of Bruce Bohor and Don Chesnut who reviewed the manuscript.

## REFERENCES CITED

Blatt, H., Middleton, G., and Murray, R., 1980, Origin of Sedimentary Rocks, 2nd edition: Prentice-Hall, Inc., Englewood Cliffs, New Jersey, 782 p.

Belkin, H.E. and Rice, C.L., 1989, A rhyolite ash origin for the Hazard No. 4 flint clay (Appalachian basin): evidence from silicate melt inclusions: Geological Society of America 1989 Annual Meeting Abstracts with Programs, v. 21(6) p. A360.

Bohor, B., and Triplehorn, D.M., 1981, Volcanic origin of the flint clay parting in the Hazard No. 4 (Fire Clay) coal bed of the Breathitt Formation in eastern Kentucky, *in* Cobb, J.C., Chesnut, D.R., Hester, N.C., and Hower, J.C. (eds.) Coal and Coal-bearing Rocks In Eastern Kentucky, Guidebook, Annual Geol. Soc. Am. Coal Div. Field Trip, Nov 5-8, 1981, Kentucky Geological Survey, Lexington, Ky., 169 p.

Burger, K., 1985a, Petrography and chemistry of tonsteins of the coal basins of western Europe and North America: *in* Economic Geology; Coal, Oil and Gas (Cross, A.T., editor) 9th International Congress on the Stratigraphy and Geology of the Carboniferous (Champaign-Urbana, Illinois, 17-26 May, 1979), Compte Rendu, v. 4, p. 449-466.

Burger, K., 1985b, Die Kohlentonsteine Im Niederrheinisch-Westfälischen Steinkohlenrevier. Erkenntnisstand 1983: Proceedings, 10th International Congress on the Stratigraphy and Geology of the Carboniferous (Madrid, 12-17 September, 1983), Compte Rendu, v. 4, p. 211-234.

Burger, K., 1985c, Kohlentonsteine In Kohlenrevieren Der Erde Erkenntnistand 1983: Proceedings, 10th International Congress on the Stratigraphy and Geology of the Carboniferous (Madrid, 12-17 September, 1983), Compte Rendu v. 1, p 155-173.

Burger, K., 1985d, Kohlentonsteine Im Oberkarbon NW-Europas Ein Beitrag Zur Geochronologie: Proceedings, 10th International Congress on the Stratigraphy and Geology of the Carboniferous (Madrid, 12-17 September, 1983) Compte Rendu, v. 3, p. 433-447.

Burger, K. and Damburger, H.H., 1985, Tonsteins in the coal fields of western Europe and North America: *in* Economic Geology; Coal, Oil and Gas (Cross, A. T., editor), 9th International Congress on the Stratigraphy and Geology of the Carboniferous (Champaign-Urbana, Illinois, 17-26 May, 1979), Compte Rendu, v. 4, p. 433-448.

Carlson, J.E., 1965, Geology of the Rush quadrangle, Kentucky: U.S. Geol. Surv. Geologic Quadrangle Map GQ-408, scale 1:24,000.

Carlson, J.E., 1971, Geologic map of the Webbville quadrangle: U.S. Geol. Surv. Geologic Quadrangle Map GQ-927, scale 1:24,000.

Chesnut, D.R., 1985, Source of the volcanic ash deposit (flint clay) in the Fire Clay coal of the Appalachian basin: Dixieme Congres International de Stratigraphie et de Geologie du Carbonifere (Madrid, 12-17 September, 1983), Compte Rendu, v. 1, p. 145-154.

Connor, C.W. and Flores, R.M., 1978, Geologic map of the Louisa quadrangle, Kentucky-West Virginia: U.S. Geol. Surv. Geologic Quadrangle Map GQ-1462, scale 1:24,000.

Dobrovolny, E., Sharps, J.A., and Ferm, J.C. 1963, Geology of the Ashland quadrangle, Kentucky-Ohio and the Catlettsburg quadrangle in Kentucky: U.S. Geol. Surv. Geologic Quadrangle Map GQ-196, scale 1:24,000.

Dobrovolny, E., Ferm, J.C., and Eroskay, S.O., 1966, Geologic map of parts of the Greenup and Ironton quadrangles, Greenup and Boyd Counties, Kentucky: U.S. Geol. Surv. Geologic Quadrangle Map GQ-532, scale 1:24,000.

Eble, C.F., 1988, Palynology and paleoecology of a Middle Pennsylvanian coal bed From the central Appalachian Basin: Ph.D. thesis (unpub.), West Virginia University, Morgantown, 495 p.

Englund, K.J., Arndt, H.H., and Henry, T.W., 1979, Proposed Pennsylvanian System stratotype, Virginia and West Virginia: American Geological Institute Selected Guidebook Series no. 1, 138 p.

Giles, A.W., 1934, Partings in coal beds: American Institute of Mining and Metellurgical Engineers, Coal Division, v. 108, p.31-40.

Goddard, E.N., Trask, P.D., De Ford, R.K., Rove, O.N., Singewald, J.T., Jr., and Overbeck, R.M., 1948, reprinted 1951, 1963, 1970, 1975, 1979, Rock-color

chart: Geological Society of America, 10 p.
Hayes, P.T., and Connor, C.W., 1982, Coal geology of Adams, Blaine, Richardson, and Sitka quadrangles, Kentucky, and Louisa quadrangle, Kentucky-West Virginia: U.S. Geological Survey Bulletin 1526, 68 p.
Hennen, R.V., and Teets, D.D., Jr., 1919, Fayette County: West Virginia Geological Survey [County Report], 1002 p.
Hess, J.C., Lippolt, H.J., and Burger, K., 1988, New time-scale calibration points in the Upper Carboniferous from Kentucky, Donetz basin, Poland, and West Germany (abst.): 6th Workshop on Fission Track Dating, Sept. 5 - 9, 1988: Besancon, France.
Hoehne, K., 1957, Tonsteine in Kohlenflözen der Oststaaten von Nordamerika und Ostaustralien: Chemie der Erde, v. 19, no. 20, p. 111-129.
Hosterman, J.W. and Dulong, F.T., (in press), A computerized system for semiquantitative mineral analysis by x-ray diffraction: Clays and Clay Minerals, Special Report.
Howell, J.V., Coordinating Chairman, 1960, Glossary of Geology and related sciences, 2nd edition: American Geological Institute, 325 p. + 72 p. in supplement.
Huddle, J.W. and Englund, K.J., 1966, Geology and Coal Reserves of the Kermit and Varney area: U.S. Geol. Surv. Professional Paper 507, 83 p.
Keiser, A.F., Grady, W.C., Blake, B.M., Jr., 1987, Flint clay parting in the Hernshaw coal of West Virginia: 11th International Congress of Carboniferous Stratigraphy and Geology, Abstracts of Papers,II, p. 447.
Keiser, A.F., Blake, B.M., Jr., and Grady, W.C., 1989, Volcanic ash in West Virginia: Mountain State Geology, West Virginia Geological and Economic Survey, p. 11-17.
Lippolt, H.J. and Hess, J.C., 1985, $^{40}Ar/^{39}Ar$ dating of sanidines from Upper Carboniferous tonsteins: Dixieme Congres International de Stratigraphie et de Geologie du Carbonifere, Compte Rendu, v. 4, p. 175-181.
Lyons, P.C., Finkleman, R.B., Thompson, C.L., Brown, F.W., and Hatcher, P.G., 1982, Properties, origin, and nomenclature of rodlets of the inertinite maceral group in coals of the central Appalachian basin, U.S.A.: International Journal of Coal Geology, v. 1, p. 313-346.
Lyons, P.C., Outerbridge, W.F., Evans, H.T., Jr., and Triplehorn, D.M., in press, Carboniferous (Westphalian) volcanic ash deposits, Appalachian basin (U.S.A.): submitted to the XIII International Sedimentological Congress, (Nottingham, England, Aug. 26-31, 1990).
McFarlan, A.C., 1943, Geology of Kentucky: Lexington, Kentucky, University of Kentucky, 531 p.
Nelson, B.W., 1959, New bentonite zone from the Pennsylvanian of southwestern Virginia: Bull. Geol. Soc. Am., v. 70, no. 10, p. 1651.
Outerbridge, W.F., 1977, Geologic map of the Mazie quadrangle, eastern Kentucky: U.S. Geol. Surv. Geologic Quadrangle Map GQ-1388, scale 1:24,000.
Outerbridge, W.F., 1978, Geologic map of the Dingus quadrangle, eastern Kentucky: U.S. Geol. Surv. Geologic Quadrangle Map GQ-1463, scale 1:24,000.
Outerbridge, W.F., Lyons, P.C., Merrill, G.K., and Kosanke, R.M., 1988, Correlation of Pennsylvanian strata in the tri-state area of Ohio, Kentucky, and West Virginia: Geol. Soc. Am., Abstracts with Programs, North Central

Section Meeting (Akron, Ohio), v. 20, no. 5, March, 1988, p. 383.
Outerbridge, W.F., 1989, Correlations of coal and other key beds in eastern Kentucky, western West Virginia, and southern Ohio: U.S. Geol. Surv. Misc. Field Studies Map MF-2110.
Phalen, W.C., 1912, Description of the Kenova quadrangle [Kentucky-West Virginia-Ohio]: U.S. Geol. Survey Geol. Atlas, Folio 184, 16 p.
Pillmore, C.L. and Connor, C.W., 1978, Geologic map of the Blaine quadrangle, Lawrence County, Kentucky: U.S. Geol. Survey Geologic Quadrangle Map GQ-1507, scale 1:24,000.
Rogers, G.S., 1914, The occurrence and genesis of a persistent parting in a coal bed of the Lance Formation: American Journal of Science, v. 87, no. 220, p. 299-304.
Ryer, T.A., Phillips, R.E., Bohor, B.F., and Pollastro, R.M., 1980, Use of altered volcanic ash falls in stratigraphic studies of coal-bearing sequences: an example from the Upper Cretaceous Ferron Sandstone Member of the Mancos Shale in central Utah: Geological Society of America Bulletin, v. 91, p. 579-586.
Seiders, V.M., 1965, Volcanic origin of flint clay in the Fire Clay coal bed, Breathitt Formation, eastern Kentucky: U.S. Geol. Surv. Prof. Paper 525-D, p. D52-D54.
Severson, R.T. and Shacklette, H.T., 1988, Essential elements and soil amendments for plants: sources and use for agriculture: U.S. Geological Survey Circular 1017, 48 p.
Sharps, J.A., 1967, Geologic map of the Fallsburg quadrangle, Kentucky-West Virginia and the Prichard quadrangle in Kentucky: U.S. Geol. Surv. Geologic Quadrangle Map GQ-584, scale 1:24,000.
Sheppard, R.A. and Ferm, J.C., 1962, Geology of the Argillite quadrangle, Kentucky: U.S. Geol. Surv. Geologic Quadrangle Map GQ-175, scale 1:24,000.
Spears, D.A. and Duff, P.McL.D., 1984, Kaolinite and mixed-layer illite-smectite in Lower Cretaceous bentonites from the Peace River coal field, British Columbia: Canadian Journal of Earth Science v. 21, p. 465-476.
Spencer, F.D., 1964, Geology of the Boltsfork quadrangle and part of the Burnaugh quadrangle, Kentucky: U.S. Geol. Surv. Geologic Quadrangle Map GQ-316, scale 1:24,000.
Stevens, S.S., 1979, Petrogenesis of a tonstein in the Appalachian bituminous basin: M.S. thesis (unpub.), Eastern Kentucky University, Richmond, 82 p.
Stout, Wilbur, Shaw, M.C., Bole, G.A., and Schaaf, Downs, 1931, The Lawrence clay of Lawrence County: Geol. Surv. Ohio, 4th Ser., Bull. 36, 134 p.
Tankard, A.J. and Horne, J.C., 1979, Paleoenvironmental interpretation of a flint clay facies in eastern Kentucky: *in* Carboniferous Depositional Environments in the Appalachian Region, Ferm, J.C. and Horne, J.C. (eds.) University of South Carolina Coal Group, p. 238-244.
Triplehorn, D.M., 1976, Volcanic ash partings in coals: characteristics and stratigraphic significance *in* Fritsche, A.E., Ter Best, H. Jr., and Wornardt, W.W., eds., The Neogene Symposium, Papers presented at the Pacific Section, American Association of Petroleum Geology-Society of Economic Paleontologists and Mineralogists Annual Meeting, San Francisco, California, 1976, p. 9-12.
Triplehorn, D.M., and Bohor, B.F., 1983, Goyazite in kaolinitic altered volcanic

ash beds of Cretaceous age near Denver, Colorado: Clays and Clay Minerals, v. 31, p. 299-304.
Ward, D.E., 1978, Geologic map of the Adams quadrangle, Lawrence County, Kentucky: U.S. Geol. Surv. Geologic Quadrangle Map GQ-1489, scale 1:24,000.
Welton, J.E., 1984, SEM Petrology Atlas: American Association of Petroleum Geologists, Methods in Exploration Series; no. 4., 237 p.
Williamson, I.A., 1970, Tonsteins, their nature, origin, and uses: Mining Magazine, v. 122 no. 2, p. 120-125 and v. 3 p. 203-310.
Zaritsky, P.V., 1971, Intercoal kaolinite layers (kaolin-kohlentonstein) of the Donetz basin and their correlative significance: Proceedings, 6th International Congress on the Stratigraphy and Geology of the Carboniferous, p. 1629-1637.

# AN ANOMALOUS MASS-FLOW DEPOSIT IN THE LEE FORMATION (PENNSYLVANIAN), EASTERN KENTUCKY COAL FIELD

STEPHEN F. GREB
DONALD R. CHESNUT, JR.
OSCAR B. DAVIDSON

*Kentucky Geological Survey*
*University of Kentucky*
*Lexington, KY 40506*

RENE RODRIGUEZ

*Geocoh Exploration*
*Lexington, KY 40502*

## ABSTRACT

Magnetic and gravity anomalies along the Rockcastle River in Laurel County, Kentucky, are interpreted to represent a fault. East of this fault, the Lee Formation contains a complex mosaic of matrix-supported, shale-clast conglomerates and fine-grained sandstones informally called the Poison Honey beds. This type of lithology has not been previously reported in the coal measures of the Appalachian Basin.

Matrix-supported conglomerates were deposited by mass flows. The complex mosaic of conglomerate and sandstone lithotypes resulted from multiple surges of mass flows in a small tributary drainage that drained an upthrown fault block. Fault control of the Poison Honey beds is suggested by (1) the rarity of mass flows in this part of the section and the location of the flows along a fault, (2) the abundant brittle shale clasts indicating short transport distances and the proximity of Breathitt Formation shales west of the fault, (3) a siderite-pebble source west of the fault, and (4) the reversal in sedimentation direction from southwest in the underlying sandstone to east and toward the direction of downthrow in the Poison Honey beds. Periodic flooding in a tributary may also have instigated flows.

## INTRODUCTION

A sequence of unique rocks in the coal measures of the Appalachian Basin is exposed along outcrops on Kentucky Highway 80 in the Billows Quadrangle, Laurel County, Kentucky (Figure 1). The unit is informally termed the "Poison Honey beds." The Poison Honey beds pose several sigificant problems to interpretations of local depositional history. The unit (1) is texturally different from other sandstones described in this part of the basin, (2) exhibits paleocurrents opposite those in surrounding units, and (3) may indicate Pennsylvanian fault movement.

### Geologic Setting

The Poison Honey beds are located on the western outcrop margin of Pennsylvanian rocks in the Eastern Kentucky Coal Field (Figure 1). Several hypotheses have been proposed for the margin of the Lee Formation in this area. Along Highway 80, 1.4 kilometers west of the Rockcastle River, shales and coals

mapped as the Lower Tongue of the Breathitt Formation (McDowell and others, 1981) are apparently juxtaposed against quartzose sandstones of the Lee Formation. The sandstones are 30 meters thick in outcrops 1.2 kilometers west of the river and are absent 1.5 kilometers west of the river (Greb and Chesnut, 1989). The juxtaposition of lithofacies has been interpreted as a possible fault (Greb and Chesnut, 1989), an abrupt facies transition along a delta front (Amig, 1988), and a fluvial channel/sand-belt margin similar to other Lee sandstones (Rice and Weir, 1984; Chesnut, 1988). The limit of the Rockcastle Sandstone Member of the Lee Formation as mapped by Hatch (1963) suggests a fluvial, sand-belt margin (Figure 1).

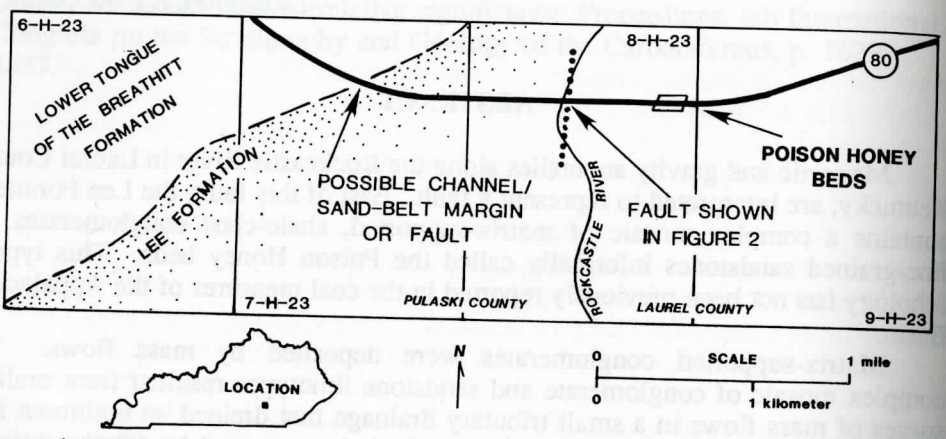


**Figure 1. Plan view map of study area showing outcrop locality, margin of the Rockcastle Sandstone Member of the Lee Formation, and a fault at the Rockcastle River (after Hatch, 1963, with presenty accepted nomenclature from McDowell and others, 1981).**

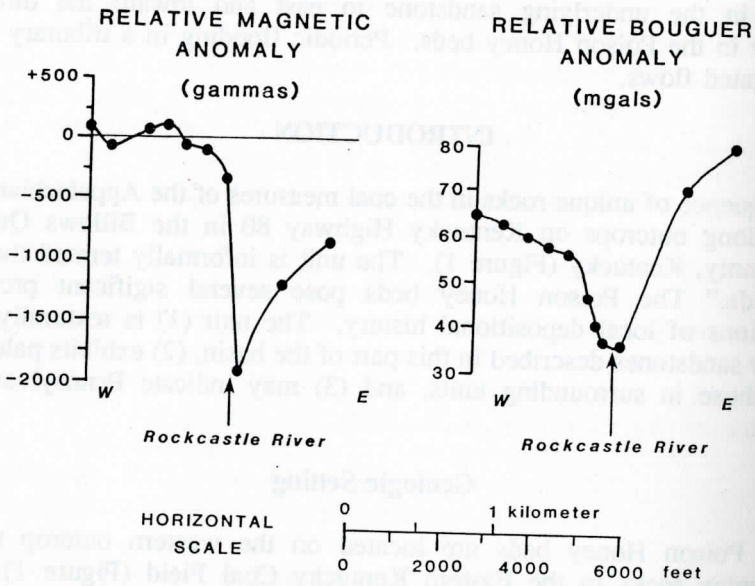


**Figure 2. Gravity and magnetic lines along Kentucky Route 80 intepreted to delineate a fault at the Rockcastle River.**

East of the Lee Formation margin, along the Rockcastle River, magnetic and gravity anomalies suggest the presence of a fault on the east side of the Rockcastle River valley (Figures 1-2). Because geophysical surveys were only made along Highway 80 in the vicinity of the Rockcastle River, the trend of this previously unknown fault is not known, although the straightness of the river in this area may suggest a north-south orientation (Figure 1). Offset along the fault is minimal (0 to 5 meters as determined from the stratigraphy on both sides of the river).

The Poison Honey beds outcrop on Highway 80 just east of the fault on the Rockcastle River (Figure 1). The beds are only exposed in the roadcuts on Highway 80, and do not continue beyond the limits of the hillside bounding the Rockcastle River and Pine Creek (Figure 1). Stratigraphically, they sharply overlie an informal member of the Lee Sandstone Formation called the Pine Creek sandstone (Greb and Chesnut, 1989) and are truncated by unnamed channel-fill deposits of the Lee Sandstone Formation (Figure 3).

## LITHOFACIES DESCRIPTION

The Poison Honey beds consist of a complex mosaic of matrix-supported, shale-clast conglomerates and fine-grained sandstones. Analysis of the vertical and lateral distribution of lithotypes indicates that the Poison Honey beds consist of a lower and upper conglomerate-dominated unit separated by zones of fine-grained sandstones (Figures 3-4).

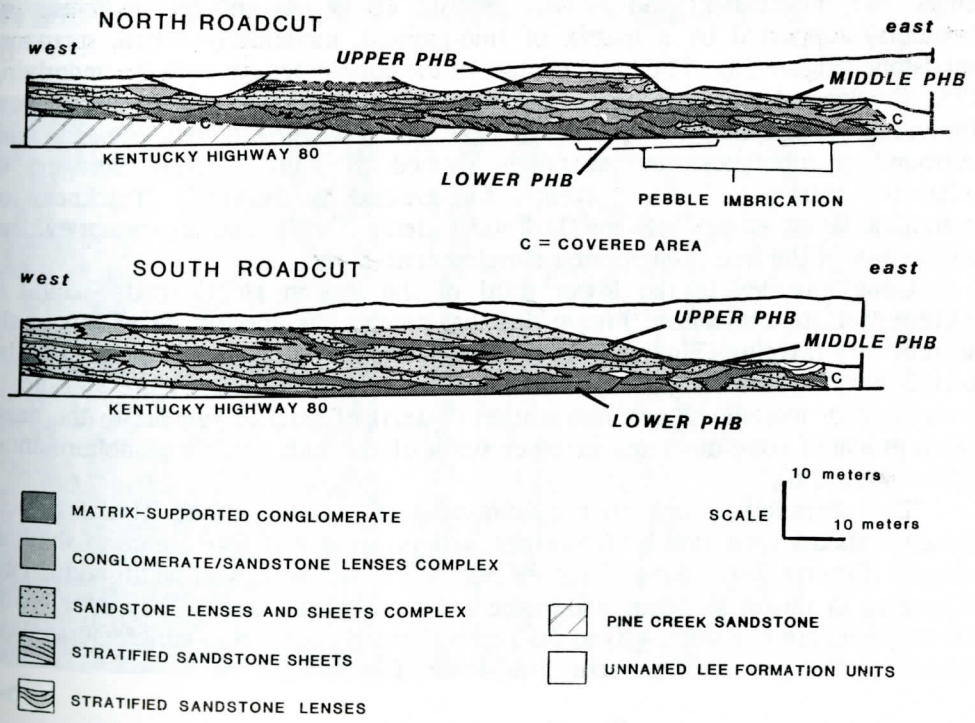


Figure 3. Roadcut sections along Kentucky Highway 80 illustrating complex mosaic of lithotypes in the Poison Honey beds.

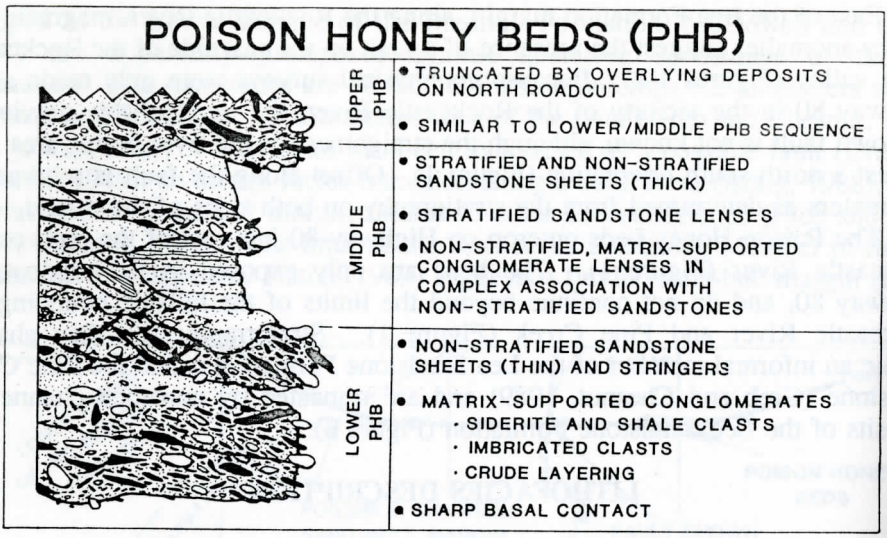


**Figure 4. Generalized geologic section.**

## Matrix-Supported Conglomerates

The lower and upper thirds of the Poison Honey beds are dominated by matrix-supported conglomerates. The conglomerates consist of detrital shale clasts (as chips and megaclasts) and detrital siderite clasts (as cobbles, pebbles, and boulders) supported by a matrix of fine-grained, moderately sorted, quartzose sandstone (Figure 5a). The basal contact of the conglomerates with the underlying Pine Creek sandstone is sharp. Pebble injection along this contact is common. Individual conglomerate layers may have sharp or gradational contacts with surrounding lithotypes, and are often capped by thin sheets or stringers of relatively clast-poor (<10 percent), fine-grained sandstones. Thickness of individual layers ranges between 0.04 and 1 meter. Grading trends are not evident within any of the matrix-supported conglomerate layers.

Conglomerates in the lower third of the Poison Honey beds exhibit a preferred clast imbrication (Figure 5b) that creates the appearance of low-angle accretionary layering (Figures 3-4). Pebble-fabric measurements (Figure 6) in the accretionary layered conglomerates (eastern end of Lower PHB, Figure 4) indicate a moderately well-developed imbrication (a-axis) of siderite pebbles to the east. Nonimbricated conglomerates in other parts of the unit exhibit a subhorizontal fabric (Figure 6).

The accretionary layered conglomerates of the lower third of the Poison Honey beds are truncated by lense-form scours, similar in appearance to shallow troughs (Figures 3-4). Several scours from 0.3 to 4.5 meters in width and 0.1 to 0.7 meter in thickness occur within the lower conglomerates. The minor scour fill may contain clast-rich (10 to 50 percent) matrix-supported conglomerates or relatively clast-poor (<10 percent) sandstones (Figure 5c).

## Fine-Grained Sandstones

The conglomerates of the Poison Honey beds may be truncated or grade into clast-poor (>10 percent), moderately sorted, fine-grained sandstone lithotypes that

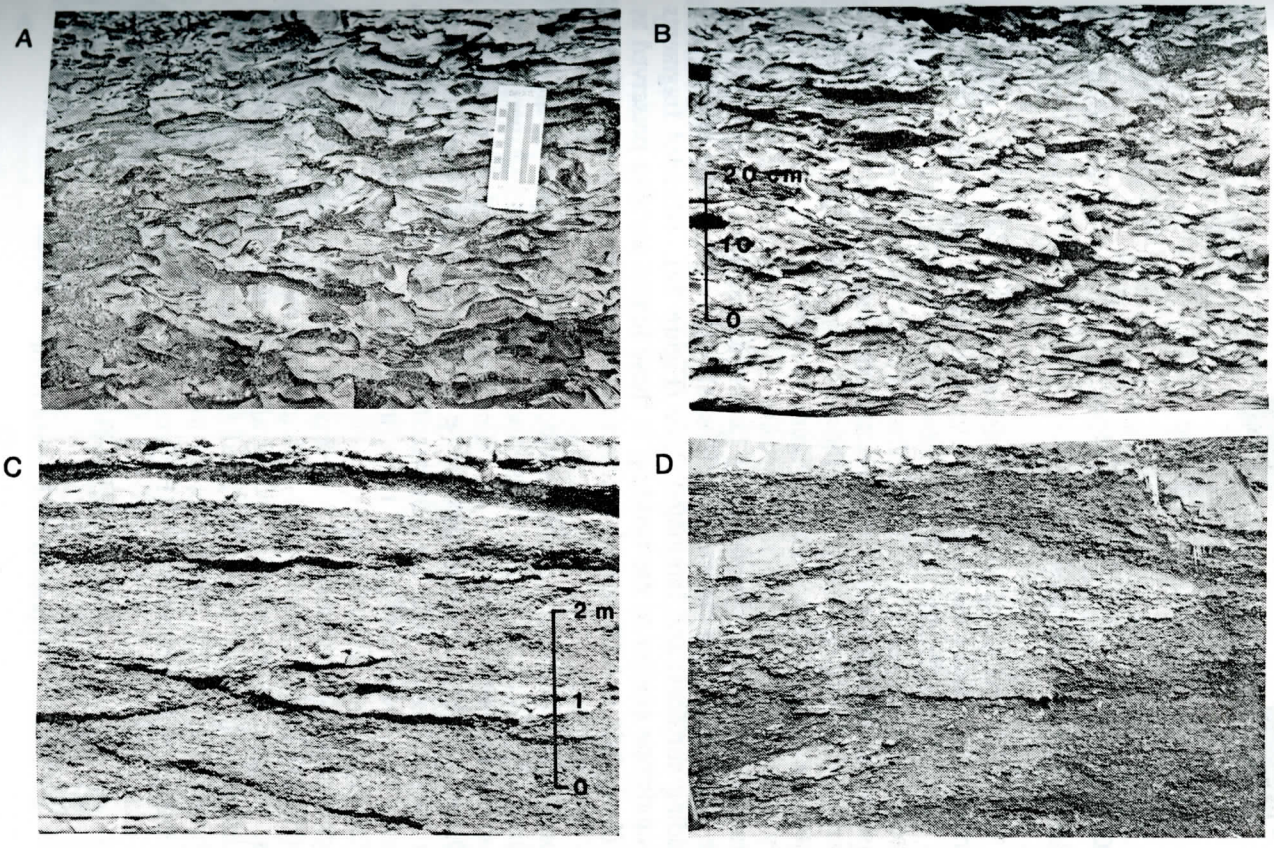


Figure 5. Photographs of conglomerates: (a) Matrix-supported shale and siderite clasts. (b) Imbricated clasts create accretionary layering. (c) Crosscutting troughs or lenses. (d) Complex interfingering of conglomerates and fine-grained sandstones (hammer for scale in bottom left corner).

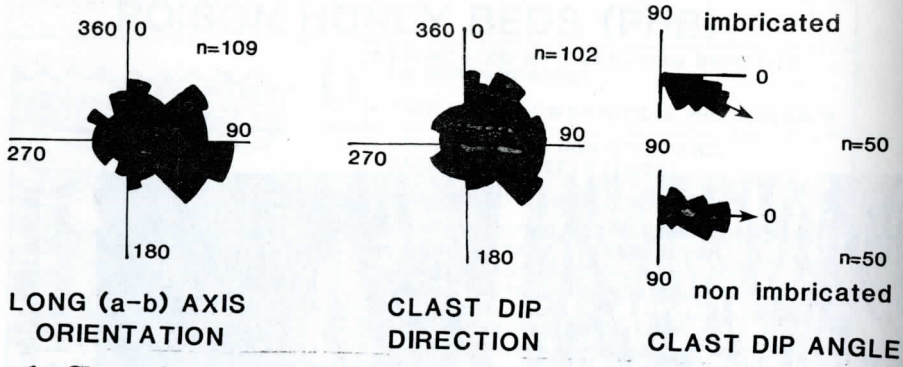


**Figure 6. Clast orientation in conglomerates.**

exhibit both lenticular and sheet-form geometries (Figures 3-4). The trough or lensoid layering exhibited in the conglomerates complexly interfingers with the fine-grained sandstones (Figure 5d). Sandstones also occur as distinct (conglomerate-free) lenses ranging in length from 1 to 6 meters. Sandstone lenses are highly discontinuous and cannot be correlated between outcrops (a distance of only 10 meters). Many appear to grade to the west into sheet-form sandstones.

Near the eastern end of the roadcut (Figure 3) a few of the sandstone lenses are distinctly stratified. These lenses consist of a sequence of flat-bedded sandstone grading upward into horizontally laminated sandstone (laminations in the sandstone are formed from chips of detrital shale rather than being distinct clay layers or bedding surfaces) and laminated shale (Figure 7a). Abraded fragments of stratified sandstone similar to the bedding in these lenses are also preserved as rip-up clasts (from 0.01 to 1.10 meters) in the conglomeratic portions of the Poison Honey beds (Figures 7b-d).

Sandstones with sheet-form geometries occur as thin stringers in the lower and upper third of the Poison Honey beds, and as thick persistent layers in the middle Poison Honey beds (Figures 3-4). Sandstone sheets range in thickness from 0.1 to 0.6 meter. Thin sheet sandstones (< 0.3 meter) in the lower and upper thirds of the Poison Honey beds are not stratified, and often separate layers of conglomerates. The lower contacts of these thin sheets are usually gradational with underlying lithotypes (Figures 7c-d).

The thicker sheet sandstones (> 0.3 meters) in the middle part of the Poison Honey beds (Figure 3) may exhibit small-scale planar crossbedding with eastward paleocurrents. These sheets exhibit both gradational and sharp contacts with surrounding lithotypes. Many exhibit soft-sediment deformation and minor offset along slip planes. The overall distribution of the thick sheet sandstones suggests an eastern stepping of successive sheets (Figure 3).

## INTERPRETATION

### Depositional Environment

Matrix-supported, conglomeratic sandstones are commonly inferred to represent mass-flow deposits (Harms and others, 1975; Middleton and Southard, 1978). The classification of mass-flow deposits is based on the inferred rheology (fluid versus plastic behavior) and the clast-support mechanisms of the flow

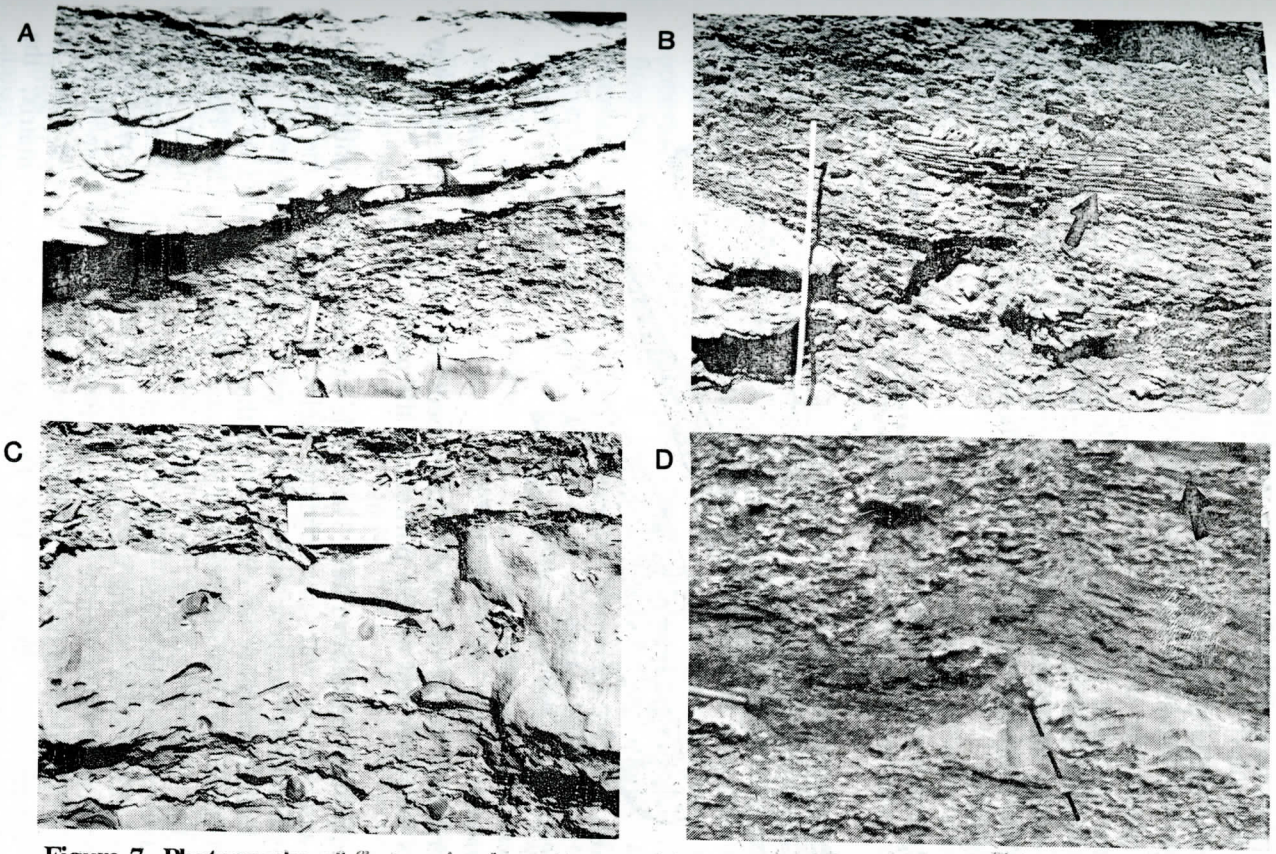


Figure 7. Photographs of fine-grained sandstones: (a) stratified sandstone lens with thinning upward bedding (hammer for scale). (b) Transported clast of statified sandstone (arrow) with bedding similar to the bedding at the top of Figure 6a. (c) Thin, sheet sandstone capping conglomerate layer. (d) Sheet sandstone capping conglomerate. Note minor faulting (dashed line), broken and transported stratified clast (arrow), and the differences in clast orientation above (nonimbricated conglomerate in upper Poison Honey beds) and below (imbricated conglomerates in lower Poison Honey beds) the sandstone sheet.

during transport (Lowe, 1982; Postma, 1986).

Most mass flows pass through a continuum of rheologic conditions and clast-support mechanisms that change as physical conditions change during transport (Middleton and Southard, 1978; Lowe, 1982; Lash, 1984). Thus, a flow might be initiated as a slump that becomes liquefied or remolded into a grain flow, liquefied sediment flow, or debris flow before it is deposited. The final form may mask the rheologic path taken by any one flow surge (Middleton and Southard, 1978; Lowe, 1982; Postma, 1986).

Of the many types of classified mass flows, the Poison Honey beds most closely resemble the subaerial mass-flow models of Nemec and Steele (1984). Composite conglomeratic units, with discontinuous and complexly interbedded sandy zones, are common in subaerial mass flows (Nemec and Steele, 1984; Schultz, 1984; Pierson and Costa, 1987). Composite units result from changes in flow rheology during individual surges, and from the stacking of multiple surges with different flow behavior. The Poison Honey beds are interpreted as composite mass flows (Figure 8).

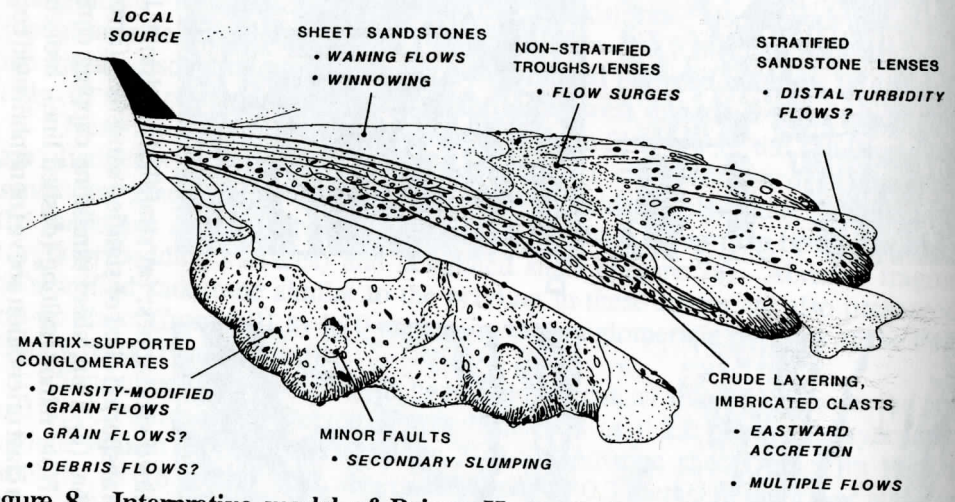


**Figure 8. Interpretive model of Poison Honey beds mass flows. The cut-away view represents the lower and middle portions of the north outcrop.**

**Matrix-Supported Conglomerates:** The crude layering, pebble imbrication, and complex associations with surrounding facies exhibited by the matrix-supported conglomerates suggest mass flows with high-concentration fluid conditions and limited mobility of clasts rather than plug flow with no mixing during transport (Enos, 1977; Middleton and Southard, 1978; Lowe, 1982; Postma, 1986). Also, the lack of grading, and imbrication of detrital clasts in the accretionary layered conglomerates suggest that the dominant clast-support mechanism was laminar shear during the final stages of flow (Fisher, 1971; Enos, 1977; Lewis and others, 1980; Nemec and Steel, 1984; Postma and Roep, 1985).

The Postma (1986) classification of mass flows describes several types of laminar, high-concentration flows. The fine-grained sandstone matrix, the orientation of clasts parallel to flow, the accretionary layering, and the pebble-injection structures exhibited in the conglomerates of the Poison Honey beds are similar to laminar, high-concentration mass flows called grain-flows. However, the conglomerate layers of the Poison Honey beds do not exhibit the inverse

grading common in grain flows (Lowe, 1976; Middleton and Southard, 1978; Nemec and Steele, 1984; Postma, 1986). Mass flows that share similarities with grain flows but exhibit no grading have been interpreted as density-modified grain flows (Lowe, 1982; Lash, 1984; Todd, 1989). Because of the wide diversity in clast concentration and orientation in the conglomeratic lithotypes, individual layers of the Poison Honey beds were probably deposited by the range of high-concentration mass flows (Figure 8), including density-modified grain flows, grain flows, and true debris flows (Lowe, 1976; Lash, 1984; Todd, 1989). Modern mass flows involving some combination of density-modified grain flows, grain flows, and debris flows have been discussed by Schultz (1984), Pierson and Costa (1987), and Todd (1989).

**Fine-Grained Sandstones:** The fine-grained, lensoid sandstones of the Poison Honey beds are problematic because they interfinger and truncate matrix-supported conglomerates and because they occur as (1) lenses that grade into thin sheets and stringers, (2) distinct, stratified lenses, and (3) persistant, crossbedded sheets (Figures 4, 5c-d). Possible depositional interpretations include (1) channeling and sedimentation by fluvial or brackish-bay processes between flow surges, (2) gravity winnowing, (3) high-concentration turbidity currents, and (4) waning flow conditions.

Reworking of the conglomerates into clast-poor sandstones by fluvial or brackish-bay processes is an attractive interpretation because underlying and possibly lateral sandstones are interpreted as fluvial sandstones, and overlying and possibly lateral shales are characteristic of bay-fill and tidal-channel environments (Greb and Chesnut, 1989). In near-shore environments there would be many opportunities for small-scale channeling and reworking of mass-flow tops between flow surges. However, if the lenses of Poison Honey sandstones (and interfingering conglomerates) are actually channels, the scale of channeling and the crude layering/stratification of these lenses is significantly different than lateral, underlying, and overlying facies (Greb and Chesnut, 1989).

If the sandstone lithotypes of the Poison Honey beds are not similar to surrounding facies, other mechanisms must be analyzed. Nonbedded to crudely stratified lenses of sandstone in mass flows that grade into sheet sandstones, similar to those in the Poison Honey beds, may be caused by post-movement gravity winnowing of mass-flow tops (Postma and Roep, 1985). Winnowing of flow tops might explain the common gradational contacts between the thin sandstone sheets or stringers and underlying conglomerates.

Although gravity winnowing may explain the nonstratified sandstone lenses that can be traced laterally into sandstone sheets or the thin, isolated sandstone stringers that are gradational with underlying conglomerates, other mechanisms need to be investigated for the stratified sandstone lithotypes. Stratified sandstone lenses occur at the eastern end of the roadcut (Figures 3-5a). The sequence of flat bedding, soft-sediment deformation, and upward thinning into laminated shale is similar to partial Bouma sequences (Middleton and Hampton, 1973; Walker, 1975; Nemec and Steele, 1984) commonly deposited in high- concentration turbulent flows (Lowe, 1982; Nemec and Steele, 1984). Lowe (1982) indicated that high-density turbidity currents could be produced from density-modified grain flows if the flows became turbulent. High-concentration turbulent flows that bypass the more viscous portions of mass flows (Lowe, 1982; Postma and Roep, 1985) or result from turbulence created on top of flows (Lash, 1984) have been interpreted

in many modern mass-flow deposits and may have occurred in the Poison Honey beds (Figure 8).

Sheet-sandstone lithotypes of the Poison Honey beds that have minor crossbedding also occur (middle PHB on Figure 3), and were probably not deposited by gravity winnowing processes. These thick, sheet sandstones divide the upper and lower conglomerate-dominated parts of the unit (Figures 3, 4, 9). Sheet sandstones that contain small-scale crossbedding in mass-flow deposits can result from sheet floods from lateral or intermittent fluvial sources (Wells, 1984; Todd, 1989). If the thicker, persistant sheet sandstones of the middle Poison Honey beds were the result of concomitant fluvial processes, a westward accretion would be expected, since surrounding fluvial sandstone facies exhibit southwestern paleoflow (Greb and Chesnut, 1989). However, where current bedding occurs in these sandstones, paleocurrent measurements indicate an eastward flow. Also, the eastward stepping of several sheet sandstones in the lower two-thirds of the Poison Honey beds suggests an overall eastward accretion (Figure 9).

Rather than flooding from fluvial processes, the thick sheet sandstones in the middle Poison Honey beds may have been deposited by waning flows on subaerial mass flows similar to the sandstone sheets described by Nemec and Steel (1984). The positioning of the thick sheet sandstones between conglomeratic portions of the Poison Honey beds (Figures 3, 4, 9) in repetitive layers supports a waning-flow hypothesis (Figure 8). Waning flow could cause small-scale crossbedding in the direction of movement. Also, waning flow on mass-flow tops could create turbulence and local turbidity currents, and would not preclude gravity winnowing of mass-flow-surge and -intersurge events.

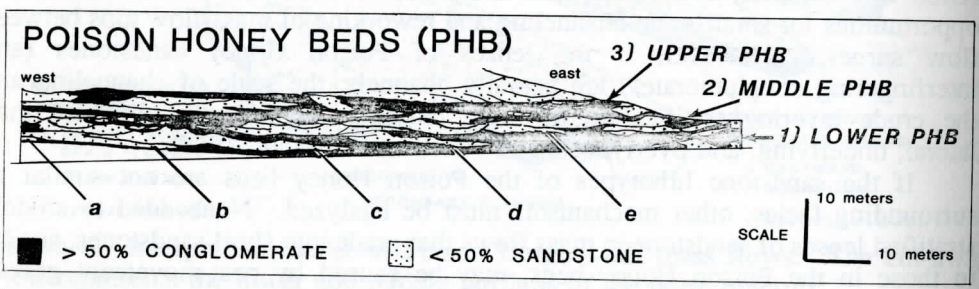


**Figure 9. Cross section of south roadcut. Note two zones (upper and lower) of conglomerate-dominated units that delineate two major mass-flow sequences. Also note sandstone-dominated sheets (a, b, c, d, e) that delineate smaller accretionary (probably intersurge) events within the major flow sequences.**

## Multiple Flows

The vertical repetition of sandstone and matrix-supported conglomerate lithotypes in the Poison Honey beds suggests repeated depositional events. There were at least two large subaerial mass flows with interflow periods of waning flow and reworking recorded by the thick sheet sandstones that divide the Poison Honey beds into upper and lower conglomeratic units (Figure 9). Within the upper and lower flows were also several accretionary (possibly intersurge) winnowing or waning-flow events of smaller scale recorded by the accretionary layering in the lower conglomerate and the repeated sequence of matrix-supported conglomerate layers overlain by thin sandstone stringers (Figure 9). Each of these events

required a mechanism to initiate flow.

Two mechanisms are discussed for the formation of the Poison Honey beds: fault control and climate control. Preservation of brittle shale clasts in the Poison Honey beds indicates a short transport distance. The most plausible local source for the abraded shale and siderite clasts of the Poison Honey beds is the Lower Tongue of the Breathitt Formation, which is juxtaposed against Lee Formation sandstones 1.4 kilometers west of the Rockcastle River Fault (Figure 1). The sharp juxtaposition of lithofacies may be another fault, or it may be a sand-belt margin. Geophysical evidence does not extend far enough west of the Rockcastle River to include the Lee sandstone margin in this area. Regardless, the shales west of the margin are still the most plausible source for the detrtial clasts of the Poison Honey beds. The location of a source horizon to the west and inferred transport of the Poison Honey beds to the east are significant, since underlying, lateral, and overlying facies exhibit southwestern paleocurrents (Greb and Chesnut, 1989).

Breathitt shales and quartz sandstones from the Lee Formation are suggested to have been mixed prior to mass flows because of the high concentration of shale and siderite clasts in the Poison Honey beds (unknown in any other Lee sandstones in this area), and because thorough mixing would be inhibited in the mass flows. One method of mixing these horizons would be by accumulating detritus in a tributary system west of the Rockcastle River Fault. Detritus may have accumulated along a scarp (either fault-bound or channel margin) at the margin of the Lee sandstones and been transported east in a small tributary drainage. The Poison Honey beds are not widespread and therefore must have been locally confined.

Potter (1957) noted locally disturbed shale-pebble breccias similar to the Poison Honey beds in the Illinois Basin along the flank of an anticline in the McCormick Fault Zone. Downslope thickening and inferred paleocurrents suggest that the deposit was triggered by movement along the structure. The Poison Honey beds may also be fault controlled, as suggested by (1) the rarity of these shale-pebble breccia and conglomerate facies in the Carboniferous of the Appalachian Basin (and in the Illinois Basin) coupled with the coincidence of the Poison Honey beds to a fault, (2) the reversal in Poison Honey beds' paleoflow (with respect to surrounding units) corresponding to the direction of downthrow on the fault, and (3) the structural control of this type of facies in other areas.

But each of the flows need not have been triggered by a seismic event. Individual flow surges in the Poison Honey beds could also have been triggered by periodic floods washing debris out of the tributary channel. In the modern Monument Creek flows (Webb and others, 1988), subaerial debris flows are washed into a river during seasonal tributary flooding. Subaerial debris flows afford analogs that allow for the relatively rapid accumulation of multiple flows, variability within individual flows, and climatic triggering mechanisms (seasonal floods in ephemeral streams) rather than multiple movements along a fault (Nemec and Steele, 1984; Schultz, 1984; Pierson and Costa, 1987; Webb and others, 1988).

## ACKNOWLEDGMENTS

This project was funded by the Kentucky Geological Survey. We gratefully acknowledge the comments and suggestions of Charles L. Rice and Thomas W. Gardner, who reviewed the manuscript for publication. Gordon Fraser gave

comments on early drafts and helped with references. We also thank Robert C. Holladay for photography and Margaret L. Smath and James C. Cobb for editorial review.

## REFERENCES CITED

Amig, B. C., 1988, Lithofacies and paleoenvironments, Lower Pennsylvanian rocks, Kentucky State Highway 80 near the Rockcastle River: Lexington, University of Kentucky, M.S. thesis, 98 p.

Chesnut, D. R., Jr., 1988, Stratigraphic analysis of the Carboniferous rocks of the Central Appalachian Basin: Lexington, University of Kentucky Ph.D Dissertation, 297 p.

Enos, P., 1977, Flow regimes in debris flow: Sedimentology, v. 24, p. 133-142.

Fisher, R. V., 1971, Features of coarse-grained, high-concentration fluids and their deposits: Journal of Sedimentary Petrology, v. 24, p. 133- 142.

Greb, S. F., and Chesnut, D. R., Jr., 1989, Geology of Lower Pennsylvanian strata along the western outcrop belt of the Eastern Kentucky Coal Field, *in* Cobb, J. C., coord., Geology of the Lower Pennsylvanian in Kentucky, Indiana, and Illinois: Illinois Basin Consortium, Illinois Basin Studies 1, p. 3-26.

Harms, J. C., Southard, J. B., Spearing, D. R., and Walker, R. G., 1975, Depositional environments as interpreted from primary sedimentary strucutres and stratification sequences: Society of Economic Paleontologists and Mineralogists Short Course 2, 161 p.

Hatch, N. L., Jr., 1963, Geology of the Billows Quadrangle, Kentucky: U.S. Geological Survey Geologic Quadrangle Map, GQ-228.

Lash, G. G., 1984, Density-modified grain-flow deposits from an early Paleozoic passive margin: Journal of Sedimentary Petrology, v. 54, no. 2, p. 557-562.

Lewis, D. W., Laird, M. G., and Powell, R. D., 1980, Debris flow deposits of early Miocene age, Deadman Stream, Marlborough, New Zealand: Sedimentary Geology, v. 27, p. 83-118.

Lowe, D. R., 1976, Grain flow and grain-flow deposits: Journal of Sedimentary Petrology, v. 46, p. 188-199.

Lowe, D. R., 1982, Sediment gravity flows: II. Depositional models with special reference to the deposits of high-density turbidity currents: Journal of Sedimentary Petrology, v. 52, no. 1, p. 279-297.

McDowell, R. C., Grabowski, G. J., Jr., and Moore, S. L., 1981, Geologic map of Kentucky: U.S. Geological Survey, scale 1:250,000, 4 sheets.

Middleton, G. V., and Hampton, M. A., 1973, Sediment gravity flows: Mechanics of flow and deposition, in Middleton, G. V., and Bouma, A. H., co-chairmen, Turbidites and deep water sedimentation: Pacific Section, Society of Economic Paleontologists and Mineralogists, Short Course, p. 1-38.

Middleton, G. V., and Southard, J. B., 1978, Mechanics of sediment movement: Society of Economic Paleontologists and Mineralogists, Short Course 3, 242 p.

Nemec, W., and Steel, R. J., 1984, Alluvial and coastal conglomerates: Their significant features and some comments on gravelly mass-flow deposits, *in* Koster, E. H., and Steel, R. J., eds., Sedimentology of gravels and

conglomerates: Canadian Society of Petroleum Geologists, Memoir 10, p. 1-31.

Pierson, T. C., and Costa, J. E., 1987, A rheologic classification of subaerial sediment-water flows, *in* Costa, J. E., and Wieczorek, G. F., eds., Debris flows/Avalanches--Process, sedimentology, and hazard mitigation: Geological Society of America, Annual Review, Engineering Geology, v. 7, p. 1-12.

Postma, G., 1986, Classification for sediment gravity-flow deposits based on flow conditions during sedimentation: Geology, v. 14, p. 291-294.

Postma, G., and Roep, T. B., 1985, Resedimented conglomerates in the bottomsets of Gilbert-type gravel deltas: Journal of Sedimentary Petrology, v. 55, no. 6, p. 874-885.

Potter, P. E., 1957, Breccia and small-scale Lower Pennsylvanian thrusting in southern Illinois: American Association of Petroleum Geologists Bulletin, v. 41, p. 2695-2705.

Rice, C. L., and Weir, G. W., 1984, Sandstone units of the Lee Formation in eastern Kentucky: U.S. Geological Survey Professional Paper 1151-G, 53 p.

Schultz, A., 1984, Subaerial debris flow deposition in the Upper Paleozoic Cutler Formation, western Colorado: Journal of Sedimentary Petrology, v. 54, p. 749-772.

Todd, S. P., 1989, Stream-driven, high-density gravelly traction carpets—Possible deposits in the Traberg Conglomerate Formation, SW Ireland, and some theoretical considerations of their origin: Sedimentology, v. 36, p. 513-530.

Walker, R. G., 1975, Generalized facies models for resedimented conglomerates of turbidite association: Geological Society of America Bulletin, v. 86, no. 6, p. 737-748.

Webb, R. H., Pringle, P. T., Reneau, S. L., and Rink, G. R., 1988, Monument Creek debris flow, 1984: Implications for formation of rapids on the Colorado River in Grand Canyon National Park: Geology, v. 16, no. 1, p. 50-54.

Wells, N. A., 1984, Sheet debris flow and sheetflood conglomerates *in* Cretaceous cool-maritime alluvial fans, South Orkney Islands, Antarctica, in Koster, E. H., and Steel, R. J., eds., Sedimentology of gravels and conglomerates: Canadian Society of Petroleum Geologists, Memoir 10, p. 133-145.

# DEFORMATION HISTORY OF AN OUTCROP-SCALE FAULT SYSTEM IN THE CENTRAL APPALACHIANS

PHILIP B. SCOTT

WILLIAM M. DUNNE[1]

*Department of Geology and Geography*
*West Virginia University*
*Morgantown, WV 26506*

## ABSTRACT

A outcrop-scale imbricate fan deforming middle Silurian rocks is well exposed in a cut of the B&O railroad. The fan has a two-stage deformation history. Footwall imbrication and thrust-tip folding preceded buckle folding with minor hangingwall imbrication. The fan is unusual because two thrusts curve into different bedding detachments for short distances before terminating, almost forming a duplex. The beds immediately above the fan accommodated fan formation by passive folding, backthrusting along small separate faults and bedding, and localized cleavage with flattening or volume loss.

## INTRODUCTION

The structural style of Alleghenian deformation in the Valley and Ridge Province of the central Appalachians consists of a blind thrust system in Cambro-Ordovician carbonates that is overlain by a cover or roof sequence (Geiser, 1988) of middle Ordovician to Permian(?) rocks. This cover deformed separately and usually in advance of the blind system (Perry, 1978) by layer-parallel shortening (Geiser, 1988) that involved cleavage (Geiser, 1974; Meyer and Dunne, 1990), faulting and folding (Kulander and Dean, 1986). The faulting is concentrated in stronger stratigraphic units (Dean and others, 1985; Kulander and Dean, 1986) and may be linked (Jacobeen and Kanes, 1974) or isolated (Kulander and Dean, 1986). The purpose of the present paper is to present one of the best-exposed outcrop-scale examples of this faulting in the entire central Appalachians (Woodward, 1989; Engelder and others; 1989). The example will be used to demonstrate: (1) faulting is intimately involved with folding; (2) deformation was locally both in and out-of-sequence; and (3) faulting is isolated by other structures compensating for the displacement. It is hoped that this example will provide a comparative template for other workers dealing with less exposed structures in the Valley and Ridge Province.

## COVER GEOMETRY

The outcrop-scale fault system described in this study is located at Cedar Cliff along a B & O railroad cut on the northern bank of the North Branch Potomac River at the Maryland-West Virginia border (Figure. 1a). The regional structure is dominated by the Wills Mountain anticline, which is the surficial expression of an

[1]Department of Geological Sciences, University of Tennessee, Knoxville, TN 37996-1410, for reprint request.

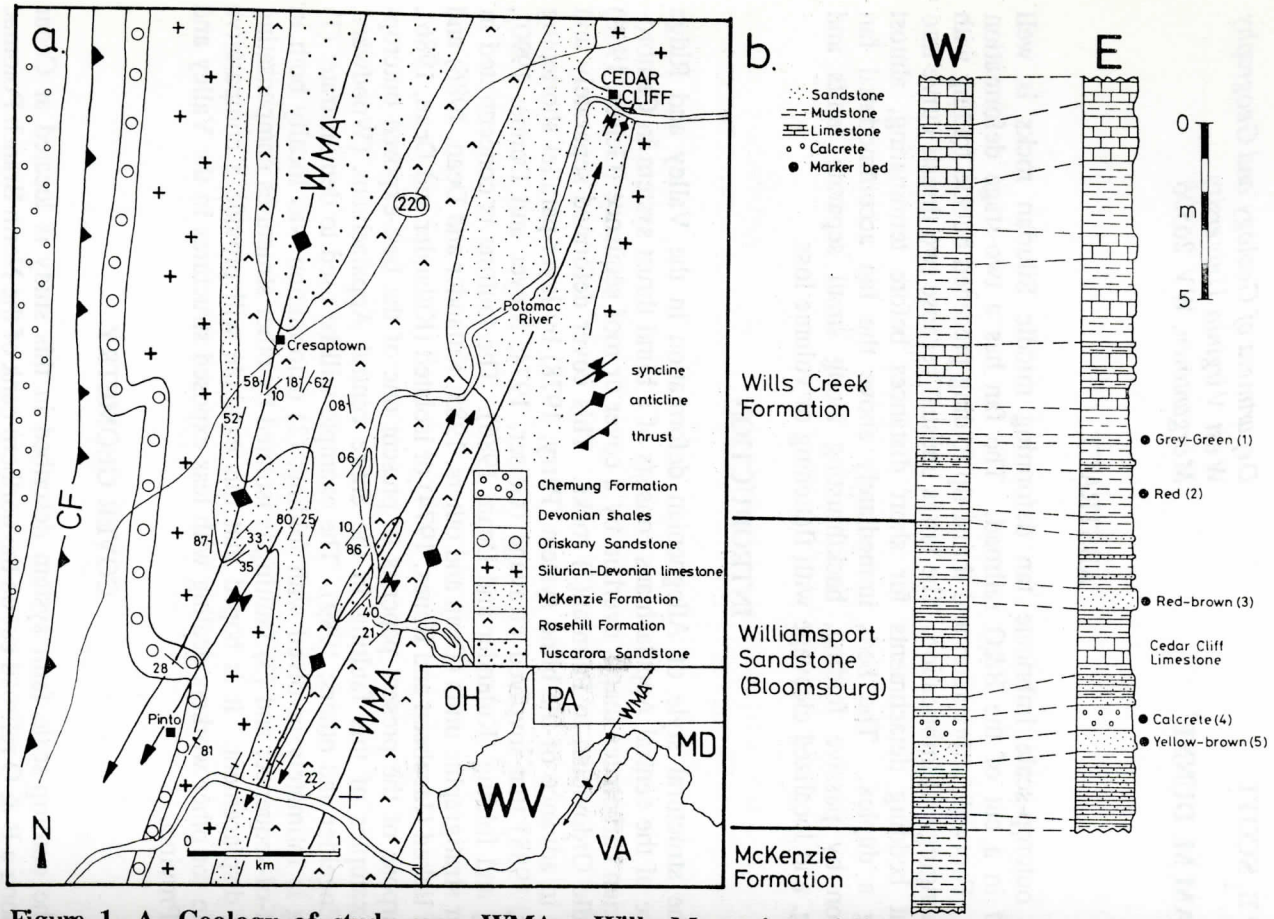


**Figure 1. A, Geology of study area. WMA - Wills Mountain anticline; DF - Dawson fault; CF - Cresaptown fault; Cedar Cliff in northeast corner of map. Inset map shows location of study area (S). B, Stratigraphy at Cedar Cliff, Maryland. Numbered beds are marker beds.**

underlying thrust horse in the Cambro-Ordovician carbonates (Gwinn, 1964; Perry, 1978). Earlier workers (Reger and Tucker, 1924; Dennison and Naegele, 1963; Cardwell and others, 1968) believed that the hinge trace for the Wills Mountain anticline curves continuously through the area, as is schematically shown in the inset map of Figure 1. However, detailed mapping during the present study demonstrates that the anticline consists of several en echelon folds that have the regional northeast trend (Figure 1a). The folds systematically plunge out within the area, transferring fold amplitude northwards from the southeastern the northwestern side of Wills Mountain anticline.

## STRATIGRAPHY AT CEDAR CLIFF

The outcrop-scale system deforms middle Silurian rocks. The sequence changes upward, from the carbonate-dominated McKenzie Formation, to the siliciclastic-dominated Williamsport Sandstone, to the carbonate-dominated Wills Creek Formation (Figure 1b) at the top. At the base of the sequence, thin-bedded limestones and calcareous shales are capped by a 2m thick, dark-grey calcareous shale in the upper McKenzie Formation. The overlying Williamsport Sandstone is dominated by fluvio-deltaic rocks, which vary from thin-bedded and bioturbated sandstones with thin interbedded mudstones to two thick sandstone beds with cross-bedding (beds 3 and 5, Figures 1b, and 2). The Williamsport Sandstone also contains two unusual lithologies, a pale lime-green mudstone with calcrete nodules (bed 4, Figures 1b, and 2), and the marine Cedar Cliff limestone (Woodward, 1941). The Williamsport Sandstone is the western deltaic equivalent of the fluvial Bloomsburg Formation (Woodward 1941, p. 150; Patchen, 1973). The overlying Wills Creek Formation consists of thick, grey calcareous mudstones alternating with buff-colored, mud-cracked, fine-grained limestones, which locally contain ostracod-rich layers.

Lithostratigraphy was measured in two separate sections along the railroad cut about 150m apart. The western section (W, Figures 1b, and 2a) was measured in relatively undeformed, gently dipping rocks of the western limb of an open upright syncline. The more-intensely deformed eastern section (E, Figures 1b, and 2) was measured in the hanging wall of the fault system (Figure 2b, A to B), which contains contraction faults, cleavage, bed-parallel slickensides, and other veins. The two sections were used to determine (1) if the eastern section at the fault system was tectonically thickened or thinned; and (2) if detachments in the thrust system extended to the same stratigraphic level in the western section.

Correlating marker beds (beds 1 to 5, Figures 1b, and 2) between sections demonstrates an absence of systematic thickness change from strain in the more-deformed eastern section. Observed thickness changes were controlled by lateral change in original sedimentary lithology and geometry. Also, bedding-parallel slickensides or faults are absent in the western section. Thus, the detachments in the eastern section do not extend even as far as the western section.

## STRUCTURAL GEOMETRY AT CEDAR CLIFF

### Major Folds and Thrusts

The fault system involves an M-shaped anticline that is completely exposed above the horizontal lines in Figure 2a-b except for the dashed fault segments at

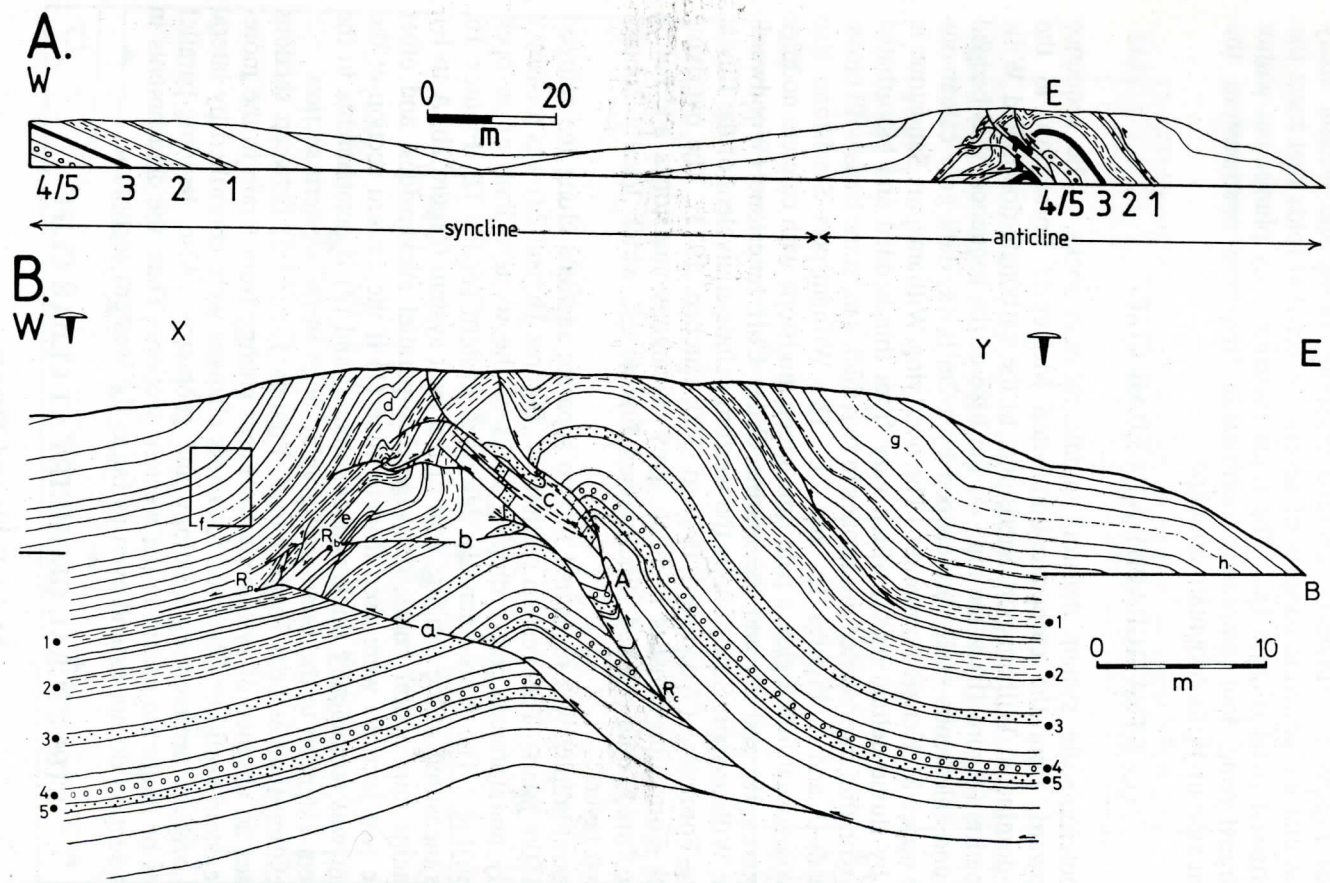


Figure 2. Profile at Cedar Cliff of thrust system with adjacent syncline. Ornamented and numbered beds are marker beds of Figures 1b and 2b. B, Enlarged profile of surface geology for thrust system with interpreted subsurface geology between pinpoints at Cedar Cliff. Dot-dash lines are bedding-parallel slickenside veins.

"c". The fold limbs are not curved, but instead are straight segments with narrow hinges or kink folds for dip changes through the anticline. The fold trends 025-205° and plunges a few degrees northeast or southwest depending on position (Figure 3a).

The thrusts appear in the anticlinal core at the ground surface, strike subparallel to fold trend (Figure 3b), and contain grooved and unstepped crystal-fiber slickensides, which pitch within 5° of the thrust dip-direction. A tempting interpretation for these relationships would be that the anticline was deformed by secondary hinge contraction-faults. Yet, all thrusts have the same displacement sense rather than symmetrically displacing the hinge in both directions, which argues against a contraction origin (Mattauer, 1973). Also, different thrusts have different relative ages to the fold. For example, the lowest exposed thrust (b, Figure 2b) is folded across the bottom anticlinal hinge zone, whereas upper thrusts (left of c, Figure 2b) are straight and hence, unfolded by the same hinge.

This geometry contrasts sharply with an adjacent upright syncline to the west (Figure 2a). The two folds have similar wavelength, but the syncline has less amplitude, a greater interlimb angle (Figure 3c), straighter limbs dipping less than 25 degrees, and a single, simple subrounded hinge. Only the outer anticlinal limb-segments have the same style.

## Secondary Structures

The only parasitic folds in the anticline are located in the western limb (d, Figure 2b). A disharmonic anticline-syncline couplet verges into the anticline and abruptly decreases in amplitude into the footwall as it crosses a gently dipping thrust.

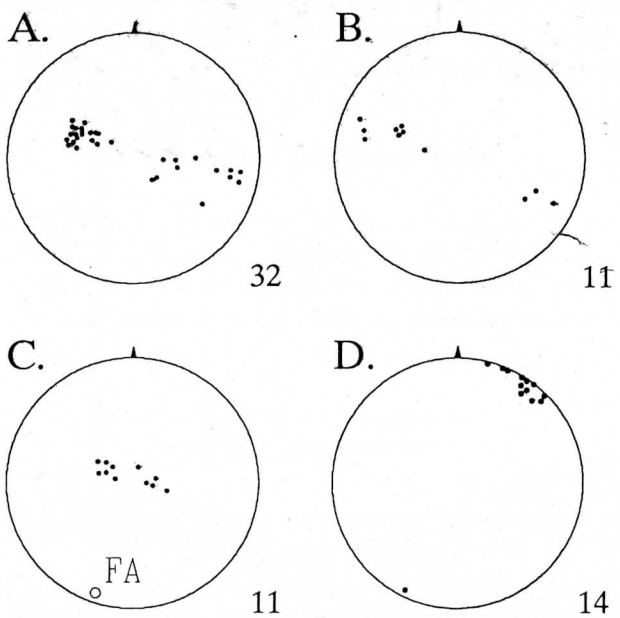


**Figure 3. Lower hemisphere equal-area stereonets. A, bedding of anticline. B, faults. C, bedding in syncline. D, cleavage to bedding intersections. FA - fold axis; numerals at lower left of each net are the number of measured structures.**

Small backthrusts (e, Figure 2b) displace rocks about 0.1m to 0.5m up the western limb. Several backthrusts are rooted in layer-parallel slip zones and only offset one or two beds. Two backthrusts displace the lowest exposed major thrust (b, Figure 2b), implying that they are younger.

Thin bed-parallel slickenside quartz veins with well defined mineral fibers occur along sandstones in the anticlinal core. Other bed-parallel, calcite slickenside veins occur in the anticlinal fold limbs within the calcareous mud-

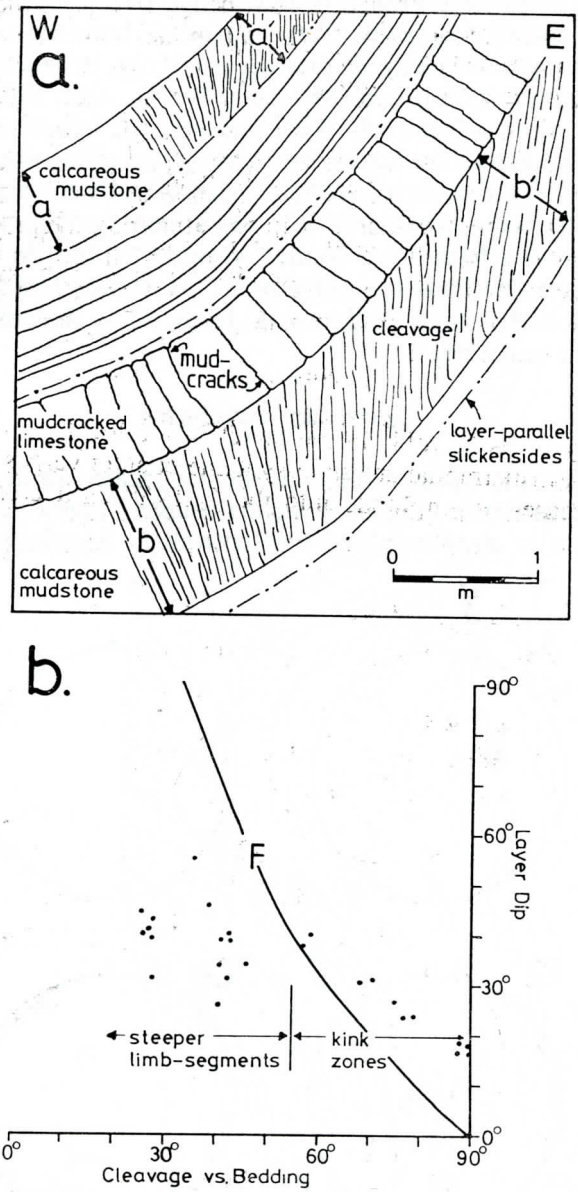


**Figure 4. A, Cleavage to bedding geometries and bed-thinning for steeper western limb-segment (to right of "f" in Figure 2b). Beds thin by 25% into steeper limb-segment (from a,b to a',b'). B, Graph of cleavage-to-bedding angles vs. layer dip. "F" curve represents predicted flexural-flow geometry without volume loss (Ferrill & Dunne 1989).**

stones of the Wills Creek Formation and pitch within 5° of the layer dip-direction. These calcite veins are not evenly distributed between fold limbs. Only two calcite slickenside veins are present in the eastern limb. They are less than 2mm thick, and extend through the entire limb (Figure 2b). In the western limb, six slickenside veins are present. They are up to 10mm thick, and terminate where the limb dip decrease sharply (f, Figure 2b). Thus, slickensides in the western limb are more frequent, thicker, and restricted to steeper limb segments unlike in the eastern limb. This stronger development could result from greater uplimb and hingeward motion in the western limb. Also, these slickenside veins define the only bed-parallel movement zones in both limbs. All other bedding surfaces are intact and "welded", demonstrating that interlayer slip is concentrated along the slickenside veins (Tanner, 1989).

Cleavage is restricted to only the steeper anticlinal limb-segments and to only the calcareous mudstones of the Wills Creek Formation (f,g, and h, Figure 2b). The cleavage to bedding intersects plunge northeast parallel to the fold axes (Figure 3d). The steeply inclined, closely spaced disjunctive cleavage disappears abruptly where limb dip decreases without changing morphology (Figure 4a).

The cleavage-to-bedding angles change from a common 30-40° in steeper limb segments (Figure 4b) to 90° across the kink folds where the cleavage disappears (Figure 4a). Beds thin by 19 to 27% from the uncleaved, gentler dipping limb-segments to the cleaved, steeper limb-segments (e.g. Figure 4a), implying syn-cleavage flattening or volume loss in the steeper limbs.

In the steeper limb-segments, the bedding-to-cleavage angles are too small for simple flexural flow (F, Figure 4b), but are consistent for flexural-flow with flattening or volume loss (Ramsay, 1967; Gray, 1981). Flattening by volume loss would also have caused the bed-thinning. This strain increment is restricted to the cleaved calcareous mudstones, as interbedded buff limestones contain mudcracks that remain at 90° to bedding, regardless of layer dip. The mudcracked limestones record a pre- thrusting layer-parallel shortening strain as the polygons are weakly deformed and are still oriented at 90° to layering.

## RESTORED CROSS-SECTION

The purpose of the restored cross-section (Figure 5) is to produce a kinematically viable and structurally admissible interpretation of the subsurface beneath the exposed thrust system (Figure 2b) (Dahlstrom, 1969; Elliott, 1983). This interpretation would then aid in establishing the deformation history.

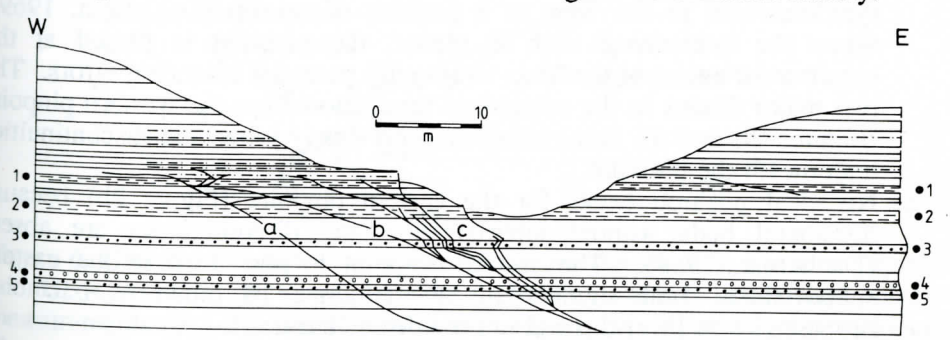


**Figure 5. Restored cross-section for Cedar Cliff profile between pinpoints (Figure 2b). Letters correspond to Figure 2b.**

## Constraints for Section Construction

The constraints for the construction of the subsurface geology in Figure 2b and the restored cross-section of Figure 5 are:

1. *Structural style—*
   a. Surficial thrust geometry and positions restrict style and positions of subsurface thrust geometry.
   b. Open-fold style of adjacent syncline and outer anticlinal limbs is indicative of fold geometry at depth within the anticline.
   c. Position of kink folds in anticlinal limbs may indicate the positions for trajectory changes of subsurface faults (Suppe, 1983; 1985).
   d. The higher stratigraphic levels in the gentle eastern limb segment requires folding, because the levels of the two gentle anticlinal limb-segments would match if only thrusts with a common extensive basal detachments are present.
   e. Measurable bed lengths and dips in outcrop constrain the range of possible bed lengths in the balanced section, and the subsurface bed geometries.
2. *Stratigraphic position of proposed floor thrust—*
   a. Convergence of surface thrusts in the fold core indicates a common origin in the subsurface. Also, at ground level the hanging-wall rocks are subparallel to the thrusts, indicating that the thrusts pass into bedding.
   b. In the hanging wall of the thrust system, hinge collapse and fold tightness of the anticlinal core indicate a local detachment stratigraphically beneath the core rocks.
   c. Decreasing amplitude of the hangingwall anticlines approaching the thrusts (b and c, Figure 2b) indicates a rootless origin for the fold and a proximity to the decollement horizon.
   d. Using criteria 2a to 2c, a relatively weak, 2m thick mudstone unit in the upper McKenzie Formation (W, Figure 1b) was chosen as the site for the floor thrust.
3. *Section construction-controls—*
   a. Given the lack of pervasive tectonic strain, it was only necessary to balance bed lengths from the floor thrust to the top of marker bed 2 (Figure 5). Beds above this level are too eroded to be balanced. Beds below this level are beneath the floor thrust, and therefore are unlikely to balance locally (Dahlstrom, 1969).
   b. The western pinpoint (Figure 2a) could have been positioned in the synclinal core to the west as a position of no-slip (Dahlstrom, 1969). Since the intervening limb is planar, the pinpoint is placed at the easternmost extent of the limb, to magnify potential balancing errors. The two major thrusts in the subsurface terminate before the western pinpoint (Figures 2b and 5), eliminating the only likely kinematic discontinuities underneath the pinpoint.
   c. No ideal position exists for the eastern pinpoint (Figure 2b) because horizontal beds without internal kinematic discontinuities are absent (Dahlstrom, 1969). The eastern pinpoint is positioned in the eastern subhorizontal limb-segment of the anticline to minimize balancing problems from layer-dip and unseen discontinuities.

The chosen kinematic solution satisfies the requirements of structural style and balances with less than 2% error (Figure 5). The interpretation involves both an open anticline and an unexposed blind imbricate thrust (a, Figure 2b). Alternative geometries with just folds or thrusts do not satisfy the constraints. For example, a single subsurface anticline would not produce the dip segments at the surface, and would produce insufficient shortening below marker bed 1. Alternatively, one or a combination of subsurface imbricate thrusts would not produce differing stratigraphic levels in the anticlinal limbs, and would cause excess shortening below marker bed 1.

To compare the interpreted thrust geometries to other thrust geometries with a known sequence of evolution, distance-displacement graphs were plotted (Williams and Chapman, 1983; Chapman and Williams, 1984). Although the mechanism proposed by Williams and Chapman (1983) to account for the relationships in distance-displacement graphs has been shown to be suspect, the graphs still provide a powerful tool for comparing geometries and sequences of thrust evolution (Chapman and Williams, 1984; Ellis and Dunlap, 1988). For the method, arbitrary reference points were chosen for each fault ($R_a$ to $R_c$, Figure 2b), distances from the reference points to beds with their displacements were measured, and the results were plotted (Figure 6).

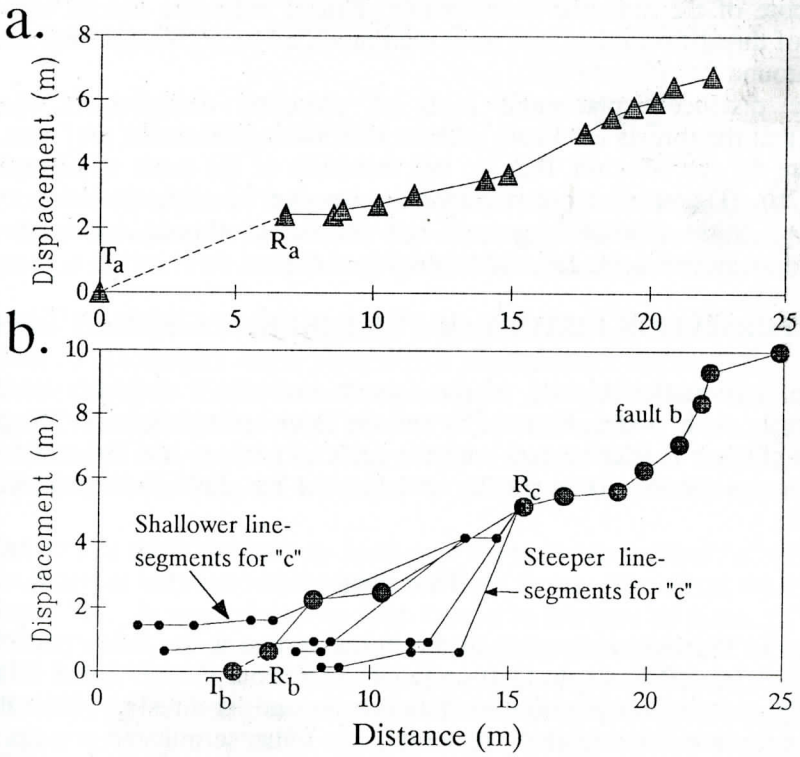


**Figure 6. Graphs of distance vs. displacement for thrusts (a,b, and c in Figures 2b and 5). A, thrust a. B, thrusts b, and c including its splays. Reference points for measurements ($R_a$, $R_b$, and $R_c$) located in Figure 2b. $T_a$ and $T_b$ are termination distances to the west of the reference points for thrusts "a" and "b", respectively. triangles - thrust "a"; solid circles - thrust "b"; dots - thrust "c" and splays.**

The upper thrusts (around c, Figure 2b) plot as two line segments. The first line-segments ($R_c$, Figure 6) have a 50° slope. Thus, the anticline above the faults at "c" (Figure 2b) is a fault-propagation or thrust-tip anticline to the thrusts (Chapman and Williams, 1984). The second line-segments are horizontal and this change in slope indicates a second stage of fault propagation with respect to the anticline (Ellis and Dunlap, 1988). During the second stage, thrusts displaced a pre-existing anticline, producing matching cutoffs. Not only do the cutoffs match, but the reconstructed fault trajectories through bed 2 (Figure 5) have the distinctive perpendicular and backwards attitudes that are related to younger, possibly out-of-sequence thrusts cutting pre-existing folds (Morley, 1988). The second stage of thrust propagation also offset the syncline-anticline fold pair immediately to the west of "c" (Figure 2b).

The western rootless anticline is above thrust "b" (Figure 2b), which plots with a 25° slope (Figure 6). This slope indicates that thrust "b" with its similar cutoffs formed the anticline at its thrust tip and offset it during growth. Both anticlines have subvertical to overturned limbs (Figure 2b) as would be expected for thrust-tip folds that generate these slopes.

The postulated, unexposed thrust (a, Figure 2b) plots with a 16° slope (Figure 6). This slope would result from a thrust with similar cutoffs that displaced a thrust-tip fold during late-stage folding.

Thus, the cutoff relationships for Cedar Cliff demonstrate that the tight M-shaped core of the anticline is the result of three imbricate thrusts with varying degrees of thrust-tip folding that were then modified by additional displacement on thrusts around "c" (Figure 2b).

The distance-displacement plots of changing displacement magnitudes indicate that the thrusts terminate without establishing extensive roof flats ($T_a$ and $T_b$ Figure 6). In addition, they do not terminate at the same stratigraphic level (Figure 2b). Therefore, these structures do involve thrust-tip or fault-propagation folding as Mitra (1986) suggested, but the linked thrusts are more usefully described as an imbricate fan, rather than as a duplex.

## DEFORMATION HISTORY OF THE IMBRICATE THRUST SYSTEM

The deformation history of the system involves a sequence of the three main thrusts (a, b, and c, Figure 2b) and the later open anticline. The proposed sequence (Figure 7) is consistent with the surficial geology, the deformed-state and restored cross-sections (Figures 2b, and 5), and the distance-displacement plots (Figure 6).

### First Stage

**Part 1:** The oldest structure in the thrust system is the lower part of thrusts "c" (Figure 7a). This single fault propagated to about marker bed 5 (Figure 2b), producing a large fault-propagation anticline beyond its thrust tip. The thrust did not curve up into bedding along its length, but rather terminated at a tip.

**Part 2:** The second structure to form was thrust "b" (Figure 7b), as a footwall imbricate from the same floor thrust. The thrust generated the second thrust-tip anticline, forming the M-shape of the anticline at Cedar Cliff. The second thrust-tip anticline is not a rootless fault-bend fold because the fold increases amplitude with decreasing thrust displacement. At the present ground

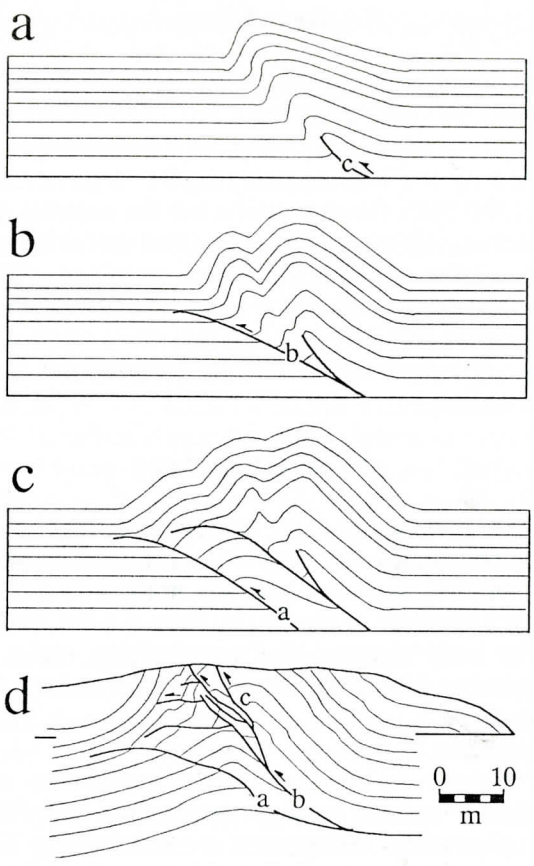


**Figure 7. Reconstruction of deformation history. a,b, and c. First stage--formation of footwall-imbricating fan with some curved thrust ends. d. Second stage--folding by an open anticline with some hangingwall imbrication from reactivated thrusts.**

surface, the thrust curves into bedding underneath marker bed 1, but observable decreasing displacements when plotted in a displacement-distance plot (Figure 6) demonstrate that the fault terminates a short distance along bedding in the subsurface. Thus, the geometry of thrust "b" is intermediate between a ramp-flat with a roof thrust and an imbricate splay with a tip-line (Boyer and Elliott, 1982). In addition, thrust "b" was unlike thrust "c", which was much shorter and had no flat.

**Part 3:** The third structure to form was the postulated thrust "a" (Figure 7c), also as a footwall imbricate along the same floor thrust. The thrust weakly folded older thrust "b". A small thrust-tip fold formed in advance of thrust "a".

Thrust "a" is interpreted to curve into bedding above marker bed 1 (Figure 2b), unlike thrust "b". The differing detachment level results from the older upper flat of older thrust "b" being too short to influence the position of thrust "a". Also, the presence of several closely spaced weaker beds provided several possible decollement horizons for the younger thrust "a". Thrust "a" is an intermediate imbricate thrust similar to thrust "b" because the thrust-tip only extends a short distance (6m) along layering (Figures 2b and 6). As can be seen, no common roof thrust links these three faults and consequently this system can not be characterized as a duplex. Instead, the system is an imbricate fan with some curved fault-ends.

## Second Stage

Structures that formed during this stage were the lower open anticline, and reactivations of thrusts "b" and "c" (Figure 7d). The anticline probably developed coevally with the western adjacent syncline of the same style and orientation, and was probably located by the heterogeneity in the sequence of the imbricate fan. The anticline folded the three thrusts, producing the external gentle limb-segments of the surficial anticline. However, the upper thrusts (c, Figure 2b) and imbricate splays from thrust "b" are straight, and hence unfolded. These younger thrusts with their out-of-sequence, matching cut-off geometries are hangingwall imbricates with respect to thrust "b". They may be younger than the anticline, but a syn-folding age would provide a cause for hangingwall imbrication after first-stage footwall imbrication.

## "Cover" Structures

Most thrusts terminate at about the stratigraphic level of marker bed 1. As a result, the overlying beds acted as a "cover" to the blind imbricate fan (Woodward and others, 1985) in the sequence beneath marker bed 1. The cover is not separated by a major kinematic discontinuity from the fan, and therefore must have compensated for the body motions in the underlying rocks. The compensation was achieved by passive fold amplification and secondary structures, which are concentrated in the cover.

Secondary structures in the cover include:

1. *Cleavage* that formed in the calcareous mudstones with a flexural-flow component, aiding uplimb motion during fold amplification, and with a flattening or volume-loss component accommodating horizontal shortening.
2. *Coeval backthrusts* with a cumulative displacement of less than 2m formed in the steeper western limb-segment. The faults allowed underthrusting beneath the "cover" by the imbricate fan.
3. *Abundant layer-parallel slip-zones* formed in the steeper western limb-segment, aiding both underthrusting from the east and uplimb motion during fold amplification.

## Discussion

The deformation history produced a total profile shortening of 28% (Figures 2b and 5). At the base of the sequence, the strain partitioning is 4% by the anticline and 24% by the imbricate fan. At the top of marker bed 2, the partitioning is 22% by the anticline and 6% by the fan. If bed-length balancing is attempted in the eroded cover at the fifth bedding surface above marker bed 1, the anticline causes 25% shortening and 3% is unaccounted for. The only other structure that could cause a 3% internal strain in the cover is the spaced disjunctive cleavage. The locallized 20% horizontal bed-thinning in the three calcareous mudstones would accommodate the overall 3% shortening difference. Thus, the shortening in the sequence shifts upward from the imbricate fan to the anticline with some cleavage in the cover.

Therefore, the deformation history may be considered as two-stage: (1) formation of the footwall-imbricating fan with some curved thrust-ends; and (2) folding by an open anticline with some hangingwall imbrication from reactivated

thrust. The overlying "cover" above the imbricate fan developed secondary structures, which allowed underthrusting, fold amplification, and horizontal shortening. Although localized, the cleavage was the most important of the secondary structures.

## CONCLUSIONS

1. The imbricate fan at Cedar Cliff has a two-stage deformation history, where a footwall-imbricating fan and fault-propagation folds were deformed by folding with hangingwall imbrication. The fan is unusual, because both footwall and hangingwall imbrication developed and some thrust-ends curve into bedding, almost forming a roof thrust. Although the fan is locally a linked-fault system, it is isolated by lateral terminations.
2. The local "cover" sequence above the blind imbricate fan compensated for the thrust system by folding, by formation of locallized flattening or volume-loss flexural-flow cleavage, by backthrusting, and by more intense interlayer-slip in the western limb. The cleavage accommodated the uplimb motion and an additional horizontal shortening. This deformation may be analogous in detail to cover deformation above larger blind thrust systems.

## ACKNOWLEDGMENTS

The authors thank Steven Wojtal for commenting on an earlier versions of the manuscript and for the review by Mark A. Evans.

## REFERENCES CITED

Boyer, S.E., and Elliott, D., 1982, Thrust systems: American Association of Petroleum Geologists Bulletin, v. 66, p. 1196-1230.

Cardwell, D.H., Erwin, R.B., and Woodward, H.P., 1968, Geologic map of West Virginia: West Virginia Geological and Economic Survey, Map 1, 1:250,000, 2 sheets.

Chapman, T.J., and Williams, G.D., 1984, Displacement-distance methods in the analysis of fold-thrust structures and linked-fault systems: Journal of the Geological Society of London, v. 141, p. 121-128.

Dahlstrom, C.D.A., 1969, Balanced cross sections: Canadian Journal of Earth Science, v. 6, p. 743-757.

Dean, S.L., Kulander, B.R., and Lessing, P., 1985, Geology of the Capon Springs, Mountain Falls, Wardensville, Woodstock, and Yellow Spring Quadrangles, Hampshire and Hardy Counties, West Virginia: West Virginia Geological and Economic Survey Map-WV26, 1:24,000 scale, 1 sheet.

Dennison, J.M., and Naegele, O.D., 1963, Structure of Devonian strata along Allegheny front from Corriganville, Maryland, to Spruce Knob, West Virginia: West Virginia Geological and Economic Survey Bulletin B-24, 42p.

Elliott, D., 1983, Construction of balanced cross-sections: Journal of Structural Geology, v. 5, p. 101-103.

Ellis, M.A., and Dunlap, W.J., 1988, Displacement variation along thrust faults: implications for the development of large faults: Journal of Structural Geology, v. 10, p. 183-191.

Engelder, T., Dunne, W.M., Geiser, P.A., Marshak, S., Nickelsen, R.P., and

Wiltschko, D., 1989, Structures of the Appalachian Foreland Fold-Thrust Belt: 28th International Geological Congress Field Trip Guidebook T166, 88p.
Ferrill, D.A., and Dunne, W.M., 1989, Cover deformation above a blind duplex: an example from West Virginia, U.S.A.: Journal of Structural Geology, v. 11, p. 421-431.
Geiser, P.A., 1974, Cleavage in some sedimentary rocks of the central Valley and Ridge Province, Maryland: Bulletin of the Geological Society of America: v. 85, p. 1399-1412.
Geiser, P.A., 1988, Mechanisms of thrust propagation: some examples and implications for the analysis of overthrust terranes: Journal of Structural Geology, v. 10, p. 829-845.
Gray, D.R., 1981, Cleavage-fold relationships and their implications for transected folds: an example from southwest Virginia, U.S.A.: Journal of Structural Geology, v. 3, p. 265-277.
Gwinn, V.E., 1964, Thin-skinned tectonics in the Plateau and northwestern Valley and Ridge Provinces of the central Appalachians: Bulletin of the Geological Society of America, v. 75, p. 863-900.
Jacobeen, Jr., F., and Kanes, W.H., 1974, Structure of Broadtop synclinorium and its implications for Appalachian structural style: American Association of Petroleum Geologists Bulletin, v. 58, p. 362-375.
Kulander, B.R., and Dean, S.L., 1986, Structure and tectonics of central and southern Appalachian Valley and Ridge and Plateau Provinces, West Virginia and Virginia: American Association of Petroleum Geologists Bulletin, v. 70, p. 1674-1684.
Mattauer, M., 1973, Les D formations des Mat riaux de L' corce Terrestre, Hermann, Paris.
Meyer, T.J., and Dunne, W.M., 1990, Deformation of Helderberg Limestones above the blind thrust system of the central Appalachians: Journal of Geology, v. 98, in press.
Mitra, S., 1986, Duplex structures and imbricate thrust systems: geometry, structural position, and hydrocarbon potential: American Association of Petroleum Geologists Bulletin, v. 70, p. 1087-1112.
Morley, C.K., 1988, Out-of-sequence thrusts: Tectonics, v. 6, p. 539-561.
Patchen, D.G., 1973, Stratigraphy and petrography of the Upper Silurian Williamsport Sandstone: West Virginia Academy of Science Proceedings, v. 45, p. 250-265.
Perry, Jr., W.J., 1978, Sequential deformation in the central Appalachians: American Journal of Science, v. 278, p. 518-542.
Ramsay, J.G., 1967, Folding and fracturing of rocks: New York, McGraw-Hill Book Co., 568p.
Reger, D.B., and Tucker, R.C., 1924, Mineral and Grant Counties: West Virginia Geological and Economic Survey County Report, 866p.
Suppe, J., 1983, Geometry and kinematics of fault-bend folding: American Journal of Science, v. 283, p. 684-721.
Suppe, J., 1985, Principle of structural geology: Prentice-Hall, New Jersey, 519p.
Williams, G.D., and Chapman, T.J., 1983, Strains developed in the hanging walls of thrusts due to their slip/propagation rate: A dislocation model: Journal of Structural Geology, v. 5, p. 563-671.

Woodward, H.P., 1941, Silurian system of West Virginia: West Virginia Geological and Economic Survey Volume V-14, 326p.
Woodward, N.B., 1989, Geometry and deformation fabrics in the central and southern Appalachian Valley and Ridge and Blue Ridge: 28th International Geological Congress Field Trip Guidebook T357, 105p.
Woodward, N.B., Boyer, S.E., and Suppe, J., 1985, An outline of balanced cross sections: University of Tennessee Department of Geological Science Studies in Geology, v. 11, 170p.

# TRACE-ELEMENT GEOCHEMISTRY AND AN OCEANIC ORIGIN FOR THE HAMMETT GROVE META-IGNEOUS SUITE, SOUTH CAROLINA

**STEVEN K. MITTWEDE**

*South Carolina Geological Survey*[1]
*5 Geology Road*
*Columbia, SC 29210-9998*

**W. E. SHARP**

*University of South Carolina*
*Department of Geological Sciences*
*Columbia, SC 29208*

## ABSTRACT

Metamorphosed ultramafic and mafic rocks of the Hammett Grove Meta-igneous Suite in the southern Appalachian Piedmont, northwestern South Carolina, exhibit compositional and mineralogical changes resulting from fractionation and differentiation of a basaltic parent magma. They range from steatitized and serpentinized ultramafite through metapyroxenite, metaclinopyroxenite, metagabbro, metabasalt, and metatrondhjemite. The trace-element compositions of 27 samples collected near Pacolet Mills, South Carolina show that Cr, Ni, Co, and Zn have high concentrations in the altered (steatitized and serpentinized) ultramafites and decrease in abundance with increasing fractionation. Sr, V, Ti, Zr, and Cu are relatively depleted in the altered ultramafites and increase in concentration with fractionation and differentiation. Rb, Ba, Y, and Mo show no consistent trends, but Ba and Y generally increase in concentration with magmatic evolution. Sn, Nb, Pb, and Th are concentrated in the metatrondhjemite.

The rapid fall in the concentration of compatible elements and the moderate to strong increase in incompatible elements indicate that initial fractionation of the parental magma was governed primarily by the crystallization of olivine and chromite and secondarily by the crystallization of Ca-rich clinopyroxene. The middle and late stages of fractionation were controlled by plagioclase and Fe-Ti oxide phase(s) crystallization.

The trace-element data for the Hammett Grove Suite suggest that the plutonic and volcanic rocks had a common magmatic parent, having formed sequentially by crystal accumulation and fractional crystallization of a basaltic melt. The parental magma was probably a high-Ti, fairly low-K basalt, not unlike ocean-floor basalts. Rocks of the Hammett Grove Suite probably formed in a shallow, oceanic magma chamber, possibly as fore-arc basement to the exotic Carolina arc terrane, not in a diapiric, late- or main-stage arc intrusion of the Bear Mountain (California) type.

## INTRODUCTION

In the central Piedmont of the southern Appalachians, the late Proterozoic-early Paleozoic Hammett Grove Meta-igneous Suite and several other ophiolitic(?)

[1]Present address: Terrane Exploration Services, 2523 Huguenot Springs Road, Midlothian, VA 23113.

ultramafic-mafic bodies occur as klippen, thrust slices, or fragments along the Piedmont terrane-Carolina terrane suture (Mittwede, 1988). The Hammett Grove Suite is the only one of these bodies for which mineralogy and major-element chemistry have been published (Mittwede, 1989; Mittwede and others, 1987).

The Hammett Grove Suite is a thrust slice or klippe composed of amphibolite-facies and retrograde greenschist-facies equivalents of possibly comagmatic igneous rocks (Mittwede, 1989), including altered ultramafites (peridotitic protoliths, now mainly soapstone and serpentinite), metapyroxenite (possibly some melagabbroic protoliths), metagabbro with metaclinopyroxenite and metatrondhjemite dikes or sills, and amphibolitic metabasalt (Figure 1). Rodingite and partially rodingitized sedimentary rock occur at one locality in the Suite. The Hammett Grove Suite has a strike length of 30 km, a maximum width of 1 km, and an estimated maximum thickness of 30 m. Even though the Suite appears to be only a thin tectonic slice, its areal extent makes it one of the largest non-diapiric, ultramafic-mafic suites in the southern Appalachian Piedmont.

The present lithologic distribution and geometry of the Suite probably reflects late Paleozoic strike-slip faulting, and may have been produced by large-scale boudinage. The string of "blocks" that extend southwest from the main body of the Suite may actually be part of a melange. No continuous translational structure is discernable in the field. Concerning intra-suite contacts, some are intrusive or gradational, but many, particularly those in the narrow, southwest extension of the Suite, are undoubtedly faults.

Mittwede (1989) interpreted the Hammett Grove Meta-igneous Suite as a metamorphosed, highly dismembered ophiolite. It lacks recognizable equivalents of sheeted dikes and pillow lavas, although the amphibolitic metabasalt probably corresponds to the extrusive section of an ideal ophiolite sequence. The major-element chemistry of the Hammett Grove Suite is similar to that of other southern Appalachian ophiolites (Mittwede, 1989), namely the Halifax County complex, North Carolina (Kite and Stoddard, 1984), and the Piney Branch Complex, Virginia (Drake and Morgan, 1981). Mittwede (1989) presented discussions of the field relationships, structure, and metamorphic history of the Hammett Grove Suite.

The purpose of this paper is to examine the distribution of trace elements in rocks of the Hammett Grove Meta-igneous Suite, to elucidate patterns of trace-element variation (in part by means of a principal component analysis), and to evaluate their implications for the origin and magmatic evolution of the Suite.

## SYNOPSIS OF MINERALOGY

### Altered Ultramafites

Altered ultramafites of the Hammett Grove Suite are mainly soapstone, talc schist or, locally, antigorite serpentinite. These metasomatized ultramafites consist of talc or antigorite, tremolite-actinolite, magnetite and a chromium-rich spinel, chlorite, anthophyllite, a carbonate phase, and pyrite. At one locality, relict olivine ($Fo_{89}$) comprises about 17 percent of the ultramafite. Mineralogic and textural evidence (for example, orthopyroxene bastite) suggests that the igneous protolith for the altered ultramafites was harzburgite or lherzolite. No unequivocal primary tectonite fabric has been recognized in the altered ultramafites.

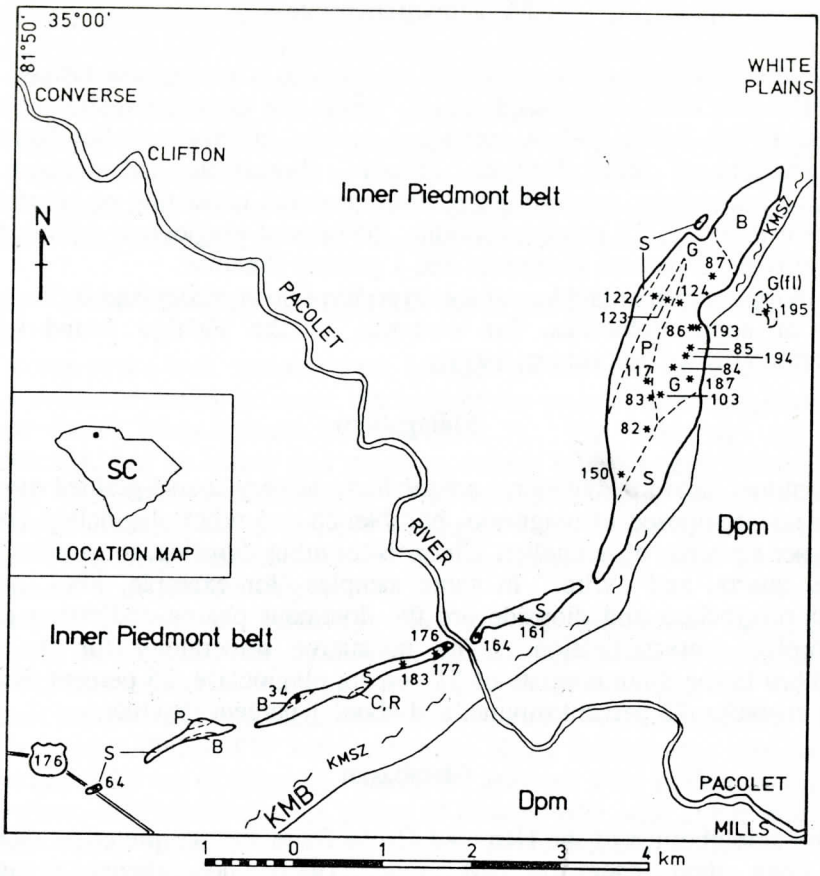


**Figure 1. Generalized geologic map of the main body of the Hammett Grove Suite and location map. Sample locations marked by asterisk, and location numbers correspond to sample numbers in Tables 1 and 2. Explanation: Hammett Grove Meta-igneous Suite lithodemes — S = altered ultramafites; P = metapyroxenite; G = metagabbro; G (fl) = metagabbro float; B = amphibolitic metabasalt; C,R = rodingitized metasediment (metachert?) and rodingite; DPM = Devonian Pacolet Mills granitic pluton; KMB = Kings Mountain belt; KMSZ = Kings Mountain shear zone.**

## Metapyroxenite

Hammett Grove metapyroxenites are coarse- to very coarse-grained (up to 4 cm) and are composed mostly of magnesio-hornblende, with lesser amounts of chlorite, actinolite, epidote, relict diopside, clinozoisite, opaque phases, and titanite. Norms suggest that the igneous parent consisted of nearly equal amounts of olivine, plagioclase (about $An_{86}$) and pyroxenes, and about 4 percent magnetite. The protolith may have been plagioclase-olivine websterite or olivine melagabbro. Compositionally similar rocks in the Marum ophiolite complex, northern Papua New Guinea and the Betts Cove ophiolite, Newfoundland have been described as plagioclase websterite (Jaques and others, 1983; analysis 11 in their Table 1) and perknites (Coish and Church, 1979; samples 61 and 65 in their Table 1), respectively.

### Metaclinopyroxenite

The metaclinopyroxenite occurs as medium- to coarse- grained dikes, sills, or pods within the metagabbro (and locally within the metapyroxenite) unit of the Hammett Grove Suite, and is composed mainly of magnesio-hornblende with lesser amounts of relict diopside, chlorite, clinozoisite and opaque phases. Normative mineralogy suggests an igneous protolith consisting of approximately 40 percent diopside, 22 percent enstatite, 20 percent plagioclase (about $An_{71}$), 9 percent olivine, 3 percent magnetite and 1 percent ilmenite.

Clinopyroxenite sills/dikes of this type have been recognized in the gabbroic section of some ophiolites, for example, in the Fidalgo Island ophiolite, Washington (Brown and others, 1979).

### Metagabbro

Hammett Grove metagabbros are medium- to very coarse-grained (up to 3 cm locally) and composed of magnesio- hornblende and relict plagioclase ($An_{82-92}$), with lesser amounts of actinolite, clinozoisite, relict diopside, muscovite, titanite, chlorite, quartz, and pyrite. In some samples (for example, #86), near end-member plagioclase and diopside are the dominant phases, indicating profound metamorphic recrystallization. The normative mineralogy for the average metagabbro in the Suite consists of 51 percent plagioclase, 25 percent diopside, 8 percent enstatite, 12 percent olivine, and about 1 percent ilmenite.

### Metabasalt

The amphibolites of the Hammett Grove Suite are interpreted as metabasalts based upon their chemistry (Mittwede, 1989); no primary textures are recognizable. The metabasalts are composed of green to olive-green hornblende, plagioclase, epidote, chlorite, biotite, titanite, apatite, and an unidentified opaque phase(s). Two norm calculations using the range of compositions observed yield 56-61 percent labradoritic plagioclase, 12-16 percent diopside, 3-16 percent enstatite, 0-10 percent olivine, 1-4 percent potassium feldspar, about 4 percent magnetite, and 3-4 percent ilmenite.

### Metatrondhjemite

Narrow, fine- to medium-grained metatrondhjemite dikes or sills, composed of plagioclase, quartz, muscovite, microcline, and minor amounts of epidote, garnet and biotite, occur within the Hammett Grove metagabbros. Normative mineralogy suggests an igneous protolith consisting of 53 percent $An_{19}$ plagioclase, 36 percent quartz, about 5.5 percent potassium feldspar, and about 2.5 percent corundum. This norm agrees well with the modal mineralogy, with normative corundum (representing excess Al) appearing modally as muscovite.

The trondhjemitic rocks of the Suite are not oceanic plagiogranite (Coleman and Peterman, 1975) but, rather, are similar to anatectic trondhjemites as described by Size (1985). Size (1985) reported that anatectic trondhjemites are commonly associated with, but not restricted to, the upper zones of ophiolites, and suggested that anatectic trondhjemites develop by a secondary process of partial melting of a low-K tholeiitic basalt. The Hammett Grove trondhjemite is dissimilar to oceanic

plagiogranite and comparable to anatectic trondhjemite of Size (1985) with regard to its $Al_2O_3$, $K_2O$, and Rb contents. Like anatectic trondhjemites, the Hammett Grove trondhjemite has a highly fractionated LREE enrichment pattern (with La 45x and Lu 4.4x chondrite; Mittwede, unpublished data).

Given the low proportion of trondhjemite in the Suite, it is possible that the trondhjemite is a simple product of fractionation of the same melt from which the gabbros crystallized. However, it is likely that the trondhjemites are second stage, anatectic trondhjemites (Size, 1985) formed by partial remelting.

## SAMPLING, PREPARATION AND INSTRUMENTATION

Twenty-seven rock samples were selected on the basis of freshness from all of those collected during geologic mapping of the main (11-km long) body of the Hammett Grove Meta-igneous Suite (Figure 1). The Suite was not sampled systematically, but an effort was made to collect samples representative of the Suite and its component lithodemes. The selected samples were trimmed on a water-cooled diamond saw to remove weathered material and organic matter. The samples were later run through a jaw crusher, and were powdered and homogenized in an agate swing mill.

The 27 samples, including six altered ultramafite samples, five metapyroxenite samples, one anomalous, partially altered metapyroxenite sample, three metaclinopyroxenite samples, ten metagabbro samples, one amphibolitic metabasalt sample, and one metatrondhjemite sample, were analyzed for 20 trace elements using a Philips PW 1404 automatic X-ray fluorescence spectrometer at the Geological Survey of Norway. All of the analyses were performed on pressed powder discs, each containing six grams of rock powder with a wax binder.

Randomized replicate analyses, shown parenthetically in Table 1, indicate good precision, five percent or less in most cases. Sub-sampling error may be responsible where precision exceeds five percent, especially if the trace element is enriched in scarce mineral grains. In most of the samples, the apparent precision for Ba is considerably poorer than for the lighter elements. Metagabbro samples 87A-1 and 122 are very coarse-grained, which may account for some of the variation between samples.

## RESULTS

Cr and Ni are strongly enriched (with up to about 7200 ppm Cr+Ni) in the altered ultramafites and decrease by one or two orders of magnitude in the cumulate and extrusive rocks; V, Ti, Sr, Y, Zr, and Ba are all depleted in the altered ultramafites relative to the cumulate and extrusive rocks of the Suite. Coleman (1977) noted that Cu is depleted in the metamorphic peridotites (14 ppm) and plagiogranites (1 ppm) of ophiolites; this behavior is paralleled in the altered ultramafites (<5 to 18 ppm) and metatrondhjemite (<5 ppm) of the Hammett Grove Suite.

Co is most abundant in the ultramafic compositions, and decreases in the mafic compositions. V is relatively depleted in the altered ultramafites, and enriched in the metabasalt and metaclinopyroxenite.

The incompatible elements Sr, Y, Zr, Ti, and Ba increase more-or-less systematically from the ultramafic through the cumulate mafic compositions; the cumulate metagabbros have the highest concentrations of Sr and Ba, probably

reflecting the accumulation of plagioclase. Y, Zr, Cu, and Ti are most concentrated in the metabasalt, an order of magnitude higher than in the altered ultramafites.

The high-Ca metaclinopyroxenites break systematic compositional trends by having more V, Y, Cr, Cu, and Mo than the other rocks of the cumulate sequence, probably due to the relative compatibility of these elements in clinopyroxene. The average Cr content of these rocks is almost as high as that of the altered ultramafites, although the Ni content is almost an order of magnitude lower. The lower Ni content is attributed to the relatively low olivine content (9 percent) of the igneous precursor as determined in the norm reported above.

Mo contents are consistently low and show little variation. Zn shows a systematic though modest decrease in concentration through the cumulate sequence, but increases sharply in the metabasalt.

Cr and Ni, which are incompatible with felsic compositions, are absent in the metatrondhjemite, as are Co, V, and Cu. Sn, Pb, and Th are absent in all lithologies except the metatrondhjemite, in which each is modestly enriched. The metatrondhjemite is also enriched in Nb.

## PRINCIPAL COMPONENT ANALYSIS

As an aid in sorting out the complex multidimensional interdependence among the trace elements, a principal component analysis (PCA) was carried out using the factor analysis procedure in the SAS computer package (Sarle and Sall, 1982). The PCA is an important tool when there are more than three variables in that: 1) the component pattern demonstrates which variables are interrelated, in this case which trace elements vary sympathetically or antithetically; and 2) the component scores provide a meaningful ordering of the data. The results show that most (53 percent) of the variance (component 1) is associated with the suite of elements Co, Cr, Ni, Zn, Sr, V, Ti, Zr, and Cu, and a smaller proportion (14 percent) of the total variance is associated with the elements V and Rb. Ideally, the essential features of the PCA should be apparent in a properly sorted table of the trace-element analyses, in which case the PCA simply acts as an aid in placing a definite order among the complex variations of the original data set.

To accomplish this, each of the samples were plotted using their component scores onto the plane of the first two principal components. From the test plots, any samples that were outliers (samples 161, 64A, 34, and 84F) were readily observed and segregated. Once these high leverage points were removed, the PCA was performed again and the sample scores were recomputed. The samples were then sorted in ascending order of the scores of the first principal component. This order was used in arranging the sample list (rows in Table 1). The columns for the elements then were segregated into three groups: those with decreasing value; those with ascending value; and those without consistent trend (Table 1). Consequently, the rows are ordered by rock type and the columns by related elements. Major elements (from Mittwede and others, 1987) were arranged in the same manner as the trace elements for easy comparison (Table 2). As an examination of the final tabulation shows all of the significant features of the PCA, the details of the PCA itself have been omitted.

A principal component analysis was also performed using the major elements to understand any associations among these. A preliminary PCA identified the same four samples as outliers and these high leverage points were removed and the

**Table 1. Trace-element analyses for rocks of the Hammett Grove Suite (in ppm).**

| Sample number | Rock type | descending | | | | ascending | | | | | without consistent trend | | | |
|---|---|---|---|---|---|---|---|---|---|---|---|---|---|---|
| | | Co | Ni | Cr | Zn | Sr | V | Ti | Zr | Cu | Rb | Ba | Y | Mo |
| (176A* | um | 112 | 2498 | 4828 | 81 | <5 | 61 | 310 | 8 | <5 | 5 | 82 | <5 | 7) |
| 164 | um | 100 | 1814 | 3420 | 86 | 23 | 14 | 46 | 12 | <5 | <5 | 22 | <5 | 10 |
| 176A | um | 110 | 2479 | 4735 | 81 | 6 | 67 | 290 | 14 | <5 | 5 | 67 | <5 | 10 |
| 183 | um | 74 | 1776 | 2959 | 96 | 6 | 26 | 290 | 13 | <5 | 6 | 62 | <5 | 7 |
| 177 | um | 66 | 1051 | 3192 | 51 | <5 | 52 | 340 | 9 | 18 | <5 | 11 | <5 | 14 |
| 64B | um | 67 | 1820 | 3204 | 62 | 11 | 50 | 840 | 9 | 15 | <5 | 19 | <5 | 6 |
| avg. | um | 83 | 1788 | 3506 | 75 | 9 | 42 | 361 | 11 | 7 | <5 | 36 | <5 | 9 |
| 150 | mp | 106 | 337 | 533 | 130 | 48 | 70 | 1080 | 18 | 8 | 7 | 58 | <5 | 7 |
| 83 | mp | 120 | 311 | 1084 | 82 | 36 | 89 | 1080 | 21 | 56 | <5 | 15 | <5 | 9 |
| 82 | mp | 85 | 377 | 2606 | 80 | 59 | 167 | 2100 | 20 | 21 | <5 | 57 | 6 | 8 |
| 85A | mp | 72 | 345 | 1129 | 55 | 79 | 107 | 1140 | 17 | 61 | 6 | 18 | <5 | 7 |
| 123 | mp | 87 | 181 | 449 | 72 | 41 | 99 | 1440 | 20 | 52 | 5 | 39 | 7 | 7 |
| avg. | mp | 94 | 310 | 1060 | 84 | 53 | 106 | 1368 | 19 | 40 | <5 | 37 | <5 | 8 |
| 187 | mcp | 68 | 328 | 3079 | 60 | 31 | 194 | 2280 | 23 | 60 | <5 | 37 | 11 | 13 |
| 117 | mcp | 73 | 226 | 3298 | 66 | 55 | 240 | 3369 | 36 | 34 | 6 | 46 | 15 | 11 |
| 194 | mcp | 53 | 292 | 2877 | 72 | 30 | 254 | 3120 | 30 | 94 | 6 | 71 | 17 | 8 |
| avg. | mcp | 65 | 282 | 3085 | 66 | 38 | 229 | 2920 | 30 | 63 | <5 | 51 | 14 | 11 |
| 193 | mg | 45 | 68 | 328 | 35 | 343 | 83 | 1260 | 21 | 61 | 13 | 68 | 7 | 10 |
| 85B | mg | 44 | 117 | 672 | 53 | 283 | 133 | 1620 | 20 | 43 | 11 | 95 | 9 | 9 |
| 86 | mg | 38 | 110 | 562 | 43 | 353 | 95 | 1380 | 23 | 39 | 5 | 97 | 6 | 6 |
| (84 | mg | 43 | 208 | 1002 | 56 | 303 | 162 | 2100 | 26 | 34 | 11 | 57 | 9 | 5) |
| 84 | mg | 42 | 208 | 1012 | 53 | 308 | 160 | 2100 | 29 | 33 | 12 | 68 | 10 | 10 |
| 195 | mg | 32 | 70 | 886 | 56 | 263 | 199 | 2760 | 35 | 41 | <5 | 22 | 17 | 7 |
| 124A | mg | 29 | 78 | 523 | 38 | 353 | 110 | 1980 | 35 | 59 | 7 | 56 | 9 | 8 |
| (87A1 | mg | 38 | 71 | 416 | 52 | 329 | 145 | 3060 | 32 | 42 | 5 | 98 | 14 | 7) |
| 87A2 | mg | 36 | 72 | 463 | 49 | 340 | 135 | 2820 | 33 | 49 | <5 | 117 | 12 | 6 |
| 87A1 | mg | 35 | 71 | 393 | 84 | 300 | 177 | 3120 | 30 | 47 | 9 | 134 | 17 | 9 |
| 103 | mg | 31 | 123 | 800 | 52 | 413 | 168 | 3720 | 36 | 86 | <5 | 74 | 12 | 9 |
| (122 | mg | 26 | 46 | 275 | 47 | 381 | 148 | 2460 | 45 | 89 | <5 | 135 | 16 | 5) |
| 122 | mg | 27 | 49 | 276 | 47 | 397 | 143 | 2400 | 48 | 90 | <5 | 130 | 18 | <5 |
| avg. | mg | 36 | 97 | 592 | 51 | 335 | 140 | 2316 | 31 | 55 | 6 | 86 | 12 | 8 |
| Outliers | | | | | | | | | | | | | | |
| 64A | um | 73 | 1590 | 2240 | 171 | 6 | <10 | 76 | 15 | <5 | 58 | 17 | <5 | 7 |
| 161 | mp | 138 | 674 | 519 | 128 | 26 | 119 | 3660 | 112 | 44 | 5 | 354 | 9 | <5 |
| (161 | mp | 126 | 672 | 530 | 128 | 26 | 117 | 3600 | 94 | 44 | <5 | 410 | 9 | <5) |
| 34 | am | 37 | 34 | 145 | 95 | 250 | 303 | 9830 | 134 | 68 | <5 | 70 | 44 | 8 |
| 84F | mt | <10 | <5 | <5 | 13 | 228 | <10 | 230 | 44 | <5 | 44 | 83 | 17 | 10 |
| (84F | mt | 12 | 8 | 7 | 15 | 228 | <10 | 220 | 47 | <5 | 42 | 47 | 17 | 8) |

* Replicate analyses in parentheses. Explanation of rock-type symbols: um = altered ultramafites; mp = metapyroxenite; mcp = metaclinopyroxenite; mg = metagabbro; am = amphibolitic metabasalt; mt = metatrondhjemite.

NOTE: Replicates and outliers (64A and 161) not included in averages Also determined, with lower limits of detection in parentheses, were Nb (5), Ag (5), Cd (5), Sn (5), W (10), Pb (10), Th (10), and U (10). Concentrations of these elements were below detection limits except as follows: sample (176A) - 6 ppm Ag; sample 164 - 7 ppm Cd; sample 177 - 7 ppm Cd; sample 161 (161) - 15 (14) ppm Nb; sample 85A - 6 ppm Cd; sample 85B - 6 ppm Ag; sample 86 - 7 ppm Cd; sample 84 - 8 ppm Ag; sample 124A - 6 ppm Cd; sample 34 - 6 ppm Nb; sample 84F (84F) - 28 (27) ppm Nb, 8 ppm Cd, 15 (15) ppm Sn, 11 ppm W, 30 (31) ppm Pb, 21 (23) ppm Th.

PCA was performed again. Because the samples were not fired before analyzing by ICP (Mittwede and others, 1987), a residual term representing loss on ignition (LOI) was calculated by subtracting the sum of the major elements from 100 percent, and this variable was included in the PCA. The results showed that most (46 percent) of the variance (component 1) is associated with the suite CaO, $Na_2O$, $Al_2O_3$, $TiO_2$, and MgO, while a smaller proportion (21 percent) of the variance (component 2) is associated with $Fe_2O_3$, MnO, $SiO_2$, and residual (Figure 2).

As chemical analyses should sum to 100 percent, this PCA is subject to correlations induced by closure. In an attempt to minimize this effect, a random

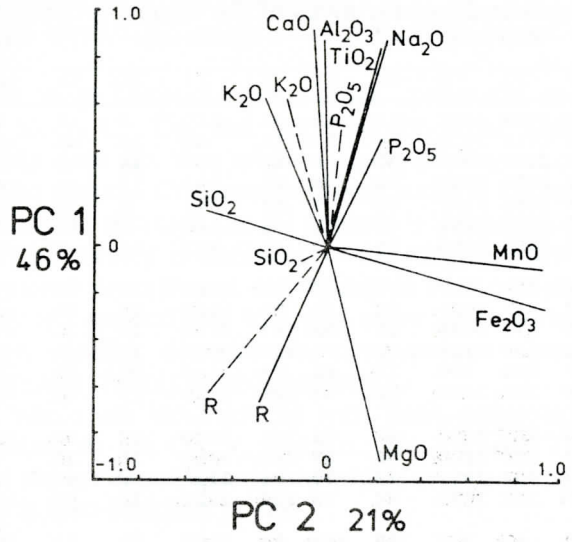


**Figure 2. Projection of the variable axes onto the plane of the first two principal components. Note the change in position of the modified axes (dashed lines) of $SiO_2$, R (residual), $K_2O$, and $P_2O_5$.**

**Table 2. Major-element analyses for rocks of the Hammett Grove Suite (in weight percent). From Mittwede and others (1987).**

| Sample number | Rock type | $SiO_2$ | $TiO_2$ | $Al_2O_3$ | $Fe_2O_3$ | MnO | MgO | CaO | $Na_2O$ | $K_2O$ | $P_2O_5$ | TOTAL |
|---|---|---|---|---|---|---|---|---|---|---|---|---|
| 176A | um | 42.50 | .05 | 2.26 | 9.56 | .16 | 34.91 | .72 | .01 | .01 | .03 | 90.22 |
| 183 | um | 57.97 | .05 | 2.21 | 6.28 | .08 | 27.18 | .26 | <.01 | .15 | .01 | 94.19 |
| 64B | um | 50.48 | .14 | 3.85 | 6.77 | .09 | 23.98 | 2.34 | .06 | .01 | .05 | 87.77 |
| 150 | mp | 41.94 | .21 | 11.81 | 12.55 | .22 | 20.03 | 7.86 | .70 | .05 | .02 | 95.39 |
| 83 | mp | 41.87 | .20 | 8.03 | 13.30 | .18 | 24.76 | 6.74 | .36 | .04 | .02 | 95.50 |
| 82 | mp | 43.93 | .38 | 7.42 | 11.02 | .17 | 21.56 | 9.06 | .22 | .07 | .04 | 93.87 |
| 85A | mp | 46.27 | .20 | 12.25 | 9.46 | .12 | 20.84 | 9.82 | .64 | .02 | .01 | 99.63 |
| 123 | mp | 43.45 | .23 | 13.51 | 11.24 | .13 | 20.40 | 8.49 | .59 | .13 | .02 | 98.09 |
| 187 | mcp | 47.07 | .41 | 7.00 | 8.12 | .14 | 18.54 | 12.53 | .83 | .23 | .04 | 94.91 |
| 117 | mcp | 49.13 | .61 | 6.96 | 8.89 | .16 | 17.36 | 12.64 | .61 | .21 | .04 | 96.61 |
| 194 | mcp | 50.17 | .58 | 5.38 | 8.48 | .16 | 17.62 | 13.67 | .58 | .10 | .05 | 96.79 |
| 193 | mg | 44.68 | .22 | 21.19 | 5.75 | .09 | 9.66 | 15.36 | .79 | .14 | .05 | 97.93 |
| 85B | mg | 44.66 | .27 | 15.33 | 6.74 | .11 | 12.85 | 13.67 | .76 | .20 | .01 | 94.60 |
| 86 | mg | 43.95 | .22 | 21.00 | 5.10 | .08 | 9.76 | 14.20 | .77 | .18 | .03 | 95.29 |
| 84 | mg | 48.34 | .36 | 12.65 | 6.99 | .13 | 13.49 | 15.85 | .55 | .49 | .04 | 98.89 |
| 195 | mg | 48.98 | .54 | 14.01 | 6.65 | .12 | 10.59 | 16.72 | .13 | .02 | .02 | 97.78 |
| 124A | mg | 48.32 | .36 | 20.51 | 5.20 | .09 | 8.73 | 17.93 | .58 | .13 | .02 | 101.87 |
| 87A2 | mg | 47.67 | .49 | 19.69 | 6.91 | .11 | 9.94 | 14.26 | .69 | .18 | .02 | 99.96 |
| 87A1 | mg | 48.71 | .58 | 17.70 | 7.88 | .14 | 10.26 | 13.98 | 1.04 | .34 | .06 | 100.69 |
| 103 | mg | 45.86 | .67 | 17.74 | 6.81 | .11 | 9.74 | 14.99 | .76 | .12 | .03 | 96.83 |
| 122 | mg | 50.05 | .46 | 19.76 | 6.15 | .12 | 7.51 | 16.29 | 1.20 | .32 | .03 | 101.89 |
| Outliers | | | | | | | | | | | | |
| 161 | mp | 45.36 | .86 | 7.04 | 14.59 | .15 | 26.24 | 1.78 | .01 | .05 | .20 | 96.28 |
| 64A | um | 53.48 | .01 | 1.68 | 4.22 | .07 | 25.51 | .90 | .01 | .26 | .02 | 86.16 |
| 34 | am | 49.98 | 1.88 | 17.55 | 11.90 | .20 | 5.61 | 11.54 | 2.37 | .22 | .14 | 101.39 |
| 84F | mt | 73.70 | .04 | 15.47 | .31 | .02 | .08 | 1.97 | 5.10 | .92 | .03 | 97.64 |

Rock-type symbols as in Table 1.

NOTE: Low totals due to unmeasured $H_2O$ content of hydrous silicates such as talc, micas, amphiboles, and serpentines, and unmeasured $CO_2$ of carbonate minerals. Major-element analyses of samples 164 and 177 gave spurious results and, therefore, were not included in this table.

term proportional to each analytical value was added:

$$\Delta x = k\ (1 - \frac{|50-x|}{(50+x)})\ N\ (0,1)$$

where $\Delta x$ is the value added to each element,
$x$ is the observed analytical value,
$k$ is a scale factor,
$N\ (0,1)$ is a random normal deviate, and
$|\ |$ means the absolute value.

This adds a random effect which tends to open up the closure by removing the normalization. By trial and error, a value of k equal to 5 percent seemed to be most effective. After adding the random term, the PCA was repeated and any changes in the results observed.

Overall, the differences are relatively minor. Again, most (43 percent) of the variance (component 1) was associated with the suite CaO, $Na_2O$, $Al_2O_3$, $TiO_2$, and MgO, while a smaller proportion (17 percent) was associated with $Fe_2O_3$ and MnO. The most notable change was the increased independence of $SiO_2$ which forms a third component carrying 12 percent of the total variance. Slight but notable changes include that the residual (LOI) becomes less associated with MgO, while $K_2O$ and $P_2O_5$ associate more with CaO and $Al_2O_3$. Finally, an ordering of the major-element analyses on the basis of descending values of the first principal component yields essentially the same order as that obtained from the trace-element PCA.

Again, examination of the table of major-element analyses (Table 2) shows the significant features of the PCA. $SiO_2$ is essentially independent of the other elements. The values of CaO, $Na_2O$, $Al_2O_3$, and $TiO_2$ are in ascending order while MgO is in descending order. Note that $Fe_2O_3$ and MnO are high in the metapyroxenite, and ordering of $K_2O$ and $P_2O_5$ is not readily discernable in the table itself.

## DISCUSSION

Many petrogenetic models and hypotheses are based upon the trace-element contents of rocks and the behavior of the trace elements in igneous processes. Trace-element behavior has been treated quantitatively with some success, especially for basaltic rocks as applied to the discrimination of tectonic environments (for example, Pearce and Cann, 1971; Beccaluva and others, 1979). Unfortunately, because of crystal accumulation and varying degrees of selectivity with which different minerals incorporate or exclude trace elements, the same sorts of tectonic discrimination diagrams cannot be applied to cumulate rocks, such as some peridotites, pyroxenites and gabbros, of which the Hammett Grove Suite is mainly composed. Since gabbros (and other cumulate rocks) mostly result from cumulate liquidus phases plus variable amounts of trapped liquid, their compositions should not define a liquid line-of-descent, but should only give a rough idea of the degree of fractionation of the parental magma(s) (Pognante and others, 1982).

Serri (1981) suggested the $TiO_2$ vs. $FeO^*/FeO^*+MgO$ diagram for gabbroic rocks to differentiate between low-Ti and high-Ti gabbroic rocks from ophiolite complexes. Low-Ti ophiolites appear to represent oceanic crust formed in the

early stages of opening of intra-oceanic back-arc basins; high-Ti ophiolites represent oceanic crust formed at accreting plate margins, either in the later stages of intra-oceanic back-arc rifting, in ensialic back-arc basins, or in major ocean basins (Serri, 1981). The Hammett Grove Suite, along with many ophiolites (Serri, 1981), falls into the broad, somewhat diverse high-Ti category (Mittwede, 1989), with $TiO_2$ contents for the metagabbros ranging from 0.22 to 0.67 weight percent, and averaging 0.42 weight percent. The Hammett Grove meta-pyroxenites and metaclinopyroxenites are also fairly Ti-rich, with respective means of 0.24 and 0.53 weight percent (Mittwede and others, 1987). Metabasalts of the Hammett Grove Suite are also high in $TiO_2$ (Mittwede, 1989), and plot in the MORB field of Sun and Nesbitt (1978).

Serri (1980, 1981), among others, has used the mafic index ($FeO^*/FeO^*+MgO$) as an indicator of differentiation, recording the extent to which a magma had fractionated at the time of crystallization of the various lithologies in an igneous suite. Application of the mafic index (M.I.) to the ultramafic and mafic rocks of the Hammett Grove Suite reveals sequential iron enrichment, with the M.I. for the altered ultramafites, metapyroxenites, metaclinopyroxenites, metagabbros, metabasalt, and metatrondhjemite of 0.18, 0.32, 0.30, 0.36, 0.66, and 0.78, respectively. The mafic index shows an abrupt increase at the altered ultramafite/metapyroxenite transition, slight increase through the cumulate sequence, and another sharp increase at the cumulate/extrusive transition. Although the metatrondhjemite occurs only within the gabbroic section, these peraluminous felsic rocks are considered end-products in the evolution of the parental magma. Some of the geochemical variation in the cumulate rocks of the Suite probably is due to the cyclic nature of fractionation and accumulation typical in many cumulate sequences (Church and Riccio, 1977).

A geochemical comparison (Figure 3) of the Hammett Grove gabbros to ophiolitic/oceanic gabbros and to diapiric, late- and main-stage arc gabbros was made using the $FeO^*$ vs. $FeO^*/MgO$ diagram (Miyashiro, 1975). The average Hammett Grove gabbro plots with a cluster of oceanic/ophiolitic (spreading center) gabbros, distinctly apart from gabbroic arc intrusions like the Slaughters suite, Alabama (Neilson and Stow, 1986) and the Charlotte belt gabbro-metagabbro complexes, North and South Carolina (McSween and others, 1984).

Covariation diagrams (Figure 4) illustrate the trace-element contents of the Hammett Grove rocks plotted against the mafic index, $FeO^*/FeO^*+MgO$. Fractionation trends displayed on these diagrams clearly show the effects of removal of olivine, pyroxene, plagioclase, and oxide phases during the evolution of the melt.

Variation of V corresponds to the crystallization of pyroxene in the early stages of fractionation, and then of the oxide phase(s) later. Cr and Co variation also was controlled by the crystallization of pyroxenes and, in the case of Cr, also by chromite or another chromian spinel. The profound separation of the altered ultramafites from other rocks of the Suite on the Ni diagram reflects the crystallization of olivine at the earliest stage of magmatic evolution. Variation in Cu generally follows the behavior of V, indicating that Cu may have entered the $Fe^{2+}$ position in pyroxenes and/or oxide phases. The Zn variation shows much scatter and is not clearly related to the crystallization of a particular mineral phase. The profound separation of the metagabbros from the other cumulate rocks of the Suite on the Sr diagram marks the crystallization of plagioclase. Zr increases gradually with evolution of the melt, possibly reflecting the crystallization of

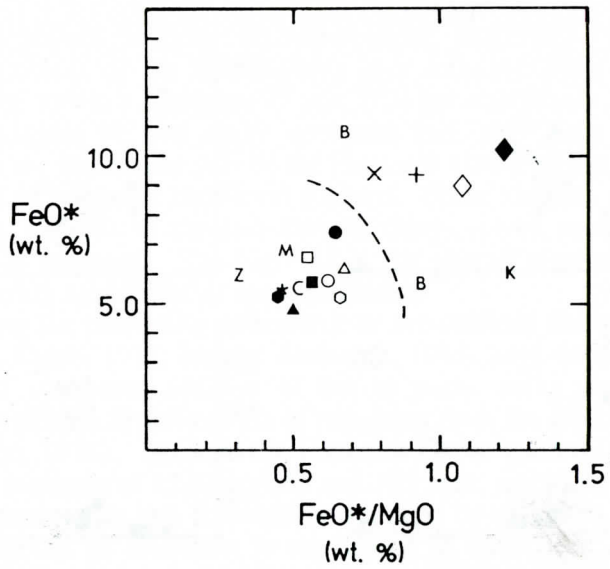


Figure 3. Binary plot of various gabbroic rocks (means or individual analyses) indicating degree of fractional crystallization/differentiation of parental magma (Miyashiro, 1975), measured by the increase in the $FeO^*/MgO$ ratio of the magma, where $FeO^*$ signifies total iron as FeO. Explanation of symbols: solid square = Hammett Grove Suite; open square = Halifax County complex, North Carolina Piedmont (Kite and Stoddard, 1984); solid circle = Piney Branch Complex, Virginia Piedmont (Drake and Morgan, 1981); open circle = northern Appenine ophiolites (Serri, 1980); solid triangle = Corsican ophiolites (Beccaluva and others, 1977); open triangle = Mid-Atlantic Ridge, Romanche Trench (Melson and Thompson, 1970); star = Tortuga ophiolite, Chile (Elthon and Ridley, 1980); solid hexagon = Papuan gabbros (Rodgers, 1975); open hexagon = Ogasawara fore-arc ophiolite (Ishii, 1985); C = ophiolitic Canyon Mountain complex, Oregon (Thayer, 1977); M = Mariana Trench (average of samples 3 and 4, Table 3 of Bloomer and Hawkins, 1983); Z = Zambales Range ophiolite, Luzon (Hawkins, 1980); solid diamond = Charlotte belt gabbro-metagabbro complexes, North Carolina-South Carolina Piedmont (McSween and others, 1984); open diamond = Slaughters metagabbro, Alabama Piedmont (Neilson and Stow, 1986); + = Pine Hill complex, California, type A gabbro (Springer, 1980); x = Emigrant Gap complex, California (average of two gabbro samples, Table 1 of James, 1971); B = Bear Mountain complex, California (two gabbro samples from Table 7 of Snoke and others, 1981); K = Kings Mountain belt metagabbro, South Carolina (Mittwede, 1988). Dashed line is approximate boundary between relatively "primitive", oceanic/ophiolitic gabbros that probably originated at or near spreading centers as part of igneous pseudostratigraphic sequences, and gabbros of diapiric, late- or main-stage arc intrusions. The most- evolved oceanic/ophiolitic gabbros and the least-evolved gabbros of arc intrusions will likely plot near or even overlap this boundary.

zircon from the later liquids and/or the substitution of Zr for Ti in the oxide phase(s). The variation of Ti generally parallels the behavior of V, Cu, and Zr. The Ba diagram shows some scatter, but Ba generally increases with magmatic evolution. The relatively high Ba content of some of the ultramafic rocks and

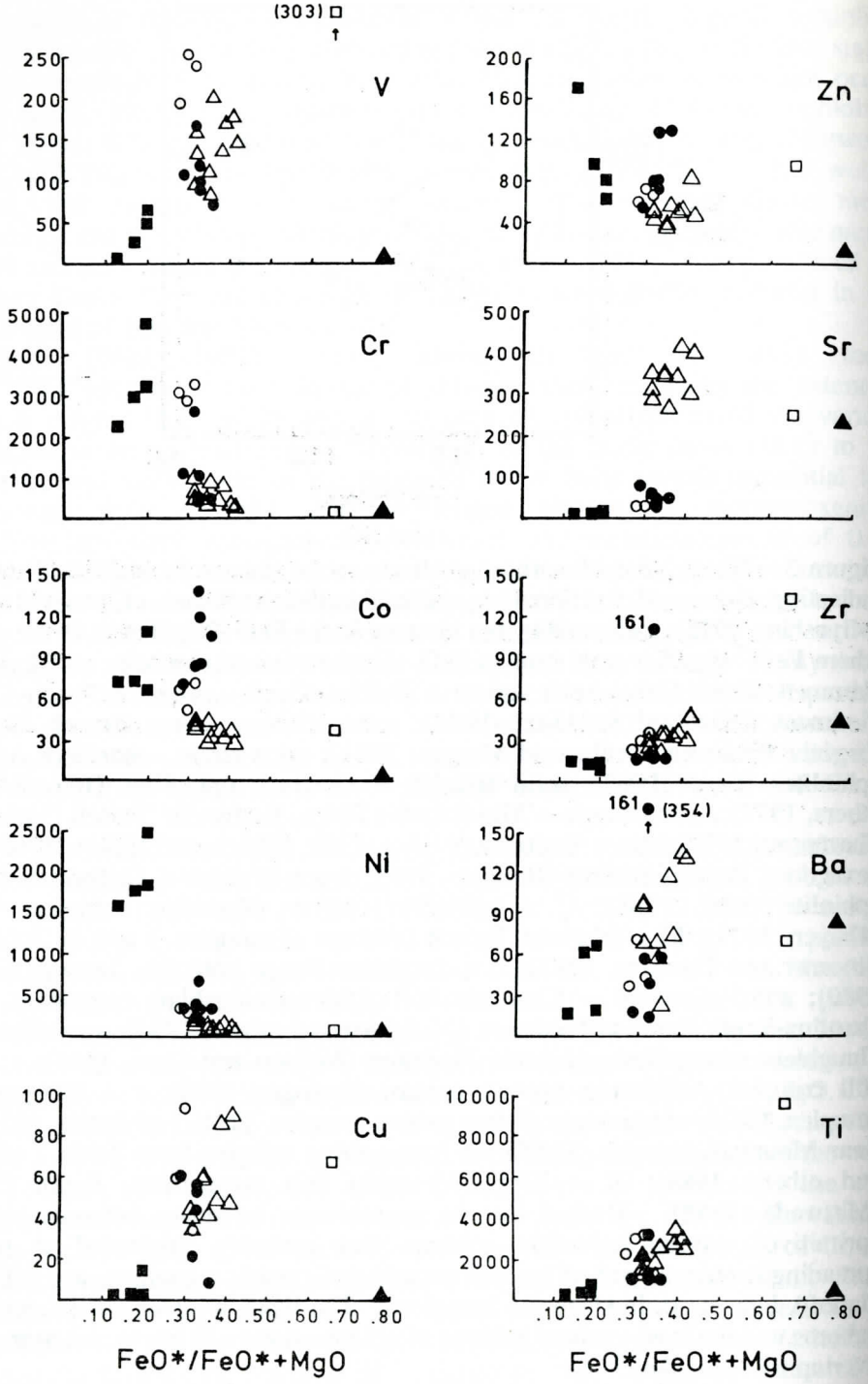


Figure 4. Trace-element covariation diagrams for rocks of the Hammett Grove Suite. Explanation: solid squares = altered ultramafites; solid circles = metapyroxenites; open circles = metaclinopyroxenites; open triangles = metagabbros; solid triangle = metatrondhjemite; open square = amphibolitic metabasalt.

gabbros may reflect seafloor or sub-seafloor alteration. Alternatively, the elevated Ba content of the metagabbros may reflect trapped liquid. The very coarse- grained gabbros (samples 87 and 122) generally have the highest Ba (as well as the highest Fe and alkali contents) and, since they occur in what is interpreted as the uppermost part of the Hammett Grove plutonic sequence, might be interpreted as relatively high-level gabbros. These virtually pegmatitic gabbros are, therefore, considered the last-formed, most-evolved rocks in the Hammett Grove plutonic sequence. The high Ba in the altered ultramafites possibly was introduced during steatitization/ serpentinization.

Regarding the possibility of seafloor or sub-seafloor alteration, many authors (for example, Coish, 1977; Ito and Anderson, 1983) have documented the loss of Ca from and consistent addition of Na to mafic rocks during hydrothermal alteration. Typically, Sr follows Ca in expulsion from the leached rock (Humphris and Thompson, 1978). Because the Hammett Grove gabbroic rocks are Ca- and Sr-rich (with averages of 15.33 percent and 335 ppm, respectively) and have fairly low alkali contents (Na and K would be supplied by seawater; Ito and Anderson, 1983), the amount of alteration is considered to have been negligible (Moody (1979) suggested that metamorphism in most ophiolite sequences dies out in the gabbro layer). If this assumption is correct, then the elevated Ba contents of the pegmatitic metagabbros mentioned above probably represent trapped liquid. However, higher concentrations of Na and K in the Hammett Grove metabasalts (sample 34, this paper; sample 221, Mittwede, 1989) may indeed reflect alkali metasomatism, with alkalis supplied and Ca removed by seawater.

Coish (1977) and Humphris and Thompson (1978) noted that Cu is also leached from mafic rocks during hydrothermal alteration. Since the Cu content of the Hammett Grove metagabbros seems to increase more-or-less systematically with fractionation, and the metabasalt sample contains less Cu than might be expected (that is, less than the most Cu- rich plutonic rocks), then the lower Cu content of the Hammett Grove metabasalt also may indicate seafloor alteration.

Although metamorphosed to the upper- or middle-amphibolite facies, the operative metamorphic process, at least in the plutonic section of the Suite, appears to have been isochemical. There are no epidosite zones or quartz veins, and there is little or no trace- or major-element evidence for any seafloor (open system) alteration in the plutonic rocks of the Hammett Grove Suite.

The Cr+Ni vs. Zr diagram (Beccaluva and others, 1977) shows Cr+Ni enrichment in the altered ultramafites and progressive depletion of these elements through the Hammett Grove plutonic section by the process of crystal accumulation (Figure 5). In the later stages of magmatic evolution, when Zr became relatively enriched in the residual liquids, fractional crystallization was operative. Relative to the marked depletion of Cr and Ni with increasing evolution, the Hammett Grove Suite shows little Zr enrichment in the more-evolved cumulate rocks (Figure 5).

The Ti vs. Zr diagram of Pearce and Cann (1973) has been applied widely in the discrimination of the tectonic setting of basic volcanic rocks (Figure 6). The single sample of Hammett Grove metabasalt plots in the ocean-floor basalt field and, although the gabbroic and ultramafic rocks of the Suite plot outside the ocean-floor basalt field, the plutonic rocks do plot on a line reflecting a differentiation trend compatible with ocean-floor basalts and/or some low-K tholeiites.

The Y vs. Zr diagram (Figure 7) shows that the behavior of Y and Zr correlate, as would be expected of two highly incompatible elements. Y and Zr (Figures 4

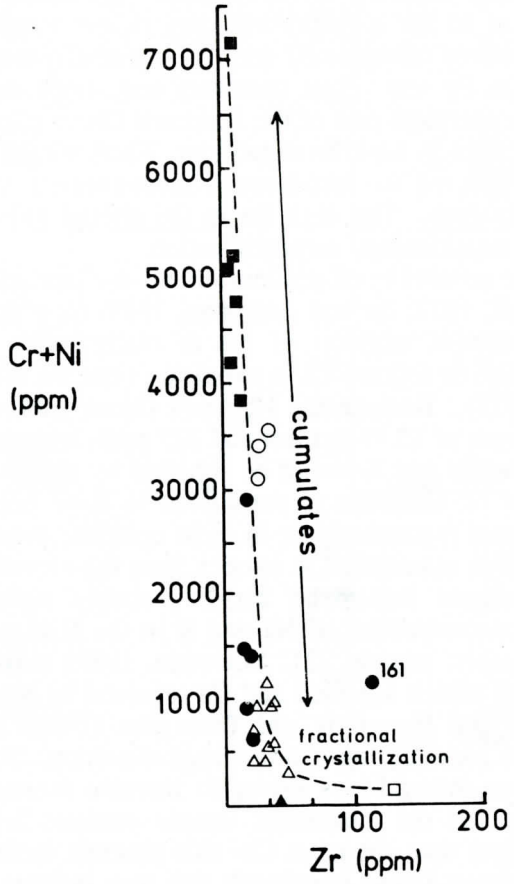


**Figure 5. Cr+Ni vs. Zr diagram (Beccaluva and others, 1977). Symbols as in Figure 4. Dashed line represents approximate crystal accumulation/residua trend and liquid line-of-descent, showing the rapid fall in compatible elements and concomitant, systematic but modest, increase in Zr with differentiation.**

and 7) show gradually increasing concentrations through differentiation, indicating their exclusion/non-accumulation during early- stage mineral formation. As in the Ti vs. Zr diagram, rocks of the Hammett Grove Suite plot on a line reflecting a trend compatible with MORB, rather than with island-arc basalts.

## QUANTITATIVE MAGMATIC MODELLING

A simple least-squares mixing model (GENMIX of Le Maitre, 1981) was used in order to evaluate the likelihood of a genetic relationship between the plutonic rocks of the Suite and the amphibolitic metabasalt. The most-evolved Hammett Grove gabbro, sample 122, was selected to be the product in the model. Relict plagioclase and relict clinopyroxene (compositions from Mittwede and others, 1987), an estimated olivine (end members Fo and Fa were mixed to give olivine that would be in equilibrium with the known clinopyroxene composition), and a basalt composition (sample 34) were used as reactants. The assumption is that the basalt represents the liquid composition. Thus the mixing model was:

relict plag + relict cpx + ol (est.) + basalt = gabbro 122

This equation yielded a least-squares solution as follows:

23.61 percent clinopyroxene
39.38 percent plagioclase ($An_{89.9}$)
4.13 percent olivine ($Fo_{86.7}$)
32.88 percent basalt.

That is, reactants in these proportions are necessary to give the gabbro product. This idealized mode is in general agreement with the observed mode which contains approximately 38 percent plagioclase and 55 percent combined magnesio-hornblende and relict clinopyroxene. Evans (1982) reported that magnesio-hornblende in isochemically metamorphosed ultramafic rocks can be regarded, to a first approximation, as substituting for the clinopyroxene of the protolith. The 55 percent "cpx" may correspond to the 23.61 percent clinopyroxene + 32.88 percent basalt (sum = 56.49 percent).

The residual sum of squares (rss) for this solution was .31, with 0 considered a "perfect" fit. However, as noted by Le Maitre (1981), apart from intuition, there is no satisfactory method of deciding whether a fit is "good" or "bad". This fit (.31) is considered good in that most of the poorness of fit comes from Na and K. Since alkalis are mobile during seafloor metamorphism (as discussed above) and are contributed readily by seawater, poorness of fit attributed to Na and K is not considered problematic. Another Hammett Grove metabasalt (sample 221; Mittwede, 1989) gave a poorer overall fit (1.09), but a better fit for Ti (difference between reactants and product of only –.04).

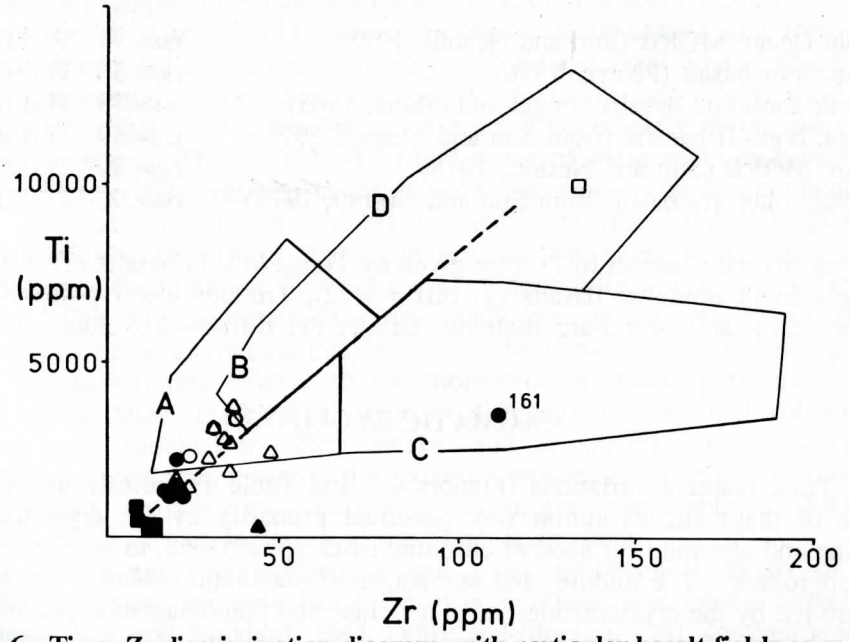


Figure 6. Ti vs. Zr discrimination diagram, with particular basalt fields as outlined by Pearce and Cann (1973). Ocean- floor basalts plots in fields D and B, low-potassium tholeiites in fields A and B, and calc-alkali basalts in fields C and B. Symbols as in Figure 4.

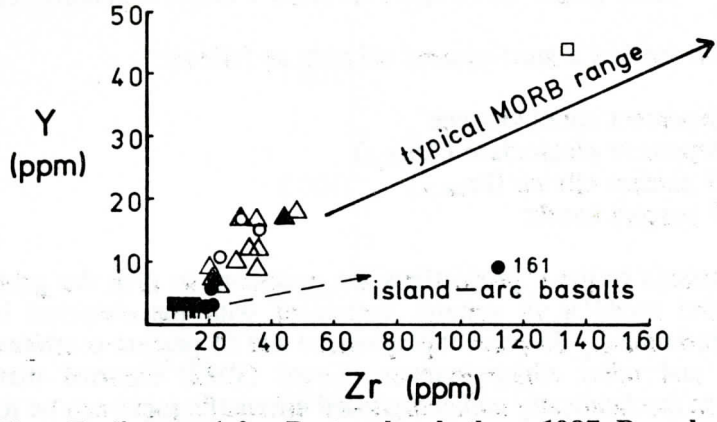


**Figure 7. Y vs. Zr diagram (after Bertrand and others, 1987; Beccaluva and others, 1977). Symbols as in Figure 4.**

A number of other basalt compositions (taken from Sun and Nesbitt, 1978) were used in the mixing model, and some (for example, Tonga low-Ti basalts and basalts from the Ming's Bight ophiolite) gave "better" overall fits (.19 and .21, respectively). Unfortunately, in these cases, the alkalis of the reactants and product were in closer agreement, but with greater disagreement for Ti. Therefore, although lower residual sums of squares can be derived, we have accepted slightly poorer overall fit to accommodate relative closeness of fit with regard to Ti (since it is widely considered an immobile trace element). Other "good" fits with respect to Ti were obtained using the following:

| | | |
|---|---|---|
| Indian Ocean MORB (Sun and Nesbitt, 1978) | rss=.74 | Ti diff.=.01 |
| ocean-floor basalt (Pearce, 1976) | rss=.56 | Ti diff.=.03 |
| oceanic tholeiitic basalts (Engel and others, 1965) | rss=.73 | Ti diff.=.05 |
| Tonga, high-Ti basalts (from Sun and Nesbitt, 1978) | rss=.59 | Ti diff.=–.06 |
| Chain, MORB (Sun and Nesbitt, 1978) | rss=.89 | Ti diff.=–.07 |
| Mariana inter-arc basin (from Sun and Nesbitt, 1978) | rss=.90 | Ti diff.=–.11 |

Poorest fits with respect to Ti were given by Tonga low-Ti basalts (Ti diff.= –.34), Ming's Bight ophiolite basalts (Ti diff.= –.32), Troodos lower pillow lavas (Ti diff.= –.22), and island-arc tholeiitic basalts (Ti diff.= –.21; Jakes and White, 1971).

## MAGMATIC EVOLUTION

Trace-element variations (Figures 4-7 and Table 1) indicate that the initial stage of magmatic evolution was governed primarily by the crystallization of olivine and chromite (or another chromium-rich spinel), and, to a lesser extent, by clinopyroxene. The middle- and late-stages of magmatic evolution were, in turn, controlled by the crystallization of plagioclase and titanomagnetite (or other Fe-Ti oxides), as indicated by the Sr and V (+ Ti) contents of the metagabbro and metabasalt, respectively (Table 1). Evolutionary trends shown in Figures 4, 5, 6, and 7 suggest that the early cumulate rocks of the Suite crystallized under relatively low $fO_2$ conditions. The later stages of magmatic evolution are

characterized by the enrichment of Fe, Ti, V, Cu, and Zr and, to a lesser extent, Ba and Y, as well as the rapid fall of compatible elements (Cr, Ni, Co, and Zn), indicating relative oxidation. This condition of oxidation is reflected in the crystallization of the Ti- bearing oxide phase(s). The crystallization of Fe-Ti oxide(s) would have shifted the scarce residual material toward silica- and alkali-rich compositions which, with likely partial melting (or concentration through remelting), led to the formation of trondhjemite.

The metaclinopyroxenites display a "hybrid" trace-element signature, with high Cr and V, and relatively low Ni and Sr. These dikes or sills may have tapped either a residual or relatively primitive (unevolved) clinopyroxene- rich liquid from the magma chamber after the removal of olivine and plagioclase, thus explaining the low Ni and Sr contents, respectively, of the resulting rocks.

The overall crystallization order inferred for the majority of the plutonic rocks of the Hammett Grove Suite is ol (Cr-sp) → opx → cpx → plag → oxides, or the type A crystallization sequence of Church and Riccio (1977). The observed rock sequence is peridotite- pyroxenite/melagabbro-gabbro (clinopyroxenite, trondhyemite) - basalt. The cumulate sequence was originally dominated by pyroxene.

## CONCLUSIONS

The geochemical study of the metamorphosed igneous rocks of the Hammett Grove Suite suggests that there are close similarities between these rocks of the southern Appalachian Piedmont and ophiolitic/oceanic analogs. Although an undisturbed igneous pseudostratigraphy is not directly observable, the inferred crystallization sequence (Mittwede, 1989) is the same as for well-documented ophiolites (for example, Coleman and Irwin, 1974; Church and Riccio, 1977).

The Hammett Grove rocks formed by crystal accumulation and fractional crystallization of a basaltic magma, possibly with little trapped liquid. Magmatic evolution apparently proceeded in a closed fractionation system; the gabbroic magma chamber that yielded the Suite was not fed periodically during the main crystallization stage. The $FeO^*/FeO^*+MgO$ ratios of these rocks suggest only slight to moderate differentiation in the cumulate sequence, with abrupt chemical changes only at the altered ultramafite- metapyroxenite and metagabbro-metabasalt transitions. These sharp changes may represent simple stages of differentiation, fractionation cyclicity, or, doubtfully, post-crystallization alteration. The altered ultramafites tentatively are interpreted as ultramafic cumulates rather than as residual mantle material by virtue of the consistent trace-element variation trends relative to the more-evolved rocks (pyroxenites and gabbros) of the Suite. In the final stage of differentiation, a small volume of remaining melt, enriched in silica, alkalis, and incompatible trace elements, crystallized as trondhjemite within the gabbroic sequence. A single metabasalt sample exhibits characteristics indicating an origin comparable to MORB, although some alkali metasomatism of the basalt is apparent.

The trace-element concentrations and gross geochemical trends of the Hammett Grove Suite are more like those of ophiolitic/oceanic crustal sequences (for example, Kite and Stoddard, 1984; Drake and Morgan, 1981; for comparison, see Mittwede, 1989) than arc-related gabbroic rocks of the Appalachian Piedmont (for example, McSween and others, 1984; Neilson and Stow, 1986; see Figure 3), suggesting that the Hammett Grove Suite may have crystallized in a small, shallow, oceanic-crustal magma chamber rather than as a diapiric intrusion within

an evolved-arc superstructure.

The position of the Hammett Grove Suite at the interpreted Piedmont terrane-Carolina terrane boundary, along with these trace-element data, suggest that the Suite is exotic relative to adjacent rocks at its present tectonostratigraphic position. The Hammett Grove Suite is interpreted to have formed as part of an ophiolite sequence in the constructional stage of Carolina-arc-terrane development and is not considered to be a disrupted, diapiric, late- or main-stage arc intrusion.

There is no evidence that the Hammett Grove Suite is a rock association of the Bear Mountain (California) type, as suggested by Dennis (1988). The lithologies, geochemistry, and interpreted tectonic environment of the Hammett Grove Suite are different than those for grossly similar associations in the Klamath Mountains-western Sierra Nevada described by Snoke and others (1982; see their Table 1 for comparison of features of various ultramafic-mafic associations). Mittwede (1989) suggested that the Hammett Grove Suite formed as fore-arc basement to the Carolina terrane. The findings of this trace-element study are consistent with that interpretation. It is likely that the Suite formed in a supra-subduction zone setting and subsequently was metamorphosed and fragmented during emplacement which coincided with terrane accretion.

## ACKNOWLEDGMENTS

This paper, a chapter from SKM's doctoral dissertation (University of South Carolina), is a product of a South Carolina Geological Survey mineral resources investigation, and is part of a cooperative program between the University of South Carolina and the Norwegian Geological Survey that was developed during the visits of WES during 1984, 1985, and 1988. Travel to and from Norway in 1984 and 1985 was supported by a National Science Foundation travel grant (INT 84 10912). The trace-element analyses reported here were performed by Bjørn Nilsen in the Geological Survey of Norway's XRF laboratory. Many thanks for helpful discussions with Scott Vetter, Debra Stakes, John Shervais and E. F. Stoddard. We appreciate the helpful, thorough critiques of earlier versions of the manuscript by M. R. Perfit, J. W. Shervais, E. F. Stoddard, R. V. Fodor, and an anonymous reviewer. However, we remain responsible for all interpretations.

## REFERENCES CITED

Beccaluva, L., Ohnenstetter, D., and Ohnenstetter, M., 1979, Geochemical discrimination between ocean-floor and island-arc tholeiites - application to some ophiolites: Canadian Journal of Earth Sciences, v. 16, p. 1874-1882.

Beccaluva, L., Ohnenstetter, D., Ohnenstetter, M., and Venturelli, G., 1977, The trace-element geochemistry of Corsican ophiolites: Contributions to Mineralogy and Petrology, v. 64, p. 11-31.

Bertrand, J., Dietrich, V., Nievergelt, P., and Vuagnat, M., 1987, Comparative major and trace element geochemistry of gabbroic and volcanic rock sequences, Montgenevre ophiolite, Western Alps: Schweizerische Mineralogische und Petrographisce Mitteilungen, v. 67, p. 147-169.

Bloomer, S. H., and Hawkins, J. W., 1983, Gabbroic and ultramafic rocks from the Mariana Trench; an island arc ophiolite, *in* Hayes, D. E., ed., The

tectonic and geologic evolution of southeast Asian seas and islands, part 2: American Geophysical Union, Geophysical Monograph 27, p. 294-317.
Brown, E. H., Bradshaw, J. Y., and Mustoe, G. E., 1979, Plagiogranite and keratophyre in ophiolite on Fidalgo Island, Washington: Geological Society of America Bulletin, v. 90, p. 493-507.
Church, W. R., and Riccio, L., 1977, Fractionation trends in the Bay of Islands ophiolite of Newfoundland; polycyclic cumulate sequences in ophiolites and their classification: Canadian Journal of Earth Sciences, v. 14, p. 1156-1165.
Coish, R. A., 1977, Ocean floor metamorphism in the Betts Cove ophiolite, Newfoundland: Contributions to Mineralogy and Petrology, v. 60, p. 255-270.
Coish, R. A., and Church, W. R., 1979, Igneous geochemistry of mafic rocks in the Betts Cove ophiolite, Newfoundland: Contributions to Mineralogy and Petrology, v. 70, p. 29-39.
Coleman, R. G., 1977, Ophiolites; ancient oceanic lithosphere?: Springer-Verlag, New York, 229 p.
Coleman, R. G., and Irwin, W. P., 1974, Ophiolites and ancient continental margins, *in* Burk, C. A., and Drake, C. L., eds., The geology of continental margins: Springer-Verlag, New York, p. 921-931.
Coleman, R. G., and Peterman, Z. E., 1975, Oceanic plagiogranite: Journal of Geophysical Research, v. 80, p. 1099-1108.
Dennis, A., 1988, Preliminary report on the geology of the Glenn Springs-Jonesville area and tectonic model, *in* Secor, D. T., Jr., ed., Southeastern geological excursions: South Carolina Geological Survey, Columbia, p. 226-249.
Drake, A. A., Jr., and Morgan, B. A., 1981, The Piney Branch Complex - a metamorphosed fragment of the central Appalachian ophiolite in northern Virginia: American Journal of Science, v. 281, p. 484-508.
Elthon, D., and Ridley, W. I., 1980, The petrology of the Tortuga ophiolite complex, southern Chile, *in* Panayiotou, A., ed., Ophiolites, Proceedings, International Ophiolite Symposium, Cyprus 1979: Cyprus Geological Survey, Nicosia, p. 507-513.
Engel, A. E. J., Engel, C. G., and Havens, R. G., 1965, Chemical characteristics of oceanic basalts and upper mantle: Geological Society of America Bulletin, v. 76, p. 719-734.
Evans, B. W., 1982, Amphiboles in metamorphosed ultramafic rocks, *in* Veblen, D. R., and Ribbe, P. H., eds., Amphiboles; petrology and experimental phase relations: Reviews in Mineralogy 9B, p. 98-113.
Hawkins, J. W., Jr., 1980, Petrology of back-arc basins and island arcs; their possible role in the origin of ophiolites, *in* Panayiotou, A., ed., Ophiolites, Proceedings, International Ophiolite Symposium, Cyprus 1979: Cyprus Geological Survey, Nicosia, p. 244-254.
Humphris, S. E., and Thompson, G., 1978, Trace element mobility during hydrothermal alteration of oceanic basalts: Geochimica et Cosmochimica Acta, v. 42, p. 127-136.
Ishii, T., 1985, Dredged samples from the Ogasawara fore-arc seamount or "Ogasawara paleoland" - "fore-arc ophiolite", *in* Nasu, N., and others, eds., Formation of active ocean margins: Terra, Tokyo, p. 307-342.
Ito, E., and Anderson, A. T., Jr., 1983, Submarine metamorphism of gabbros

from the Mid-Cayman Rise; petrographic and mineralogic constraints on hydrothermal processes at slow-spreading ridges: Contributions to Mineralogy and Petrology, v. 82, p. 371-388.
Jakes, P. and White, A. J. R., 1971, Composition of island arcs and continental growth: Earth and Planetary Science Letters, v. 12, p. 224-230.
James, O. B., 1971, Origin and emplacement of the ultramafic rocks of the Emigrant Gap area, California: Journal of Petrology, v. 12, p. 523-560.
Jaques, A. L., Chappell, B. W., and Taylor, S. R., 1983, Geochemistry of cumulus peridotites and gabbros from the Marum ophiolite complex, northern Papua New Guinea: Contributions to Mineralogy and Petrology, v. 82, p. 154-164.
Kite, L. E., and Stoddard, E. F., 1984, The Halifax County complex: oceanic lithosphere in the eastern North Carolina Piedmont: Geological Society of America Bulletin, v. 95, p. 422-432.
Le Maitre, R. W., 1981, GENMIX - a generalized petrological mixing model program: Computers in Geoscience, v. 7, p. 229-247.
McSween, H. Y., Jr., Sando, T. W., Clark, S. R., Harden, J. T., and Strange, E. A., 1984, The gabbro-metagabbro association of the southern Appalachian Piedmont: American Journal of Science, v. 284, p. 437-461.
Melson, W. G., and Thompson, G., 1970, Layered basic complex in oceanic crust, Romanche Fracture, Equatorial Atlantic: Science, v. 168, p. 817-820.
Mittwede, S. K., 1988, Ultramafites, melanges and stitching granites as suture markers in the central Piedmont of the southern Appalachians: Journal of Geology, v. 96, p. 693-707.
Mittwede, S. K., 1989, The Hammett Grove Meta-igneous Suite; a possible ophiolite in the northwestern South Carolina Piedmont, *in* Mittwede, S. K., and Stoddard, E. F., eds., Ultramafic rocks of the Appalachian Piedmont: Geological Society of America Special Paper 231, p. 45-62.
Mittwede, S. K., Ødegård, M., and Sharp, W. E., 1987, Major chemical characteristics of the Hammett Grove meta- igneous suite, northwestern South Carolina: Southeastern Geology, v. 28, p. 49-63.
Miyashiro, A., 1975, Classification, characteristics, and origin of ophiolites: Journal of Geology, v. 83, p. 249-281.
Moody, J. B., 1979, Serpentinites, spilites and ophiolite metamorphism: Canadian Mineralogist, v. 17, p. 871-887.
Neilson, M. J., and Stow, S. H., 1986, Geology and geochemistry of the mafic and ultramafic intrusive rocks, Dadeville belt, Alabama: Geological Society of America Bulletin, v. 97, p. 296-304.
Pearce, J. A., 1976, Statistical analysis of major element patterns in basalts: Journal of Petrology, v. 17, p. 15-43.
Pearce, J. A., and Cann, J. R., 1971, Ophiolite origin investigated by discriminant analysis using Ti, Zr and Y: Earth and Planetary Science Letters, v. 12, p. 339-349.
Pearce, J. A., and Cann, J. R., 1973, Tectonic setting of basic volcanic rocks determined using trace element analyses: Earth and Planetary Science Letters, v. 19, p. 290-300.
Pognante, U., Lombardo, B., and Venturelli, G., 1982, Petrology and geochemistry of Fe-Ti gabbros and plagiogranites from the western Alps ophiolites: Schweizerische Mineralogische und Petrographische Mitteilungen, v. 62, p. 457-472.

Rodgers, K. A., 1975, A comparison of the geology of the Papuan and New Caledonian ultramafic belts: Journal of Geology, v. 83, p. 47-60.
Sarle, W. S., and Sall, J. P., 1982, Proc Factor, *in* SAS User's Guide - Statistics: SAS Institute, Cary, NC, p. 308-345.
Serri, G., 1980, Chemistry and petrology of gabbroic complexes from the northern Appenine ophiolites, *in* Panayiotou, A., ed., Ophiolites, Proceedings, International Ophiolite Symposium, Cyprus 1979: Cyprus Geological Survey, p. 296-313.
Serri, G., 1981, The petrochemistry of ophiolite gabbroic complexes: a key for the classification of ophiolites into low-Ti and high-Ti types: Earth and Planetary Science Letters, v. 52, p. 203-212.
Size, W. B., 1985, Origin of trondhjemite in relation to Appalachian - Caledonide palaeotectonic settings, *in* Gee, D. G., and Sturt, B. A., eds., The Caledonide orogen - Scandinavia and related areas: John Wiley, Chichester, U.K., p. 735-744.
Snoke, A. W., Quick, J. E., and Bowman, H. R., 1981, Bear Mountain igneous complex, Klamath Mountains, California: an ultrabasic to silicic calc-alkaline suite: Journal of Petrology, v. 22, p. 501-552.
Snoke, A. W., Sharp, W. D., Wright, J. E., and Saleeby, J. B., 1982, Significance of mid-Mesozoic peridotitic to dioritic intrusive complexes, Klamath Mountains- western Sierra Nevada, California: Geology, v. 10, p. 160-166.
Springer, R. K., 1980, Geology of the Pine Hill intrusive complex, a layered gabbroic body in the western Sierra Nevada foothills, California: Geological Society of America Bulletin, v. 91 (part II), p. 1536-1626.
Sun, S., and Nesbitt, R. W., 1978, Geochemical regularities and genetic significance of ophiolitic basalts: Geology, v. 6, p. 689-693.
Thayer, T. P., 1977, The Canyon Mountain complex, Oregon, and some problems of ophiolites, *in* Coleman, R. G., and Irwin, W. P., eds., North American ophiolites: Oregon Department of Geology and Mineral Industries, Bulletin 95, p. 93-105.